
Editorial Office of *Earth's Cryosphere (Kriosfera Zemli)*
Institute of Geography, Russian Academy of Sciences
37 Vavilov str., office 22, Moscow, 117312, Russia
Editorial staff: *N.V. Arutyunyan*, *N.G. Belova, O.M. Lisitsyna, G.E. Oblogov*
Phone: 8(985) 957-10-01, e-mail: kriozem@gmail.com

Journal promoted by
Russian Academy of Sciences, Siberian Branch, Novosibirsk
Earth's Cryosphere Institute, Tyumen Scientific Centre SB RAS, Tyumen
Melnikov Permafrost Institute, SB RAS, Yakutsk

Editorial Manager *M.A. Trashkeeva*
Designed by *N.F. Suranova*
Typeset by *N.M. Raizvikh*

RUSSIAN ACADEMY OF SCIENCES
SIBERIAN BRANCH
EARTH'S CRYOSPHERE INSTITUTE, TYUMEN SCIENTIFIC CENTRE

EARTH'S CRYOSPHERE
SCIENTIFIC JOURNAL

Founded in January 1997	6 issues per year	Vol. XXV, No. 6	November–December 2021

CONTENTS

FUNDAMENTAL ISSUES OF EARTH'S CRYOSPHERE

Melnikov V.P., Osipov V.I., Broushkov A.V., Badina S.V., Drozdov D.S., Dubrovin V.A., Zheleznyak M.N., Sadurtdinov M.R., Sergeev D.O., Okunev S.N., Ostarkov N.A., Osokin A.B., Fedorov R.Yu. Adaptation of Arctic and Subarctic infrastructure to changes in the temperature of frozen soils 3

ECOLOGICAL PROBLEMS IN PERMAFROST ZONE

Zakharchenko A.V., Tigeev A.A., Pasko O.A., Kolesnichenko L.G., Moskovchenko D.V. Spatial distribution of geochemical characteristics of snow cover within and outside Tomsk-Seversk industrial agglomeration 13

GEOTHERMAL FIELDS AND THERMAL PROCESSES IN CRYOSPHERE

Sysolyatin R.G., Zheleznyak M.N. Thermal regime of cryolithozone at Ytymdzha Depression, Aldan Shield 23

GEOLOGICAL CRYOGENIC PROCESSES AND FORMATIONS

Nesterova N.B., Khomutov A.V., Leibman M.O., Safonov T.A., Belova N.G. The inventory of retrogressive thaw slumps (thermocirques) in the north of West Siberia based on 2016–2018 satellite imagery mosaic 34

SURFACE AND GROUND WATERS IN TERRESTRIAL PERMAFROST REGION

Galakhov V.P., Samoilova S.Yu., Mardasova E.V. Assessment of the amount of winter precipitation in mountain basins and their influence on flood formation (Charysh and Anuy river basins, Altai as a case study) 42

Glotov V.E. Subpermafrost waters in the East Chukotka's Upland 52

EARTH'S CRYOSPHERE
SCIENTIFIC JOURNAL

Earth's Cryosphere, 2021, vol. XXV, No. 6, pp. 3–12 http://earthcryosphere.ru/

FUNDAMENTAL ISSUES OF EARTH'S CRYOSPHERE

ADAPTATION OF ARCTIC AND SUBARCTIC INFRASTRUCTURE TO CHANGES IN THE TEMPERATURE OF FROZEN SOILS

V.P. Melnikov[1–4], V.I. Osipov[5], A.V. Brushkov[6], S.V. Badina[7,8], D.S. Drozdov[1,9,10], V.A. Dubrovin[10], M.N. Zheleznyak[11], M.R. Sadurtdinov[1], D.O. Sergeev[5], S.N. Okunev[12], N.A. Ostarkov[13], A.B. Osokin[14], R.Yu. Fedorov[1,2]

[1] *Earth Cryosphere Institute, Tyumen Scientific Centre SB RAS, Malygina str. 86, Tyumen, 625026, Russia; melnikov@ikz.ru*
[2] *Department of Methodology for Interdisciplinary Cryosphere Research, Tyumen Scientific Centre SB RAS, Malygina str. 86, Tyumen, 625026, Russia*
[3] *Tyumen State University, Semakova str. 10, Tyumen, 625003, Russia*
[4] *ANO "Gubernskaya Academia", Malygina str. 86, Tyumen, 625026, Russia*
[5] *Sergeev Institute of Environmental Geoscience RAS, Ulanskiy per. 13, bldg 2, Moscow, 101000, Russia*
[6] *Lomonosov Moscow State University, Faculty of Geology, Department of Geocryology, Leninskie Gory 1, Moscow, 119991, Russia*
[7] *Plekhanov Russian University of Economics, Stremyanny lane 36, Moscow, 117997, Russia*
[8] *Lomonosov Moscow State University, Faculty of Geography, Laboratory of Geoecology of the Northern Territories, Leninskie Gory 1, Moscow, 119991, Russia*
[9] *Ordzhonikidze Russian State University for Geological Prospecting, Mikluho-Maklaya str. 23, Moscow, 117997, Russia*
[10] *FSBI "Gidrospecgeologiya", Marshal Rybalko str. 6, bldg 4, Moscow, 123060, Russia*
[11] *Melnikov Permafrost Institute SB RAS, Merzlotnaya str. 36, Yakutsk, 677010, Russia*
[12] *LLC NPO "Fundamentstrojarkos", Novatorov str. 12a, Tyumen, 625014, Russia*
[13] *Ministry of Far East and Arctic Development, Burdenko str. 14, Moscow, 119121, Russia*
[14] *ITC LLC "Gazprom dobycha Nadym", Pionerskaya str. 14, Nadym, 629730, Russia*

The problem of sustainable economic development is acutely manifested in the Arctic regions, which is due to the vulnerability of the Arctic infrastructure to climate change and landscape transformations. The reasons for the deformations of buildings and structures in the Russian Arctic are considered. The permafrost monitoring network is identified as the basis for the development of technical solutions for adapting the Arctic infrastructure to climate change; the problems and prospects for its development are considered. The analysis of technological solutions for controlling and ensuring the reliability of the bearing capacity of foundations by regulating the state of permafrost soils is presented, and a preliminary analysis of the economic efficiency of protective measures is carried out. Their cost is at least an order of magnitude less than the expected damage to infrastructure by the middle of the 21st century.

Keywords: *Arctic zone of the Russian Federation, permafrost, frozen ground, climate change, adaptation of infrastructure, thermal stabilization.*

INTRODUCTION

One of the key problems of sustainable economic development is the adaptation of civil and industrial infrastructure to global climate change [*Infrastructure..., 2011; Zimmerman, 2011*]. This problem is especially acute in the Arctic regions, where, on the one hand, warming occurs faster than global trends [*Larsen et al., 2014*], and on the other hand, the vulnerability of the Arctic infrastructure is high under growing air and soil temperature and transforming permafrost and landscapes. In the Arctic zone of the Russian Federation (AZRF) more than 90 % of nickel and cobalt, 60 % of copper, and more than 96 % of platinum metals are mined, and about 80 % of gas and 60 % of oil from the all-Russian production are extracted [*Bryukhovetsky et al., 2014*]. For this zone, warming became a dangerous factor of economic and geoecological risks.

Due to an increase in temperature, the bearing capacity of frozen soils decreases, in many places they thaw from the surface, and destructive cryogenic (permafrost) processes develop. Thus, in the European North, modern climatic changes for the period from 1984 to 2019 caused an increase in soil temperature at a depth of 10 m by 0.5...1.5 °C. At the same time, the southern boundary of the discontinuous permafrost has significantly shifted to the north (in the Pechora lowland – on average by 30–40 km, on the plains near the Urals – up to a maximum of

80 km). In Western Siberia, in the northern taiga and forest-tundra at a latitude of 65–66 N, the mean annual ground temperatures increased by an average of 1–2 °C. In Yamal, in a typical tundra zone (68–71 N), according to more than 40-year observations, the temperature of permafrost at a depth of 10 m increased on average at a rate of 0.05 °C/year [*Melnikov et al., 2021*]. As a result, the increase in the mean annual permafrost temperature compared to the background state in the 1970s–1980s was from 1.5 to 2 °C [*Osokin, 2016*].

As a result of such changes, industrial complexes of the Russian Arctic and the cities serving them that have been created over the past 100 years are under threat. Today they require adaptation to the changed climatic and permafrost environment. Without this, the accident rate of geotechnical systems increases. For example, the number of deformed objects is 25–50 % of their total number. Thus, in Amderma, the number of collapsing buildings is about 40 %, in Dikson – 33 %, in Tiksi – 22 %, and in Pevek – 50 % [*Brushkov et al., 2021*]. The cryogenic factors cause a significant number of failures of technical systems in the oil and gas industry. In a number of studies, including this one [*Melnikov et al., 2021*], estimates of the material damage expected as a result of warming are given for the territory of the Russian Arctic [*Shiklomanov et al., 2019; Streletskiy et al., 2012, 2019*]. It becomes obvious that the design of new infrastructure should be carried out focusing not on modern, but on the predicted permafrost-climatic conditions.

CAUSES OF DEFORMATIONS OF BUILDINGS AND STRUCTURES IN THE ARCTIC

In areas with continuous permafrost, construction is mostly carried out according to the "principle I", i.e., with the preservation of the frozen ground. To maintain the frozen state, a ventilated crawl space is mainly used as a cooling system, the design of which at the time of construction provides a frozen state of the base. However, in many cases, due to salinity, and now due to warming, the soils are in a plastic-frozen state, and often have high ice content. As a result, as observations in the cities and towns of Amderma, Dikson, Tiksi, Pevek, and others show, the buildings continue to deform for decades. Accordingly, the calculation of the foundations would have to be carried out taking into account both bearing capacity and deformations. However, in practice, this requirement is still rarely met.

Ideally, in built-up areas, soil temperatures should be lower than in natural conditions, due to the removal of snow and cooling ventilated crawl spaces. So, in Yakutsk, wherein the natural conditions of the taiga or open spaces, soil temperatures are –3...–5 °C, in the built-up area they drop to –7 °C. The greatest drop in ground temperature under the building occurs in the first 2–3 years after the start of operation [*Ershov, 1989*]. Here, modern construction is carried out on pile foundations, crawl spaces are ventilated, and snow on the streets is removed or compacted, as a result of which the temperature of the soil under the building is generally lower than in the surrounding

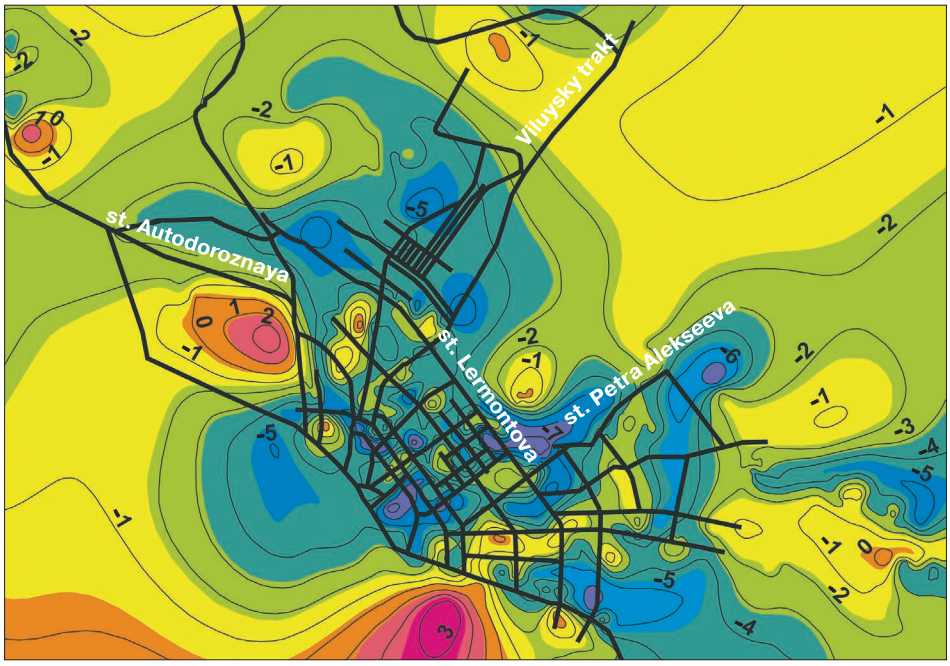

Fig. 1. Isotherms of permafrost soils in Yakutsk and its environs in 2015.

Provided by the Ministry of Construction of the Republic of Sakha (Yakutia), © P. Semenov.

areas (Fig. 1). However, at the same time, the intraquarter space is often poorly drained, and due to the disturbance of the flow and leaks, new paths for the movement of heating water are formed. This leads to an increase in the temperature of the bases and subsequent deformation of some buildings. In general, unfavorable areas are not typical for Yakutsk, while in other settlements such areas are common, and favorable trends in the change in the thermal state of frozen soils in settlements are not always observed.

As shown by the studies of I.N. Esau and colleagues [*2019*], for example, in Tiksi settlement the temperature of the soil averages about –7 °C, and outside the settlement is up to –12 °C, in Amderma, respectively, –3 °C within the build-up area, and –4.5 °C in undisturbed conditions outside the settlement. Within the city of Nefteyugansk, the ground surface temperature is higher than outside the city by about 3 °C. The main reasons are the irrational redistribution of surface runoff, leaks from water supply and sewerage networks, and the practice of untimely and insufficient snow removal.

Snow drifts are a problem, especially on the Arctic coast. Many settlements in the Arctic are located in areas with an average winter wind speed of more than 7 m/s. The built-up area is an obstacle to the wind flow, and therefore large masses of blown snow are deposited here. At the same time, snow, as a rule, has a strong warming effect, which also causes surface subsidence and deformations of buildings and structures.

An important task during construction remains the maximum possible preservation of the moss and vegetation cover in the immediate vicinity of the building and beyond, capable of cooling the soil by 1–2 °C and more.

Thermal abrasion causes significant damage to structures in small settlements that were built in dangerous proximity to the sea. When the sea coast retreats at a rate of more than 3 m/year, a zone near the coast with buildings, roads, piers, warehouses for fuels and lubricants, and other materials becomes hazardous and requires protection or relocation of facilities. The destruction caused by thermal abrasion occurred in Dikson, Tiksi, Varandey, Amderma, Kharasavey, Se-Yakha, and other settlements.

Usually, the direct cause of deformations of the foundations of buildings and structures is a violation of the temperature regime of soils during construction and operation, mainly due to the thermal effect of buildings and the ingress of wastewater into the base. There are other organizational and technical reasons for the deformations of buildings. The most frequent among them is insufficient resistance of materials to external factors (for example, to salt waters) and low frost resistance of concrete of building structures. This is manifested in the Arctic (Norilsk) and further south, in areas with a subarctic continental climate (Yakutsk). Apart from foundations, pipes and communication lines are affected. According to *S.S. Vyalov* [*1992*], most of the failures of foundations of buildings and structures (on average 45 %) are due to their improper operation: errors of surveyors and designers account for an average of 22 % and defects of builders – an average of 33 %.

Geotechnical systems (GTS) of the oil and gas complex dominate among the engineering facilities in the Arctic and the North as a whole. Here, most of the hazardous situations develop already in the first 2–3 years of operation of the GTS. Technogenic impact on permafrost is one of the main causes of emergencies, regardless of the stage of the object's life cycle. For example, at the operating gas production facilities of the Yamburg and Medvezhye fields, the permafrost table at the base of some structures decreased over time to 7.5–8.0 m, which exceeded the pile-laying depth and caused a loss of the bearing capacity of the foundations and the occurrence of emergency situations [*Remizov et al., 1997*]. Main pipelines with a product temperature different from the temperature of the enclosing ground are subject to deformation. Technogenic taliks are formed around pipelines with a positive temperature of the transported product, which is accompanied by surface subsidence, thermokarst, thermal erosion and pipeline floatation. A frozen halo appears around the "cold" pipelines, which loiters the ground runoff in the seasonally thawed layer and the underflow runoff in the valleys, initiating other processes. Many problems are associated with old production wells, which were built without proper insulation methods for the casing. The high positive temperature of the gas in the reservoir (up to +36 °C) for the Cenomanian gas of the Medvezhye and Urengoy gas fields has a warming effect on the entire permafrost strata, which is accompanied by the formation of thawing halos around the wellbores, the formation of near-well funnels, the development of thermokarst and collapse of the production strings themselves [*Bereznyakov et al., 1997*].

Thus, examples and causes of deformations of buildings and engineering structures in the Arctic are numerous; they are of natural, man-triggered, and mixed origins. When the need arises, the cost of repairing and restoring of buildings, as shown below, is 25–100 % of their initial cost, depending on the speed of action.

Permafrost monitoring as a basis for the development of technical solutions for adapting the Arctic infrastructure to climate change

State monitoring of the permafrost zone should be an inter-agency system of regular observations, collection, accumulation, processing, and analysis of information (a) to assess the state of permafrost in natural and man-triggered disturbed conditions,

(b) to make forecasts of its changes under the influence of natural factors, land and subsoil use, industry, construction, housing and communal services, (c) to develop methods for regulating the state of permafrost for the protection and rational use of cryogenic resources and sustainable development of the permafrost zone.

For observations, a specialized network is being created, including polygons, stations, and monitoring sites both in natural conditions and within infrastructure facilities [*Melnikov et al., 2018*]: (1) observation wells for a comprehensive study of the geological (geocryological, hydrogeological, etc.) section and for regular measurement of the ground temperature, which is one of the main indicators of the permafrost stability; (2) observation sites for regular measurement of the parameters of the active layer (annual cycle of the depth of freezing and thawing and changes in moisture/ice content); (3) observation platforms for recording the dynamics of exogenous (including cryogenic) processes, changes in hydrogeological, hydrological and landscape conditions.

In Western Siberia, the permafrost stationary (monitoring observations) sites have been laid since the early 1970s in connection with the exploration and the beginning of the development of the largest oil and gas fields. Long-term monitoring observations could be organized only at certain points (Igarka, Yakutsk, Nadym, Marre-Sale, the area of the Urengoy field, etc.). In general, permafrost monitoring remains largely local. Monitoring studies of the permafrost state in the Central Siberian and Yakutsk sectors of the Russian Arctic are not being carried out sufficiently. Regular control points include only five sites near the settlements of Igarka, Tiksi, Chersky, Zhigansk, and on Samoilovsky Island.

Enterprises and companies of land and subsoil users interested in the efficiency of their activities, as well as municipalities, conduct object geotechnical monitoring (GTM), including permafrost observations. However, not everyone realizes the necessity of GTM. In addition, the systemic disadvantage of department-based permafrost GTM is that the regime network covers exclusively the areas of direct impact of engineering facilities and does not contain sites for monitoring the background state of permafrost.

An integral part of monitoring is not only observations but also the analysis of all available data, primarily on the foundations of buildings and structures, as well as the development of technical solutions for the engineering protection of economic and social facilities based on methods of controlling the bearing capacity of foundations by means of regulation methods. Without the development of such solutions, observations are largely irrelevant. An inalienable requirement in all these activities is an environmental component.

Therefore, it is necessary to come to an understanding that both the background and geotechnical permafrost monitoring should be parts of a unified structure of state interdepartmental monitoring of the permafrost zone [*Drozdov, Dubrovin, 2016*]. Background monitoring is carried out in undisturbed natural conditions at special stations and sites of periodic visits, covering, if possible, all the variety of landscape and permafrost conditions of the permafrost zone. Geotechnical monitoring is carried out in the area of industrial and civil buildings. Background monitoring is important for understanding the general and regional trends in the development of the permafrost zone. Geotechnical monitoring solves specific problems of ensuring the stability and reliability of the operation of buildings and structures and provides a comprehensive information basis for the development of regulatory documents. In other words, geotechnical monitoring of natural and technical (geotechnical) complexes should be understood as a system for monitoring, forecasting, and managing their condition to ensure the operational reliability of economic objects at all stages of the life cycle in compliance with environmental safety.

The pioneer in the organization of the institutional GTM system in the oil and gas industry is PJSC Gazprom, where, earlier than others, it was realized the need to introduce into production activities an integrated system for managing the state of GTS built on frozen grounds (back in 2003, a comprehensive program was developed and implemented to ensure the reliability of the operation of engineering structures in the permafrost zone). The current standard "Foundations and foundations on permafrost soils" [*SP 25.13330.2012, 2012*] presupposes carrying out geotechnical monitoring but does not give specific recommendations for its organization.

As in other industries, the main common drawback of the existing GTM system at all facilities of the oil and gas industry is the absence of background sites in the GTM network to control the temperature regime of permafrost, the dynamics of the development of exogenous processes, hydrological and hydrogeological regimes of the territory, the state of ground covers and other important indicators of the permafrost geosystems state in undisturbed natural conditions. Thus, despite the organization of geotechnical monitoring at the facilities of the oil and gas complex, the absence of simultaneous background monitoring reduces the efficiency of both. A similar one-sidedness in observations is typical for municipalities that monitor permafrost in their settlements (Yakutsk, Salekhard). And, most importantly, there is no single center for the collection and analysis of geocryological information. And this leads to a situation in which the scientific community and society as

a whole, in fact, do not know what actually happens to the permafrost, especially in built-up areas, in cities and towns, and in the foundations of engineering structures.

A comparison of the organization of geocryological monitoring in Russia and other countries shows that the Nordic countries are developing background permafrost monitoring on the basis of scientific and geological organizations: in the USA and Canada – on the basis of geological services, in Switzerland and Norway – on the basis of universities under the state program, in China – on the basis of the Academy of Sciences together with manufacturing enterprises.

Ensuring reliable bearing capacity of foundations by means of regulation

When building on permafrost soils, the currently used methods can effectively ensure sustainability only for a certain time, since they take into account the peculiarities of the state of the environment before construction (including climatic and hydrological conditions). There are two ways to control the mechanical interaction of structures with frozen foundations: (1) constructive, in which the limits of the stress state, deformations, and creep of frozen soil, ground ice, and structure material are ensured; (2) thermal engineering, in which the temperature regime of the foundations and materials of structures is maintained within the limits ensuring their sufficient strength. These methods, as a rule, are applied simultaneously [*Dostovalov, Kudryavtsev, 1967; Tsytovich, 1973*]. There are also two main methods used for permafrost construction. The so-called *1st principle* assumes the preservation of permafrost soils in their natural state during the entire service life of a building or structure. This method is used in areas of discontinuous or continuous permafrost. *2nd principle* involves thawing permafrost prior to or during construction. This method is used mainly in areas of sporadic permafrost.

Most buildings built according to the 1st principle have a ventilated crawl space, which ensures the preservation of the temperature regime of the frozen ground. The height of the crawl space in Russia for buildings on permafrost according to [*SP 25.13330.2012, 2012*] should be chosen according to the conditions for ensuring its ventilation, but not less than 1.2 m from the crawl space surface to the bottom of the protruding floor structures. In such cases, as a rule, a pile foundation is used (Fig. 2) [*Ladanyi, 1984; Vyalov, Gorodetskiy, 1984*]. The piles are frozen into the permafrost and can withstand heavy loads if they are frozen before installation, primarily due to the lateral freezing surface, The difficulty of maintaining ventilated crawl spaces is that they can be covered with snow and wet in the absence of proper drainage.

Recently, the operation of facilities built according to the 1st principle has been complicated by climatic factors. Over the past 30–40 years of the ascending branch of climatic changes, the bearing capacity of frozen soils of the foundations, for example, in Western Siberia, has decreased due to warming by 5–30 %, and the belt of the maximum reduction in bearing capacity runs approximately along the Salekhard – Nadym – Novy Urengoy – Norilsk line. This is an area of oil and gas development at the end of the 20th century, and everything built here at that time is at risk, since the margin of safety on the ground is exhausted [*Streletskiy et al., 2019*].

Both natural and man-made changes in the temperature of frozen soils require compensation. Since

Fig. 2. The building of the dormitory on reinforced concrete piles in continuous permafrost zone, Kharasavey settlement, the Yamal Peninsula.

Photo by A.B. Osokin.

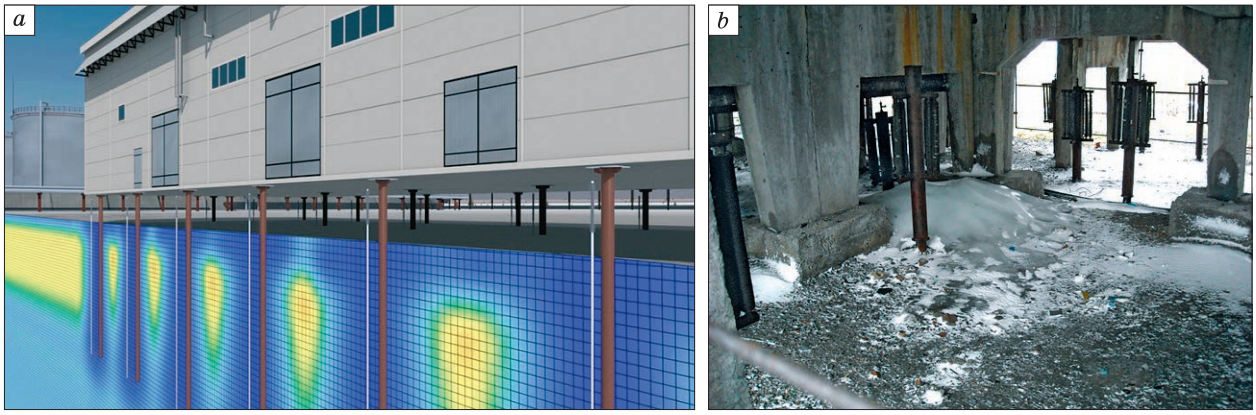

Fig. 3. Thermal stabilizers used to lower the temperature of the base of the building in permafrost zone:

a – along the perimeter of the building (*at the top* – the appearance of the building; *at the bottom* – a diagram of lowering the soil temperature by thermal stabilizers: yellow – positive temperatures, blue – negative); *b* – thermal stabilizers under the building.

the 1950s, in Alaska and in Russia [*Long, 1966; Gapeev, 1969*], the so-called thermosyphons or seasonally-cooling units have been introduced. The thermosyphon operates based on the natural circulation of a heat carrier in a metal pipe that cools down on the surface in winter. Initially, kerosene was used for this, and later carbon dioxide or ammonia. Nowadays, thermal piles are becoming more widespread – these are the piles with a built-in thermosyphon. In several years, the soil temperature around the pile decreases by several degrees, but at a short distance from it – up to about 1.5 m. When using thermal piles, the possibility of secondary heaving of frozen soils should be taken into account when they are additionally cooled. Several structures were damaged in this way, for example, a sports complex in the center of Yakutsk and a compressor station on the Yamal–Center gas pipeline. Nevertheless, the thermosyphon (thermal stabilizer) is today an important part of many construction projects in the cryolithozone (Fig. 3).

Ventilation ducts are one of the most well-known and widely used methods for cooling the foundation of embankments and other bankings [*Recommendations..., 1985*]. In the body of the embankment, culverts or air ducts with a diameter of 0.5–1.0 m are laid in order to let the cold winter air through themselves (in the summer the air ducts are muffled). In the PRC in Tibet, this method is used in addition to transport embankments for airfield facilities; in Canada in Inuvik – for cooling the foundations of oil reservoirs and related structures. To cool the base and slope of the embankments, rock placement [*Minaylov et al., 1985; Ashpiz, 1989*] and shading visors [*Kondratyev, 2013*] are also used. The latter significantly improved the cooling of the Tommot-Kerdem railroad embankment and the problem section of the Baikal-Amur Mainline at 1841 km.

Examples of maintaining the reliability of the bearing capacity of foundations by means of regulation

The use of thermal stabilizers is probably the most effective method among considered above, which is especially common in operational practice. Let's look at some examples.

In the city of Norilsk, Talnakh district, a residential building, which is deformed as a result of the increase in soil temperature, was stabilized with vertical thermostabilizers. In conditions of general warming and groundwater filtration, the temperature of the building base by the beginning of 2020 reached +1.4 °C. The operating system of temperature stabilization for the winter periods of 2020/21 lowered the temperature of the soil directly under the foundation to –7.2 °C (according to the data of "Fundamentstroyarkos").

In the city of Nadym in the 1990s–2000s, about a dozen buildings were subjected to deformations (5–7 % of the total number of permanent structures in the city), which was caused by uneven subsidence of foundations due to the thawing of icy soils at their base. Four residential multi-storey buildings, which received unacceptable damage, were dismantled. The load-bearing capacity of the frozen basement of two other residential buildings, which had decreased due to thermal effects, was restored by forced freezing with the use of vapor-liquid heat stabilizers. In two more buildings, the bearing capacity of the soils of the building foundations was restored by pumping cement mortar (according to the data of *A.B. Osokin*).

In the Amderma settlement, the building of the diesel boiler house of the Building and Construction Department built according to 2nd principle (on Proterozoic fractured shales on a strip foundation without a ventilated crawl space), experienced subsid-

ence. The use of about ten simpler thermosyphons filled with diesel fuel made it possible to partially freeze the base, ensure its stabilization and prevent further development of deformations.

Ensuring the reliability of the bearing capacity of the foundations of buildings and structures by means of redundancy

When designing the infrastructure of the Bovanenkovo gas field (PJSC "Gazprom"), optimization of the location of well pads was carried out on the basis of zoning of the territory according to geocryological conditions. For obvious reasons, reserving extra reliability of foundations taking into account climate warming causes additional investment in construction. But the positive operational effect made the requirement "on reserve reliability of foundations on permafrost soils adjusted for warming" became a standard in Gazprom when developing technical specifications for the design of new construction and reconstruction. Redundancy of the reliability of foundations is achieved not only due to the design of foundations (depth of immersion of piles, the method of immersion, and diameters of the piles used) but mainly due to the use of thermal stabilization systems. The calculated temperature regime of permafrost soils of foundations is justified when designing objects by means of modeling using specialized software products that implement non-stationary numerical methods of calculation, taking into account the predicted trend of air temperature. Unfortunately, the approaches used in the gas industry have not yet found their continuation in other industries.

Cost-effectiveness of protective measures

During the construction of wells at the PJSC "Gazprom" field, a complex thermal engineering solution was used, which ensures the preservation of the host deposits of the wells in a perennially frozen state. The experience of the first years of operation has shown that the implemented technical solutions justify themselves. In addition, the thermal stabilization of the wellhead zones made it possible to bring wells in the cluster closer from the traditional 40 m to 20–15 m, which significantly (up to 30 %) reduced the cost of arranging the cluster pads [*Melnikov et al., 2019*].

Another example is the use of thermal stabilizers when laying power lines. This makes it possible to shorten the length of the piles for the foundation of the supports. For example, during the development of the Lodochnoye field (Krasnoyarsk Territory, 130 km west of Igarka), about 20 million rubles were saved, or 26 % due to the cost of the foundations of the supports.

However, despite the obvious efficiency, the failure rates of thermostabilizers in the permafrost zone are still high (for the thermosyphons it is up to 20–30 %) [*Strizhkov, 2015*]. They fail due to corrosion, damage during operation, and factory defects. To increase the reliability of the operation of seasonally operating cooling devices, it is advisable to conduct a technological audit of the manufacturers and to increase the competition between them.

Heat pumps are one of the alternatives to thermal stabilizers and freezing units [*Koloskov, Gamzaev, 2015*]. In a heat pump, the condenser is a heat exchanger that generates heat for consumer needs (for example, for heating buildings), and the evaporator is a heat exchanger that removes heat from the soil mass. It was proposed to use heat pumps during construction in the permafrost zone abroad [*Stenbeak-Nielson, Sweet, 1975*] and in Russia [*Perlstein et al., 2000*]. The technical and economic efficiency of using heat pumps is determined by the density of heat fluxes entering the evaporator during the cooling of the soil [*Kibl, 1983*]. Heat pumps are the basis of a technical solution for low-rise buildings under the program of resettlement of residents from nearby villages to Vorkuta. It is planned to build 40 such houses with a heating system and thermal stabilization of the base, which will optimize the construction in terms of timing and reliability [*Koloskov, Gamzaev, 2015*]. A specific calculation of the economic efficiency of using heat pumps in the permafrost zone was carried out by G.Z. Perlstein in 2012 for the conditions of Yakutsk [*Report..., 2012*] and showed that, as a result, the annual savings per building can be approximately 41 thousand rubles. However, heat pumps have not yet become widespread.

The cost of adapting the housing stock to changing permafrost conditions on the example of the city of Norilsk

Approbation of the proposed approach to assessing the cost of ensuring the sustainability of buildings at a large object in the permafrost zone was carried out using the example of the urban district of Norilsk. According to forecasts [*Melnikov et al., 2021*], the maximum damage under a moderate warming scenario and established management practices will reach about 600 billion rubles in Norilsk by the beginning of the second half of the 21st century. At the same time, according to the authors' estimates, the total cost of buildings and structures in 2020 prices on the territory of the urban district is about 631 billion rubles, of which: 117 billion rubles – the cost of the housing stock, 514 billion rubles – the cost of buildings and construction of the industrial sector, that is, such key sectors as industry, agriculture and forestry, construction, transport, sectors of market and non-market services. For a clear understanding of the scale of the likely damage, it should be noted that the budget of Norilsk for 2020 amounted to only 20.6 billion rubles (only 61 % of them are own income).

The cost of thermal stabilization consists of the costs of manufacturing, transportation, construction, and installation of thermal stabilizers. The selection of their number and geometrical arrangement is carried out according to the results of thermal engineering modeling. According to average estimates, in the zone of continuous permafrost, on average, one thermal stabilizer is needed to maintain two piles of a residential building [*Gamzaev, Kronik, 2016*]. The number of piles per unit area of a building is determined by its design features. For example, for a two-storey residential rotational complex for 850 people at the Vankor field in the Krasnoyarsk Krai (according to "Fundamentstroyarkos" [*Volkova, 2021*], etc.), 12 thermal stabilizers are needed per 100 m^2 of the object area. On average, according to "Fundamentstroyarkos", one average thermal stabilizer provides a freezing area of about 4 m^2 [*Anikin et al., 2013*], and, thus, about half of the area of its base is frozen at this object.

The unit cost of stabilizing 1 m^2 of frozen soil in the building plan ranges from 10,000 to 80,000 rubles/m^2. Such a range of prices is associated with technical solutions and prices depending on the category of soil and drilling depth. The work [*Svetlyshev, 2018*] gives an example of a 9-storey 4-entrance residential building made of prefabricated reinforced concrete structures with a reinforced concrete monolithic strip foundation in Nadym (building dimensions 101.0 by 14.4 m). According to the author's data, the costs of setting up a soil thermal stabilization system, i.e. further application of the first principle of construction, amounted to 47 million rubles. Of these: temperature stabilization of the soil – 19 million rubles, emergency restoration work on the repair of the foundation and supporting structures – 28 million rubles at the cost of construction of a similar building in comparable prices – 127 million rubles.

Based on the structure of the Norilsk housing stock (Table 1), the authors calculated the average area of the foundations of residential buildings of various series. The approximate cost of thermal stabilization systems was calculated at the rate of 10 thousand and 80 thousand rubles per 1 m^2 of the base. This did not take into account the costs of transportation and installation of systems. The calculation results are presented in Table 1. Panel 9-storey dormitories series 1-464.D-82 were excluded from the calculation. Unlike the others, they are primarily subject to gradual demolition and will not be either reconstructed or major repaired.

Thus, as a first approximation, it was possible to estimate that the costs of thermal stabilization of the Norilsk housing stock will be from 10 to 81 billion rubles, while the cost of the existing housing stock is estimated by us at 117 billion rubles. According to our estimates, the damage to the housing stock in Norilsk may amount to about 60 billion rubles by 2050 [*Melnikov et al., 2021*]. Close proportions of the costs of preventing negative consequences and the magnitude of the probable damage, apparently, are typical for the rest of the urbanized territories of the permafrost zone of the Russian Arctic, depending on how early measures are taken to thermostabilize the soils of the foundations. It should be emphasized that the maintenance of the thermal regime of the bases must be carried out not only with the help of thermal stabilizers (the reliability of which must be increased in the future) but also with other, proven methods (ventilated crawl space) and new methods, including the use of heat pumps.

Table 1. **The cost of thermal stabilization of the housing stock in Norilsk**

Building type	Number of buildings	The total area of the foundations of the houses, m^2	Number of floors	Estimated cost of thermal stabilization*, million rubles
Houses designed in the 1960–1970s	305	334 601	5	3346/26 768
K-69	62	95 828	9	958/7666
Series-84	255	257 675	9	2577/20 614
Series 111–112	140	153 592	9	1536/12 287
NK-12	15	21 553	12	216/1724
Houses designed in the 1930–1950s	44	91 379	5	914/7310
Hotel-type houses**	12	14 584	9	146/1167
Brick apartment buildings in Snezhnogorsk settlement	6	7389	5	74/591
Total dormitories, including:	26	30 809	–	308/2465
general type (5-floor)	8	8955	5	90/716
apartment type (9-floor)	18	21 854	9	218/1749
Total:	865	1 007 410	77	10 075/80 592

* *Left*: based on the coast of 10,000 rubles per 1 m^2 of frozen soil; *right*: based on the coast of 80,000 rubles per 1 m^2 of frozen soil.

** Gostinka (hotel-type house) – a type of dwelling, which is a small one-room apartment or a room with a kitchen niche and a bathroom.

CONCLUSIONS

Current trends in the state of permafrost are largely determined by global climatic changes. According to the ideas existing today, climate warming inevitably contributes to the emergence of trends toward quantitative and qualitative changes in the state of the Arctic cryolithozone.

Changes in the thermal state of permafrost under the influence of climatic variations occur over many years but have not reached their maximum. This circumstance significantly increased the risks in construction, land and subsoil use, and increased epidemiological and environmental threats in the Russian Arctic, and in the permafrost zone as a whole. Everywhere in the Arctic zone, there is a loss of the bearing capacity of the soils of the foundations of buildings and structures. The overwhelming majority of data on the state of the permafrost, as well as on its interaction with infrastructure facilities, need to be updated and renewed.

Over the past 35–40 years, the temperature in the upper part of the permafrost under natural conditions has increased by 0.5–2.0 °C, and on the plains of Western Siberia built up with gas industry facilities – by 2.0 to 4.0 °C. The bearing capacity of frozen soils of the foundations of structures at the same time, only due to natural changes, decreased by 5–30 %, depending on local geocryological conditions.

Technogenesis is seriously complementing the impact of background climate change. As a result of the combined influence of climate warming and large-scale anthropogenic impacts on the permafrost, a cumulative effect arises, the consequences of which already lead to the loss of stability of the frozen ground, major accidents, environmental disasters and, in general, to an increase in the risk of natural resource use in the developed areas of permafrost zone.

For an economically justified response to ongoing changes, a system of state monitoring of permafrost should be created, including background permafrost observations and object-based geotechnical monitoring with a unified system of data accumulation and forecasting. This will help to significantly reduce the managing risks in the permafrost zone, to solve planning issues, and to evaluate the effectiveness of design solutions and protective measures. In this case, the cost of protective measures, in particular, thermal stabilization, turns out to be an order of magnitude lower than the possible damage in case of its absence, and, thus, the effectiveness of protective measures is quite high.

An approach to the design of permanent construction projects in the permafrost zone seems to be justified and subject to dissemination, assuming redundancy of the reliability of foundations through the use of thermal stabilization and other methods that compensate for the predicted decrease in the bearing capacity of permafrost soils caused by climatic and technogenic factors. With a relatively small amount of additional investments (the first percent of the cost of construction), reliability redundancy will ensure the stability and mechanical safety of facilities.

Acknowledgements. *The article was prepared within the framework of the state assignment and the research plan of the IEG RAS on the research topic AAAA-A19-119021190077-6; state assignment of the Earth's Cryosphere Institute of Tumen Scientific Centre SB RAS No. 121042000078-9; agreement between FASI "Eastern State Planning Center" and FSBI "Gidrospetsgeologiya" No. K-26092/1-1-2020; directions of exploratory and fundamental research SB RAS 1.5.12. "Cryosphere of the Earth and its space-time evolution", with the support of the YaNAO administration.*

References

Anikin, G.V., Plotnikov, S.N., Spasennikova, K.A., 2013. Calculation of soil freezing dynamics under the influence of a single thermosyphon. Kriosfera Zemli [Earth's Cryosphere], XVII (1), 51–55.

Ashpiz, E.S., 1989. Assessment of reliability of operation of embankments constructed according to the II principle of use of permafrost soils as a base. In: Interuniversity Collection of Scientific Works. MIIT, Moscow, vol. 823, pp. 27–30 (in Russian).

Bereznyakov, A.I., Griva, G.I., Popov, A.P. et al., 1997. Problems of stability of producing wells of Yamal Peninsula oil fields. IRC Gazprom, Moscow, 159 pp. (in Russian).

Brushkov, A.V., Drozdov, D.S., Dubrovin, V.A. et al., 2021. Geocryological monitoring: what is it for and how it is carried out. Part II. Science: Ecology. May 19, 2021 (in Russian). – URL: https://goarctic.ru/regions/geokriologicheskiy-monitoring-dlya-chego-on-nuzhen-i-kak-provoditsya-chast-ii/

Bryukhovetskiy, O.S., Drozdov, D.S., Laukhin, S.A., Yashin, V.P., 2014. On the share of subsoil use in accumulated environmental damage of the Arctic zone of the Russian Federation. Izvestiya vuzov: Geologiya i razvedka [News of universities: Geology and exploration], No. 6, 59–63.

Gamzaev, R.G., Kronik, Ya.A., 2016. Soil thermal stabilization systems during construction in cryolithozone. In: Proc. of the Fifth Conference of Geocryologists of Russia (Moscow, 14–17 June 2016). Universitetskaya kniga, Moscow, pp. 245–252 (in Russian).

Gapeev, S.I., 1969. Strengthening of frozen foundations. Stroyizdat, Leningrad, 104 pp. (in Russian).

Dostovalov, B.N., Kudryavtsev, V.A., 1967. General cryology. MGU, Moscow, 404 pp. (in Russian).

Drozdov, D.S., Dubrovin, V.A., 2016. Environmental problems of oil and gas exploration and development in the Russian Arctic. Earth's Cryosphere XX (4), 14–25.

Ershov, E.D. (Ed.), 1989. Geokriologiya SSSR. Geocryology of the USSR. Eastern Siberia and the Far East. Nedra, Moscow, 515 pp. (in Russian).

Esau, I., Miles, V., Varentsov, M. et al., 2019. Spatial structure and temporal variability of a surface urban heat island in cold

continental climate. Theoretical and applied climatology, 137, iss. 3–4, 2513–2528.

Infrastructure, Engineering and Climate Change Adaptation – ensuring services in an uncertain future., 2011. (Anon). The Royal Academy of Engineering, London, 107 pp.

Kibl, D., 1983. Application and economics of heat pumps. In: Environmental Energy and Construction Engineering. Stroyizdat, Moscow, pp. 56–65 (in Russian).

Koloskov, G.V., Gamzaev, R.G., 2015. To the issue of selection of optimal systems of thermal stabilization of soils during construction in cryolithozone. Geotechnika [Geotechnics], No. 6, 4–11.

Kondratyev, V.G., 2013. Cooling of the mass of permafrost soils at the base of roads by regulating cold and heat flows. Gruntovedenie [Pedology], No. 1, 34–47.

Ladanyi (in Russian)B., 1984. Design and construction of deep foundations in permafrost: North American practice. In: Permafrost, 4th Intern. Conference, Fairbanks, Alaska. National Academy Press, Washington, DC, pp. 43–50.

Larsen, J.N., Anisimov, O.A., Constable, A. et al., 2014. Polar regions. In: Climate Change 2014: Impacts, Adaptation, and Vulnerability. Part B: Regional Aspects. Contribution of Working Group II to the Fifth Assessment Report of the Intergovernmental Panel on Climate Change. Cambridge University Press, Cambridge, pp. 1567–1612.

Long, E.L., 1966. The long thermopile. In: Permafrost Intern. Conference (Lafayette, Indiana, November 11–15, 1966). National Academy of Sciences – National Research Council, Washington DC, pp. 487–491.

Melnikov, I.V., Nersesov, S.V., Osokin, A.B. et al., 2019. Geotechnical solutions for the construction of gas wells in especially difficult geocryological conditions of the Yamal Peninsula. Gazovaja promyshlennost' [Gas Industry], 12 (794), 64–72.

Melnikov, V.P., Osipov, V.I., Brushkov, A.V. et al., 2021. Assessment of damage to residential and industrial buildings and structures during temperature changes and thawing of permafrost soils in the Arctic Zone of the Russian Federation by the middle of the 21st century. Geoekologiya. Inzhenernaya Geologiya. Gidrogeologiya. Geokriologiya [Geoecology. Engineering Geology. Hydrogeology. Geocryology], No. 1, 14–31.

Melnikov, V.P., Trofimov, V.T., Osipov, V.I. et al., 2018. The doctrine of study and protection of "permafrost" – a necessary element of the development strategy of the Russian Arctic. In: Proc. of the Conference "Modern Problems of Geocryology" (Moscow, 15–16 May, 2018). Universitetskaya kniga, Moscow, vol. 1. pp. 5–19 (in Russian).

Minaylov, G.P., Merenkov, N.D., Peretrukhin, N.A. et al., 1985. Recommendations to eliminate deformations and increase the stability of the roadbed in difficult permafrost and soil conditions. CNIIS, Moscow, 50 pp. (in Russian).

Osokin, A.B., 2016. Long-term changes in the average annual MMP temperature in the North of Western Siberia due to climate warming. In: Proc. of the Fifth Conference of Geocryologists of Russia (Moscow, 14–17 June. 2016). Universitetskaya kniga, Moscow, 69–77 (in Russian).

Perlshtein, G.Z., Gulyi, S.A., Buyskikh, A.A., 2000. Increasing the load capacity of frozen soils using heat pumps. Osnovaniya i fundamenty [Supports and Foundations], No. 3, 26–31.

Recommendations for the design of spatial ventilated foundations in permafrost soils, 1985. NIIOSP, Moscow, 38 pp. (in Russian).

Remizov, V.V., Chugunov, L.S., Popov, A.P. et al., 1997. Dynamics of the temperature regime of the soils of the foundations of gas treatment facilities in the north of the Tyumen region. In: Preparation and processing of gas and gas condensate. Overview information. IRC Gazprom, Moscow, 70 pp. (in Russian).

Report on research work on the topic: Carry out mathematical modeling of the temperature field and the stress-strain state of alluvial soils at the base of underground parking lots equipped with heat pumps. Predict the impact of construction on the surrounding structures for the facility "development of quarter No. 203 of Yakutsk", 2012. IGE RAN, Yakutsk, 91 pp. (in Russian).

Shiklomanov, N., Streletskiy, D., Suter, L., 2019. Assessment of the cost of climate change impacts on critical infrastructure in the circumpolar Arctic. Polar Geography, No. 42, 267–286. – https://doi.org/10.1080/1088937X.2019.1686082

SP 25.13330.2012, 2012. Foundations and foundations on permafrost soils, Moscow. – URL: https://docs.cntd.ru/document/1200095519 (last visited: 28.08.2021).

Stenbeak-Nielson, H.C., Sweet, L.R., 1975. Heating with ground heat: an energy saving method for home heating. The Northern, 7 (1), 20–25.

Streletskiy, D.A., Shiklomanov, N.I., Nelson, F.E., 2012. Permafrost, infrastructure and climate change: a GIS based landscape approach to geotechnical modeling. Arctic, Antarctic, and Alpine Research, No. 44, 368–380. – http://doi.org/10.1657/1938-4246-44.3.368

Streletskiy, D.A., Suter, L., Shiklomanov, N.I. et al., 2019. Assessment of climate change impacts on buildings, structures and infrastructure in the Russian regions on permafrost. Environment Research Letters, No. 14, 025003. – http://doi.org/10.1088/1748-9326/aaf5e6

Strizhkov, S.N., 2015. Improving the reliability of geotechnical systems using seasonal cooling devices. Geotekhnika [Geotechnics], No. 6, 34–41.

Svetlyshev, D.A., 2018. Deformations of buildings and structures in the cryogenic zone of Western Siberia. YurGu, Chelyabinsk, AS-279, 69 pp. (in Russian).

Tsytovich, N.A., 1973. Mechanics of frozen soils. Vysshaya Shkola, Moscow, 448 pp. (in Russian).

Volkova, E.V., 2021. Results of a comparison of geocryological monitoring of temperature stabilization systems for soils of foundations of different manufacturers. NPO Fundamentstroyarkos LLC, Tyumen. – URL: https://www.npo-fsa.ru/rezultaty-sravneniya-geokriologicheskogo-monitoringa-sistem-temperaturnoy-stabilizacii-gruntov-0

Vyalov, S.S., 1992. Problems of foundation construction on permafrost soils. In: Foundations and foundations on permafrost soils. Stroyizdat, Moscow, pp. 5–13 (in Russian).

Vyalov, S.S., Gorodetskiy, S.E., 1984. Thermal seedlings in construction in the North. Stroyizdat, Leningrad, 146 pp. (in Russian).

Zimmerman, K.O. (Ed.), 2011. Resilient Cities: Cities and Adaptation to Climate Change. Proceedings of the Global Forum 2010. New York, Springer, 463 pp.

Received July 29, 2021
Revised August 2, 2021
Accepted August 26, 2021

Translated by A.V. Muravyov

EARTH'S CRYOSPHERE
SCIENTIFIC JOURNAL

Earth's Cryosphere, 2021, vol. XXV, No. 6, pp. 13–22 http://earthcryosphere.ru/

ECOLOGICAL PROBLEMS IN PERMAFROST ZONE

SPATIAL DISTRIBUTION OF GEOCHEMICAL CHARACTERISTICS OF SNOW COVER WITHIN AND OUTSIDE TOMSK-SEVERSK INDUSTRIAL AGGLOMERATION

A.V. Zakharchenko[1], A.A. Tigeev[1], O.A. Pasko[2], L.G. Kolesnichenko[3], D.V. Moskovchenko[1,4]

[1] *Institute of the Problems of Northern Development, Tyumen Scientific Centre SB RAS, Malygina str. 86, Tyumen, 625026, Russia; avzakh@gmail.com, ttrruubbaa@mail.ru*
[2] *Agrophysical Research Institute, Grazhdansky ave. 14, St. Petersburg, 195220, Russia; pasko@agrophys.ru*
[3] *Tomsk State University, Lenina str. 36, Tomsk, 634050, Russia; klg77777@mail.ru*
[4] *Tyumen State University, Semakova str. 10, Tyumen, 625003, Russia; moskovchenko1965@gmail.com*

The ability of snowpack to accumulate airborne substances allows analyzing spatiotemporal geochemical patterns and detecting polluted areas. Spatial features of geochemical regional distribution of dust deposited in the snow cover in areas remote from industrial centers are determined. The snowpack of Tomsk, Shegarka and Kozhevnikovo districts in the Tomsk Oblast was chosen to be the object of this research. The observations were carried out in the period from 1995 to 2000. The measurements of snow meltwater filtrate included: pH, concentrations of nitrate and ammonia nitrogen, phosphorus, potassium, calcium, magnesium, sodium, chlorine, while the solid residue was analyzed for heavy metal contents (Cu, Zn, Cd, Pb, Co, Mn, Cr, Ni) using atomic absorption spectrophotometry method. The average thickness of snowpack is evenly distributed within the study area and varies from year to year. Contents of dust, ammonia (NH_4^+), phosphorus (P_2O_5), Mg in snow on the forest floor significantly differ (an upward bias) from arable land areas. Ions NO_3^-, NH_4^+, alkaline and alkaline-earth elements show an increasing trend (relative to the background values) near the industrial zone. The levels of siderophilic and lithophilic elements, copper and zinc tend to be enhanced in proximity to the industrial zone of the Tomsk city agglomeration. Lead shows a mosaic distribution throughout the study area. In individual localities (Batkat village, Komarovo swamps), dust and heavy metals contents in snowpack were found to be higher relative to the background values.

Keywords: *solid aerosols, snow, heavy metals, dust, trace elements.*

INTRODUCTION

The seasonal phenomenon of the cryosphere of Western Siberia functions as a system-forming factor in many natural landscapes, which is controlled inter alia by horizontal fluxes of natural and anthropogenic substances [*Bordon, 1996*]. Although the formation of the chemical composition of snowpack in the West Siberian Plain is known to be affected by zonal peculiarities, the macro- and microelement transport (elementary fluxes) into rivers and lakes during the spring flood remains largely underestimated [*Ermolov et al., 2014; Shevchenko et al., 2017*]. The Northern Hemisphere climate warming trends [*AMAP, 2011*] in the Arctic geosystems dynamics marked by a reduction in snow and ice cover and longer ice-free periods of water bodies, have significantly changed major and trace element (TE) fluxes.

Three main approaches which are currently used for monitoring the geochemical properties of an object [*RD 52.04.186-89, 1991*] include: 1) impact estimation (e.g. gas flares), 2) TE pathway analysis, and 3) probabilistic-statistical methods. The impact estimation method is used to investigate objects expressly affecting the snow chemistry [*Chernyaeva et al., 1978; Ermilov et al., 2002; Filimonenko et al., 2013; Yanchenko et al., 2013; Onuchin et al., 2014; Talovskaya et al., 2014a,b; Krest'yannikova et al., 2015*]. The TE pathway method deals with external controls, e.g., natural local climate zones [*Ermolov et al., 2014; Shevchenko et al., 2017*]. The probabilistic-statistical approach is the most appropriate in the absence of visible boundaries of the impact zones and a priori geographic patterns and is therefore interpreted as unbiased in the study of natural ecosystems. In this case, the study area is divided into conditional squares, with one of them selected randomly for observation.

The relevance of this study is less concerned with the identification of ecologically unfavorable areas, with the emphasis placed instead on highly topical recognition of their redistribution patterns at a considerable distance from diverse sources of pollution [*Akba et al., 2013; Xue et al., 2020*] by analyzing the snowpack chemistry, as well as geographical distribution and formation of atmospheric precipitations

laden with toxic substances and posing threats to human health.

This work aims to identify the spatial features of the region-scale geochemical distribution of dust aerosol particles deposited in the snowpack in areas located at varying distances from the industrial zone.

The snowpack geochemical monitoring commenced in the Tomsk Oblast in the 1980s included the elemental and chemical composition of snow [*Boyarkina et al., 1993*]. In the 1990s, many Russian regions were exposed to atmospheric air pollution by nitrogen and sulfur oxides (SO_x and NO_x) and heavy metals [*Walker et al., 2003*]. Also worth noting is that, previously, snowpack research was undertaken by scientists from the National Research Tomsk Polytechnic University (TPU), under the guidance of E.G. Yazikov [*Filimonenko et al., 2013; Talovskaya et al., 2014a,b, 2018a*]. This work draws heavily on the data obtained from the snowpack monitoring in the 1990s at the Soil Science Laboratory (headed by L.A. Izerskaya) of the Research Institute of Biology and Biophysics at Tomsk State University.

RESEARCH OBJECTS AND METHODS

The object of the study is the snowpack of background sites in the Tomsk Oblast (Fig. 1). The observation (sampling) points were scattered around the Tomsk-Seversk industrial agglomeration.

The background conditions for substances transport to snowpack, as this is defined by [*RD 52.04.186-*

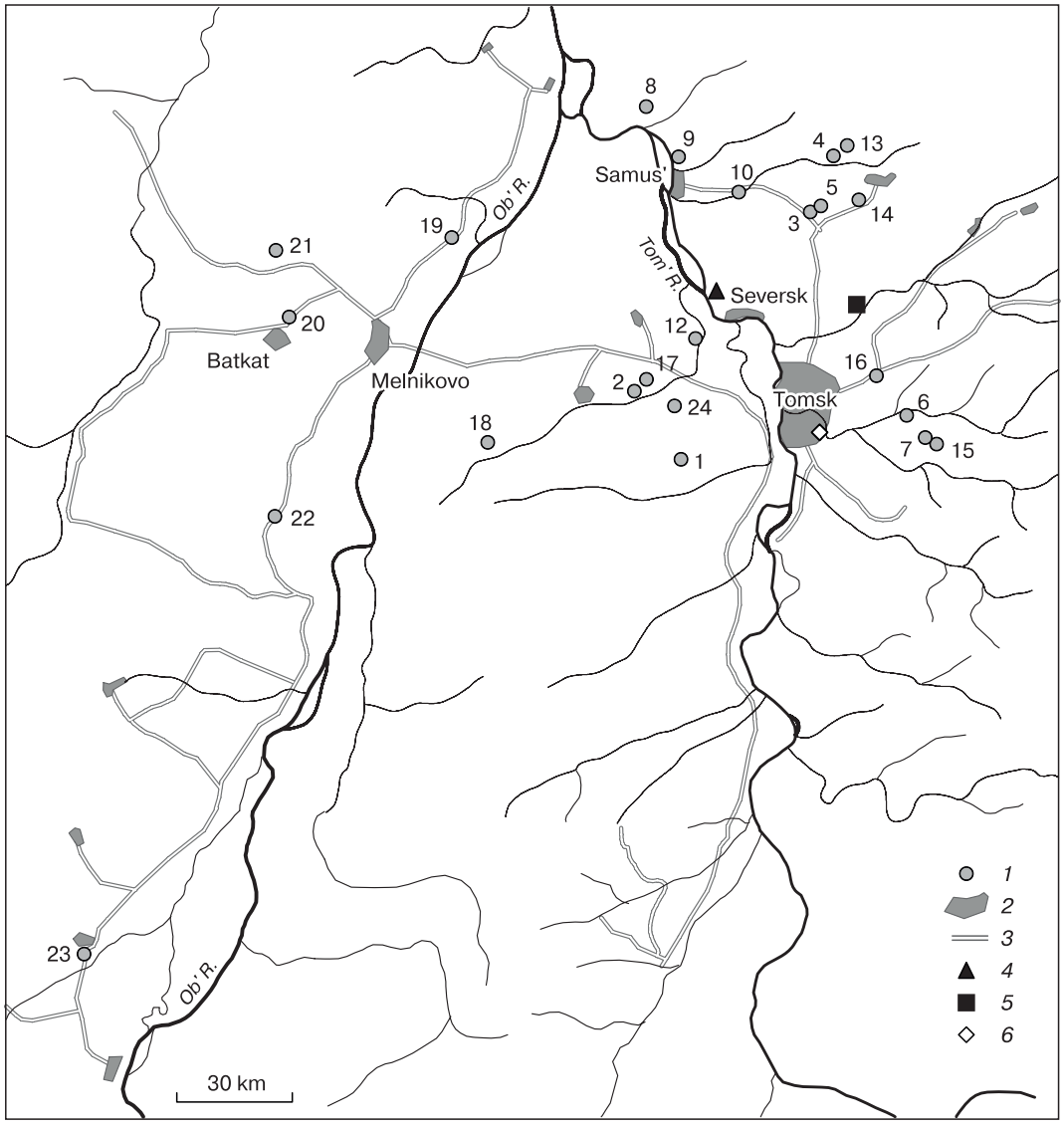

Fig. 1. Sampling points location with indications of the site number and position of air pollution sources.

1 – sampling points (SPs); *2* – settlements; *3* – roads; *4* – Siberian Chemical Combine (SCC); *5* – Tomsk Petrochemical Plant (Tomskneftekhim); *6* – Hydropower plant HPP-2.

89, 1991], were investigated to reveal interregional and transboundary transmission of solid aerosols in the winter season. Their input from Kazakhstan and subsequent transfer from the Novosibirsk Region and Altai Territory were anticipated.

While setting up the regional background monitoring network in the Tomsk Oblast, locations of sampling sites within the area were determined based on the probabilistic-statistical approach. The works commenced in 1994. Snow samples were systematically taken within a five-year period (1995–2000). The chemical composition of snow was analyzed at the monitoring sites located at different distances from pollution sources. The monitoring site selection met the following criteria: area 0.5 ha [*GOST 17.4.3.01-83, 2004*]; car accessibility.

Differentiation between the amounts of dust particles deposited in snowpack in agricultural land areas and in forests is of particular interest. To estimate the dust capture and retention capacity of tree species, the snow sampling points were in most cases paired: in the forest and in a nearby agricultural field [*Glazovskii, 2006*]. Snow samples were taken in March within one week. In Tomsk Oblast, the period with snow cover lasts 175–180 days, and the duration of snow cover averages T = 178 days [*Filimonenko et al., 2013*]. The number of prepared monitoring sites was initially 11 (0.5 ha) which increased to 18 in the first year, and to 23 in the next year; the duration of observations at the sites was 3–6 years in the period from 1995 to 2000.

Snow meltwater was sampled for the chemical analysis which was performed in compliance with generally accepted procedures [*Vasilenko et al., 1985; RD 52.04.186-89, 1991*]. Snow samples were taken by using a snow gauge (a widely used instrument for meteorological observations) through the full depth of the snowpack. In order to exclude contamination of samples by soil particles and litter admixtures, the lower 5 cm of snow was removed. After that, snow density was determined. Dust content was estimated from the cumulative sample composed of 3–5 samples depending on the snow depth.

The snowpack samples were melted in the laboratory at room temperature, and water volume was measured. The meltwater was filtered using a vacuum pump: the partitioning was achieved by passing the melted samples through the "blue ribbon" filter. The filters were dried in a desiccator at 105 °C. The filtrate analysis included determinations of: pH [*PND F 14.1-2-3-4.121-97, 1997*], concentrations of nitrates and NH_4^+ [*PND F 14.1-2.1-95, 1995*], contents of phosphates [*GOST 26204-91, 1992*] expressed as P_2O_5, potassium [*RD 52.24.391-95, 1995*] expressed as K_2O, calcium (Ca^{2+}) and magnesium (Mg^{2+}) [*GOST 26487-85, 1985*], sodium [*RD 52.24.391-95, 1995*], chlorides [*GOST 4245-72, 2010*]. The solids (dust) trapped on filters were dried at 105–110 °C and decomposed by hydrofluoric acid digestion. Total concentrations of nickel, cobalt, lead, copper, zinc, manganese, chromium, and cadmium in the resulting solution were determined by atomic absorption spectrophotometry (factorial design with eight runs). The atomic absorption analysis of trace elements yielded relative accuracy (%): 3.8 for Zn, 3.5 for Cu, 1.2 for Mn, 3.7 for Co, 4.2 for Pb, 14.3 for Cd.

The values of element concentrations in filtrates were converted to their concentration per liter of meltwater (μg/L), trace elements (TEs) inventory per unit area of snow (μg/m^2), and trace element flux (μg/(m^2·day)). Concentration coefficients were calculated as the ratio between TE content (Kc) and the background value (Kb):

$$K = \frac{\mathrm{Kc}}{\mathrm{Kb}}$$

and the total pollution index as

$$\mathrm{Zc} = \sum K - (n-1),$$

where K is concentration coefficient; n is amount of elements with $K > 1$.

Dust content was calculated using the formula

$$C = \frac{P_c}{V_w},$$

where C is dust mass concentration, g/L; P_c is dust weight in meltwater, g; V_w is the volume of water, L. The total dust input (P) was calculated as the mass of dust per unit area per unit of time. The area value was derived from the sampler diameter multiplied by the number of samples taken at one point. Sampling points (except points 20 and 21) which are located significantly away (30 km or more) from the Tomsk-Seversk agglomeration were referred to as the background values.

The dust flux emitted onto the snowpack surface was determined by the formula

$$P = \frac{P_c}{ST},$$

where P is TE flux per surface unit per time unit; P_c is the mass of trapped dust; S is the total sampling area; T is the time interval between the moment of sampling and the date of the onset of stable snow cover, days.

Geographic coordinates of the observation points were defined with GPS, and spatial distribution of trace element concentrations was analyzed using QGIS. This allowed mapping of the cluster analysis results. The distances from each observation point to the Siberian Chemical Combine (SCC) and Hydro Power Plant (HPP)-2 (i.e. potential impact factors) were measured.

The Orange software suit and appropriate Python packages were used for statistical analysis of the data. Clustering analysis with multiple variables using the algorithm K-means enabled the identification of the groups of representative points for contamina-

tion levels and pollutants inventory within the snowpack. Similar analytical procedures were used previously [*Shevchenko et al., 2017*]. The Statistica for Windows software package allowed us to assess the factors controlling pollutants intake into the snowpack.

RESULTS AND DISCUSSION

Snowpack characteristics inferred from measurement results at 24 monitoring sites are: snow depth averaging (56.4 ± 2.7) cm (Table 1); uniform distribution of snowpack within the studied area (coefficient of variation is 25.9 %). The variability of some indicators is interpreted as moderate (snow depth, pH) or high (>100) for others (contents of dust, P_2O_5, Mg^{2+}, NO_3^-).

The average snow depth values are greater for the forest versus agricultural land areas, which is corroborated by the Mann-Whitney test (at a significance level of $p < 0.05$). The dust load is shown to be on average (8.5 ± 3.6) mg/(m^2·day), approximating the background values for the Tomsk Oblast (7 mg/(m^2·day)) [*Talovskaya et al., 2014a,b*].

The average snow density is generally (0.19 ± 0.01) g/cm^3, although it tends to be higher within the agricultural land area than in the forest. This differentiation proved to have low credibility, though. The amounts of solid insoluble particles in snow meltwater average (6.8 ± 1.2) mg/L. Elevated dust concentrations were reported both at sampling points near the urban agglomeration (points 5, 6, 10, 12, 16) and away from dust emission sources (points 4, 21, 22, see Fig. 1). Average amounts of dust particles in the surface layer of snowpack are known to be about 2.74–2.91 mg/L within the background sites located in the Arctic [*Shevchenko et al., 2002, 2007*]. Our results have shown that in the territory of Tomsk Oblast, total solid impurities in snow mass are 2.5 times higher as compared to levels reported for remote Arctic regions.

Both spatial and temporal variability of this parameter is shown to be significant. The year 1997 stands out in terms of maximal snow cover depth (78.2 ± 4.7 cm) and minimal total dust content in snow (0.40 ± 0.13 mg/L) (Fig. 2).

The snowpack thickening translated to lower dust concentrations as a result of dilution by a larger snow volume. The next year, 1998, saw a remarkably enhanced flux of dust aerosol particles settled on snowpack. A comparison of the two samples – from the forest and agricultural field – of snow meltwater using the Mann-Whitney test ($p < 0.05$) showed a greater amount of dust particles in the snowpack sampled in the forest. The snow meltwater yielded a pH value varying from 5.6 to 6.6 (on average, 6.04 ± 0.13), which suggests weak alkalinity, as compared to the data obtained by other authors: pH of 5.89 for snow within the 30-km zone around the SCC [*Artamonova, 2011*], pH of 5.4 for snow in the Khanty-Mansi Autonomous Okrug (KhMAO) [*Moskovchenko, Babushkin, 2012*].

Emissions of NO_3^- into the atmosphere account for air pollution as a result of liquid fuel combustion, with sulfur and nitrogen compounds unevenly spreading within snowpack in the northern Russia [*Vetrov et al., 2014*]. The levels of NO_3^- in snowpack of the Tomsk Oblast are on average (1.4 ± 0.03) mg/L, and (0.54 ± 0.33) mg/L at sampling points located away from pollution sources. The NO_3^- concentration values amount to 0.45 mg/L for KhMAO, which is higher than the background values [*Moskovchenko, Babushkin, 2012*], while the 0.01–0.37 mg/L interval is indicative of the natural gas fields area in the Yamal Peninsula [*Ermilov et al., 2002*]. Contents of NH_4^+ in snowpack of the study objects are in the range (0.41 ± 0.04) mg/L, which is in good agreement with the available data for both the Tyumen Oblast and KhMAO. The background level was determined as (0.36 ± 0.04) mg/L. Concentrations of NO_3^-, NH_4^+ are enhanced relative to the background values in proximity to the industrial zone. Comparison of NH_4^+

Table 1. **Statistical characteristics of snow depth and pH, chemical composition of snow meltwater at the monitoring sites**

Characteristics	Snow depth, cm	pH	Concentration, mg/L								
			Dust	N_NO_3	NH_4	P_2O_5	K_2O	Ca	Mg	Na	Cl
Mean	56.44	6.05	7.08	0.14	0.42	0.08	1.06	7.34	2.48	1.03	7.46
Confidence interval*	2.69	0.13	1.31	0.03	0.05	0.02	0.17	1.13	0.75	0.13	1.09
Median value	54.95	6.10	4.90	0.05	0.35	0.06	1.00	5.41	1.22	1.00	7.00
Standard deviation	14.63	0.73	7.14	0.18	0.23	0.09	0.90	6.18	4.07	0.62	5.15
Variation coefficient	25.93	12.07	100.86	132.23	56.16	106.70	84.75	84.15	164.00	60.45	69.03
Mean value for background points	55	6	4.1	0.12	0.38	0.06	1.02	6.75	2.01	1.09	7.17
No. of background site	114	114	114	114	103	103	114	114	114	86	86

* At a significance level $p < 0.05$.

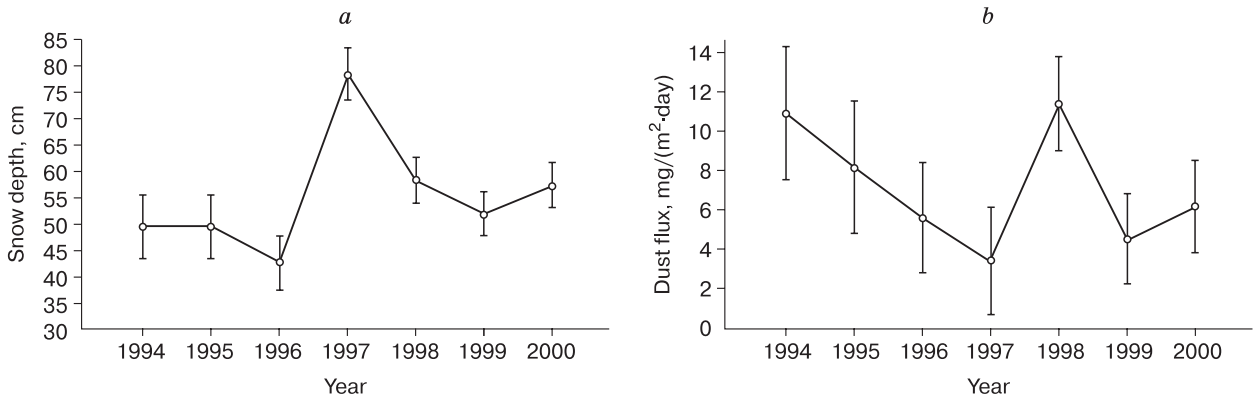

Fig. 2. Average annual snow depth (*a*) and dust aerosol flux (*b*).

contents in the forest and agricultural areas has revealed a reliable differentiation, indicating its higher levels in the forest.

The Mann-Whitney test at $p < 0.05$ confirmed the contents of phosphates in melted snow samples taken in the forest to be greater than in the field. P_2O_5 contents averaging (0.08 ± 0.2 mg/L) in snow meltwater differ only slightly from the mean value for the background sites (0.07 ± 0.02 mg/L).

Measured concentrations of potassium (K_2O) and sodium (Na^+) are on average (1.06 ± 0.16) mg/L and (1.03 ± 0.13) mg/L, respectively, and vary only slightly over the sampling points.

Results of this study has revealed that chloride-ion contents along with alkali metals represent snow contamination with readily soluble salts, which on average is (7.46 ± 1.1) mg/L. Cl^- concentrations vary only slightly at the observation points. For KhMAO, the average chloride levels within snowpack are significantly lower (3.4 mg/L) [*Moskovchenko, Babushkin, 2012*] increasing in the direction from west to east.

Abnormally high chloride-ion contents reported for the period 1997–1998 decreased dramatically later to (1.3 ± 0.5) mg/L (Fig. 2). Given that the sea influence on the coastal zone is known to spread within 200–250 km [*Zverev, Rubeikin, 1973*], this effect can be ruled out for chloride content in the analyzed samples.

With calcium contents averaging (7.3 ± 1.1) mg/L within snowpack, there is a logarithmic dependence between Ca^+ and Cl^-:

$$Cl = 3.3 \ln (Ca) + 3.2 \ (R^2 = 0.5 \text{ at } p < 0.05).$$

The presence of calcium in the snowpack is mainly associated with soil erosion [*Kutsenogii, 2006*], which suggests continental origins of the chloride ion. The study on the dissolution behavior of calcium in the eastern Tien Shan glaciers has demonstrated that calcium has the highest DFP (dissolved fraction percentage (%) calculated as the dissolved fraction divided by the sum of the dissolved and insoluble fraction) which is logarithmically regressed for the samples with SO_4^{2-} [*Wu et al., 2018*]. From a range of major mineral dust cations, Ca^{2+} has the highest solubility with chloride ion.

The content of magnesium in snow meltwater is (2.5 ± 0.7) mg/L. Spearman correlation coefficient between calcium and magnesium, magnesium and chlorine content is shown to be less than 0.3, which indicates of a weak link between them. The Mann-Whitney test at $p < 0.05$ showed that Mg content in the snowpack is higher for the forest than agricultural land area.

The distribution of trace element contents within the snowpack varies significantly between the observation points (Table 2).

The average content of nickel within the snowpack is (2.68 ± 0.33) μg/L, with its lowest levels (1.38 μg/L) reported from background site (BS) 18 (Verkh-Sechenovo village). The sampling points (SPs) which reported Ni concentrations within a confidence interval ($p < 0.05$) below the mean are: SP19 (Trubochevo v.), SPs 7 and 8 (Orlovka v.), and SP1 (Timiryazevo v.). The sampling points showing remarkably higher Ni contents at $p < 0.05$ are numbered 4, 5, 12, 14, 16, 20, and 21. Comparison of the obtained results with the data from the background sites provided a compelling evidence of enhanced Ni content in snowmelt waters sampled from within the Tomsk-Seversk industrial agglomeration. Thus, nickel concentrations range from 0.2 to 0.8 μg/L in the Ural industrial region [*Chernyaeva et al., 1978*], and equal to 0.7 μg/L within natural gas fields area in the Yamal Peninsula [*Ermilov et al., 2002*]. The average content of zinc in snow meltwaters is (26.7 ± 9.9) μg/L. Its content in the snowpack of the Tyumen Oblast reaches 81 μg/L in settlements. In the KhMAO, the most probable value for Zn concentrations is in the range of 10–27 μg/L [*Moskovchenko, Babushkin, 2012*]. The reported values for zinc concentrations range from maximal (81.7 μg/L) at

Table 2. **Averages concentrations (μg/L) of trace elements in solid residue of snow meltwater**

Sampling points*	Cr	Mn	Co	Ni	Cu	Zn	Cd	Pb	Zc
1	3.61	15.80	0.26	1.89	7.25	8.09	0.047	1.10	4.8
2	5.08	23.61	0.30	2.43	6.39	15.01	0.084	1.22	9.3
3	4.59	22.63	0.27	2.70	6.62	10.66	0.035	1.01	7.0
4	5.96	50.88	0.69	3.52	7.19	15.46	0.042	1.51	11.2
5	4.67	55.06	0.89	3.84	8.79	24.52	0.035	1.62	9.8
6	4.69	25.40	0.32	2.37	8.91	19.12	0.045	1.04	5.9
7	14.51	14.88	0.26	1.67	5.24	18.79	0.051	1.10	7.6
8	4.40	17.28	0.22	1.62	6.05	22.08	0.041	1.13	6.7
9	5.28	25.96	0.33	2.25	8.32	37.92	0.068	1.51	7.7
10	6.19	77.23	0.62	2.90	7.34	26.31	0.051	1.49	11.0
12	6.11	55.42	0.36	3.08	6.54	81.68	0.065	0.87	12.9
13	6.24	33.80	0.31	1.76	7.98	20.51	0.040	1.32	6.4
14	7.48	65.17	0.75	3.93	11.38	74.57	0.053	1.43	16.9
15	4.87	21.77	0.44	3.78	7.86	30.33	0.066	1.43	7.8
16	12.24	72.75	0.59	4.09	10.50	13.71	0.101	1.64	18.4
17	3.81	24.01	0.35	2.99	7.32	15.21	0.037	0.76	6.8
18	2.00	7.71	0.14	1.38	4.62	22.68	0.026	1.14	3.1
19	2.85	9.26	0.11	1.57	4.36	13.17	0.065	1.49	3.8
20	5.57	58.76	0.72	3.28	8.19	40.99	0.049	2.62	9.9
21	4.00	29.62	0.54	3.65	6.36	26.09	0.043	2.50	7.4
22	4.45	18.52	0.32	2.63	7.16	32.89	0.049	4.61	7.1
23	2.80	13.78	0.29	1.71	6.06	15.71	0.057	1.68	3.5
24	1.37	14.54	0.25	1.73	3.55	9.78	0.036	0.99	2.7
Mean	5.60	34.16	0.42	2.68	7.30	26.7	0.052	1.42	8.5
Background value	3.64	18.42	0.25	1.97	6.27	15.70	0.04	1.17	5.07

* Numbering of the sampling points is given in Fig. 1.

SP 12 in Kolomino village to slightly lower (74.6 μg/L) at Naumovka village. At this, high levels (within a confidence interval ($p < 0.05$) above the mean) was observed at sampling points 9 (Samus v.) and 20 (Batkat v.). While Samus village is located within the SCC impact zone [*Artamonova, 2011*], there are no industrial enterprises in the vicinities of Batkat village. Emissions of pollutants may be released by gas flares, the snowpack near which shows Zn concentrations reaching 52 μg/L [*Moskovchenko, Babushkin, 2012*]. However, Batkat village is located hundreds of kilometers away from oil fields, and the distance from the impact zone responsible for translocation of pollutants measures 5–15 km, depending on the wind rose [*Lezhenin et al., 2016*]. Coarse dust aerosol particles are dominantly (90 %) deposited within a radius of 7 km from the pollution source, and spread within a radius of 40 km [*Onuchin et al., 2014*], with snowfalls assisting both in dry and wet washout of atmospheric pollutants [*Talovskaya et al., 2014a*].

Among different types of boilers, the coal-fired boiler house in Batkat village contributes its share into the environmental impact from coal combustion which is confirmed by the reported enhanced concentration coefficients for zinc along with other trace elements [*Talovskaya et al., 2018a,b*].

The contents cobalt in snowpack have received little consideration so far [*Kutsenogii, 2006*]; within the observation sites, Co levels are reported to be higher than the average value at SPs located northeast and east of the Tomsk city agglomeration and at SP 20 (Batkat village). Dust emissions from the coal-fired boiler house are featured by elevated Co contents and greater Na and Ca concentration coefficients. Contents of metals in the snow-captured dust at least twice as higher than the background values.

The contents of lead within snowpack averages 7.6 μg/L against the background value of 6.3 μg/L. The snow dust enrichment in lead reported from SPs 20 and 22 showed Pb concentrations to be significantly higher than the background value. Although SPs 5 and 22 are located at different parts of the study area, but in proximity to highways with heavy traffic flow, they show explicable high lead levels. Sampling points 20, 21 are 1.5–3.0 km away from the highways, which makes dry washout of lead from snowpack of these points unlikely. Results of the field studies conducted around the Norilsk Mining and

Metallurgy Combine have shown a mosaic pattern of Pb deposition into snowpack [*Onuchin et al., 2014*]. Analyses of lead input in the snowpack of Tyumen showed its concentration in the solid phase, with the levels varying within a wide range, from 0 to 214 μg/L [*Krest'yannikova et al., 2015*]; its abnormal concentrations are localized.

At the studied sampling points (5, 6, 9, 10, 13–16), copper pollution encompasses the background sites located around the SCC, Tomsk Petrochemical Plant (Tomskneftekhim), where Kc > 1. Copper concentrations average (7.3 ± 0.8) μg/L. The value of Kc is reported to be high for SP 20 (Batkat village). In coals utilized as fuel, one can hardly expect high levels of copper. Enrichment of Siberian coals in lithophile and siderophile chemical elements (Cr, Ni, Co) and their depletion in chalcophile elements (Cu, Pb, Zn, Cd, etc.) is noted [*Arbuzov, 2007*]. Consequently, Cu enters the Batkat snowpack from other sources. Given that manganese is commonly used in the chemical industry, its anomalous abundancy relative to the background value should be expectable in the vicinities of SCC and Tomskneftekhim. The mean value is (34.2 ± 7.3) μg/L, the background value is 18.4 μg/L. At the sampling points (4, 5, 9, 10, 13–16) around chemical plants, Mn concentrations are 2–3 times higher than background values. At points 20, 21, the Kc values are shown to be high (3.6 and 1.8), which

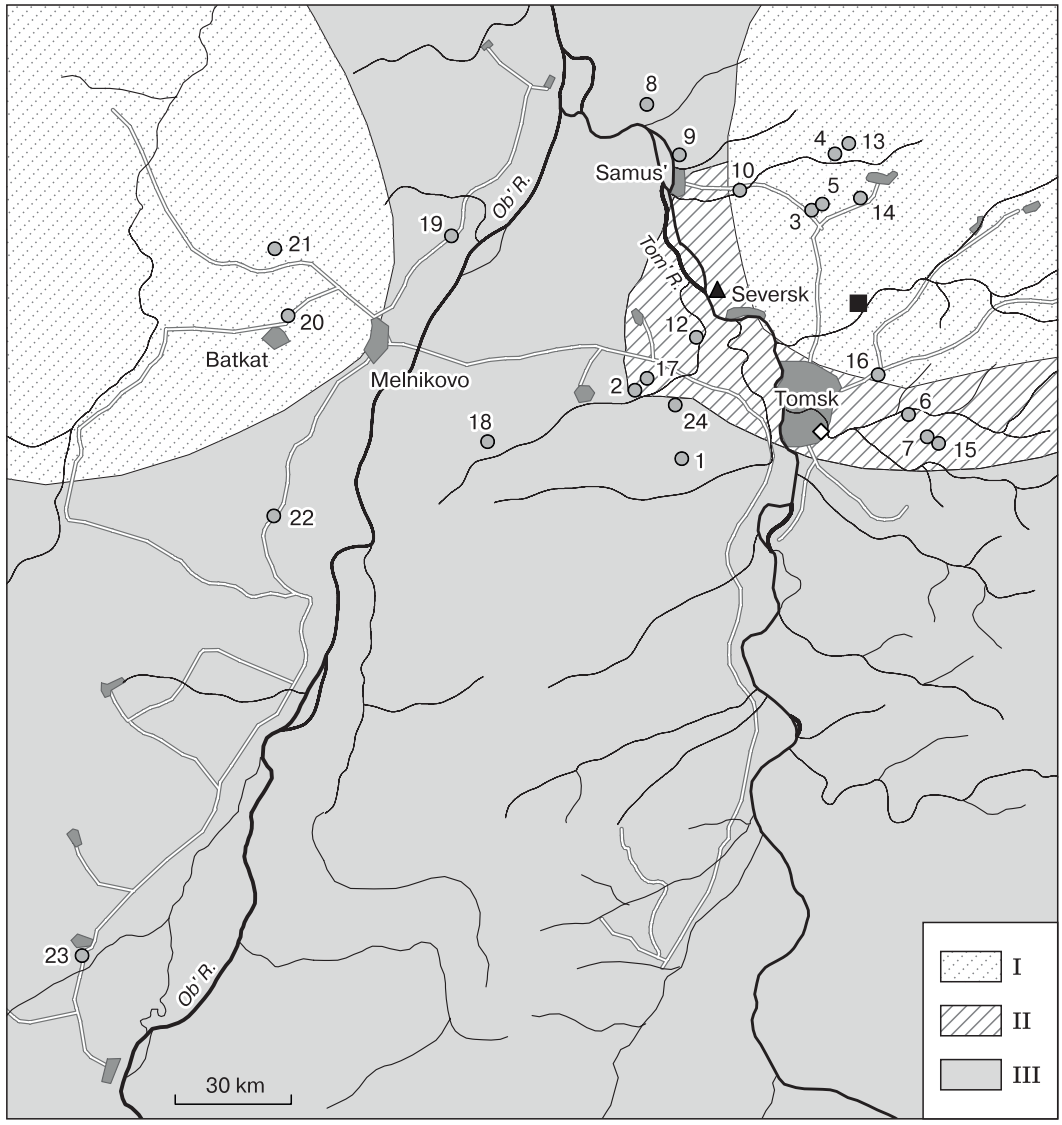

Fig. 3. Distribution of mean annual values of multivariate cluster analysis of trace element inventory (Ni, Co, Cu, Mn, Zn, Pb, Cr, Cd) in the territory of the Tomsk Oblast.

Zones showing similarity in the chemical composition: I – industrial zone, II – industrial-residential zone, III – relatively pure areas. See Fig. 1 for notations.

does not permit us to relate this phenomenon with the chemical composition of solid fuel utilized by the boiler house. Territorially, the pollution points gravitate to Tomskneftekhim and Tomsk city. Anomalies in chromium contents in the snowpack are primarily associated with the foundry production facilities [*Sergeeva, Kuimova, 2011*]. The authors attribute the chromium contamination of snowpack in Blagoveshchensk city to transboundary transmission from China, where thermal power plants are coal-fired. Although the foundry facilities remained within the Tomsky Instrument factory, the contamination did not spread beyond the city limits. However, HPP-2, which in the 1990s was partially coal-fired may continue to be the source of chromium pollution. The average cadmium content is (1.0 ± 0.2) μg/L within the snowpack. Abnormally high cadmium concentrations within snowpack are associated with the industrial and residential-transport zones [*Sergeeva, Kuimova, 2011*]. The Kc value reached maximum (1.3–2.0) at SPs 16, 2, and 9, and minimum (1.1–1.3) at SPs 15, 12, 19, and 23. All these points are located in proximity to highways, and the sampling points in proximity to the industrial zone report the highest values.

The mean value of total Zc pollution index is 8.5 ± 1.3, which varies widely (the variation coefficient is 73 %). The level of pollution is regarded as low and non-hazardous at Zc < 32 [*Kasimov et al., 2012*].

The K-means cluster analysis was used for classification of the sampling points. For simplicity, they were split into three clusters to provide a fit to the existing at the time trace elements distribution patterns in the territory of Tomsk Oblast. The averaged over the years Euclidean distances between the multivariable centers of clusters were mapped in using the QGIS (Fig. 3). For convenience, results of the classification are shown in black and white shading (notations I–III in Fig. 3). The points grouped in northeast and southeast of SCC and near Tomskneftekhim (points 10, 3, 5, 14, 4, 16) correspond to Zone I. The points 20 and 21 located at a considerable distance (70 km) from SCC are characterized by a close chemical composition. A similar situation is observed in Bratsk, where the aluminium smelter (BrAZ) is known to be a heavy metal pollution source [*Yanchenko et al., 2013*]. The sampling point located 29 km from the source shows a high concentration of contaminants, even higher than at a distance of 3 km from the production facilities. Assumingly, the pollution is caused by the boiler house, rather than the BrAZ facilities. We think, heavy metals uptake and translocation from the facilities over such distance is possible, in view of the revealed similarity in the chemical composition and elements concentrations (spectrum) at a distance of 29 km and near BrAZ.

Zone II encompasses the transitional group (points 2, 3, 6, 7, 12, 15) biased toward HPP-2 and the city-specific trace element contamination. The sampling points which are highlighted within Zone III are relatively pure in terms of elemental composition (points 1, 8, 9, 13, 18, 22–24), which largely overlaps the points within the interval below the mean Zc content.

CONCLUSIONS

1. Although the average snow depth is evenly distributed within the studied area, its variability over the years of observation is remarkable. The average snow-captured dust content is (6.8 ± 1.2) mg/L, dust load is (8.5 ± 3.6) mg/(m^2·day).

2. The variability may be regarded as moderate with respect to some parameters (snow depth, pH), or high (>100, e.g., contents of dust particles, P_2O_5, Mg, NO_3^-).

3. Comparison of snowpack in the forest and in land-use area revealed a significant difference between snow depth, contents of dust, NH_4^+, P_2O_5, Mg (towards their enhancement for the forest area).

4. Trace element levels tend to increase near the industrial zone of the Tomsk city agglomeration. Lead has a mosaic distribution pattern throughout the territory and its concentrations are confined to observation points located near highways, while cadmium concentration coefficient is reported to be high in snow samples both from the background sites and from within the industrial zone.

5. The multivariate cluster analysis allowed us to establish three groups of the observation points, namely: industrial and industrial-residential areas, and relatively pure areas.

6. Snowpack of some observation points (Batkat settlement and Komarovo swamps) which are more than 70 km away from the SCC and Tomskneftekhim facilities is shown to have anomalous contents of dust and heavy metals (1.5–2 times higher relative to the background values), whose composition is similar to those observed in the northeast of the Tomsk-Seversk agglomeration.

7. The total pollution index value indicates that all the background sites have an average value of Zc < 32, suggesting a low level of snowpack contamination with heavy metals. Thus, pollutants deposition in the studied snowpack has a focal pattern both within a 30-kilometer impact zone of the industrial facilities and at a considerable distance from them (more than 70 km).

Acknowledgements. *This research was supported by the Russian Foundation for Basic Research (Project No. 19-05-50062/19) and by the Ministry of Education and Science of the Russian Federation (Agreement No. 075-15-2020-805 dated 02.10.2020).*

References

Akba, O., Kilinc, E., Aydin, I., Erdogan, S., Aydin, F., Duz, M.Z., Hamamci, C., 2013. Major and trace element contamination of short-term snow cover during and after a dust storm and analysis by ICP-OES. Atom. Spectros, No. 34, 48–52.

AMAP, 2011. Snow, Water, Ice and Permafrost in the Arctic (SWIPA): Climate Change and the Cryosphere. Arctic Monitoring and Assessment Programme (AMAP). Oslo, Norway, 538 pp.

Arbuzov, S.I., 2007. Metal content of Siberia coals. Bulletin of Tomsk Polytechnic University, No. 1, 77–83.

Artamonova, S.Yu., 2011. Assessment of technogenic aerosol pollution of Seversk area using geochemical and GIS methods. GEOSIBIR. Izd-vo Sib. gos. un-ta geos. i tekhnol., Novosibirsk, vol. 4, pp. 2542–2558 (in Russian).

Bordon, S.V., 1996. Formation of geochemical anomalies in the snow cover of urbanized territories. Litasfera [Lithosphere], No. 5, 172–177.

Boyarkina, A.P., Baikovskii, V.V., Vasil'ev, N.V. et al., 1993. Aerosols in Siberian Natural Trays. Tomsk University Press, Tomsk, 157 pp. (in Russian).

Chernyaeva, L.E., Chernyaev, A.M., Mogilenskih, A.K., 1978. The Chemical Composition of Atmospheric Precipitations (Ural Mountains and Cis-Ural Region). Gidrometeoizdat, Leningrad, 178 pp. (in Russian).

Glazovskii, N.F., 2006. Selected works in two volumes. Vol. 1. Geochemical Flows in the Biosphere. T-vo nauchn. izd. KMK, Moscow, 535 pp. (in Russian).

Ermilov, O.M., Griva, G.I., Moskvin, V.I., 2002. Effect of Gas Industry Objects on Northern Ecosystems and Ecological Stability of Geotechnical Complexes in Permafrost. Izd-vo SO RAN, Novosibirsk, 147 pp. (in Russian).

Ermolov, Yu.V., Makhatkov, I.D., Khudyaev, S.A., 2014. Background concentrations of chemical elements in snow cover of the central regions of Western Siberia. Optics of the Atmosphere and Ocean, No. 9 (27), 790–800.

Filimonenko, E.A., Talovskaya, A.V., Yazikov, E.G., Chumak, Yu.V., Ilenok, S., 2013. Mineral composition of precipitated airborne particles in impact zones of Tomsk industrial enterprises. Mineralogiya Tecknogeneza [Mineralogy of Technogenesis], No. 14, 191–202.

GOST 26487-85 (State Standard), 1985. Soils. Determination of exchangeable calcium and exchangeable (mobile) magnesium by CINAO methods. Standard Publishing, Moscow, 14 pp. (in Russian).

GOST 26204-91 (State Standard), 1992. Soils. Determination of mobile phosphorus and potassium compounds by Chiricov method modified by CINAO. Standard Publishing, Moscow, 8 pp. (in Russian).

GOST 17.4.3.01-83 (State Standard), 2004. Nature protection. Soil. General requirements for sampling. Standard Publishing, Moscow, 4 pp. (in Russian).

GOST 4245-72 (State Standard), 2010. Drinking water. Methods for determination of chloride content. Standartinform, Moscow, 6 pp. (in Russian).

Kasimov, N.S., Kosheleva, N.E., Vlasov, D.V., Tverskaya, E.V., 2012. Geochemistry of snow cover in Eastern district of Moscow. Vestnik Mosk. Un-ta [Bulletin of the Moscow State University. Ser. 5. Geography], No. 4, 14–24.

Krest'yannikova, E.V., Kozlova, V.V., Larina, N.S., Larin, S.I., 2015. Chemical and environmental assessment of lead pollution in the atmosphere of the city of Tyumen. Izv. Samar. nauch. tsentra RAN [Izvestiya Samara Scientific Center of the Russian Academy of Sciences], 17, No. 5 (2), 679–684.

Kutsenogii, K.P. (Ed.), 2006. Aerosols of Siberia. Novosibirsk, Izd-vo SO RAN, 548 pp. (in Russian).

Lezhenin, A.A., Yaroslavtseva, T.V., Raputa, V.F., 2016. Monitoring of aerosol pollution of snow cover with ground-based observation data and satellite information. J. Sib. Fed. Univ. Eng. Technol. 9 (7), 950–959.

Moskovchenko, D.V., Babushkin, A.G., 2012. Features of formation of the chemical composition of snow cover on the territory of Khanty-Mansi Autonomous Okrug. Kriosfera Zemli [Earth's Cryosphere], XVI (1), 71–81.

Onuchin, A.A., Burenina, T.A., Zubareva, O.N., Trefilova, O.V., Danilova, I.V., 2014. Pollution of snow cover in the impact zone of enterprises in Norilsk Industrial Area. Sibirskii Ecologicheskii Zhurnal [Siberian Ecological Journal], No. 6, 1025–1037.

PND F 14.1-2.1-95 (Normative documents of Ministry of Environmental Protection and Natural Resources of Russian Federation), 1995. Method for measuring the mass concentration of ammonium ions in drinking, surface (including sea) and waste waters by the photometric method with Nessler reagent. Min-vo okhr. Okr. sredy i prirod. Res. RF, Moscow, 18 pp. (in Russian).

PND F 14.1-2-3-4.121-97 (Normative documents of Ministry of Environmental Protection and Natural Resources of Russian Federation), 1997. Quantitative chemical analysis of waters. Method for measuring pH in waters with the potentiometric method. Min-vo okhr. okr. sredy i prirod. Res. RF, Moscow, 11 pp. (in Russian).

RD 52.24.391-95 (Executive geodetic documentation), 1995. Methodological guidelines. Methods for measuring the mass concentration of sodium and potassium in the surface land waters using a flame-photometric method. Rosgidromet. Gidrokhim. In-t, Rostov-on-Don, 9 pp. (in Russian).

RD 52.04.186-89 (Executive geodetic documentation), 1991. Guidelines for air pollution control. Goskomgidromet SSSR, Moscow, 450 pp. (in Russian).

Sergeeva, A.G., Kuimova, N.G., 2011. Snow cover as an indicator of the state of atmospheric air in the system of sanitation and environmental monitoring. Bulletin of Pathology and Physiology, No. 40, 100–104.

Shevchenko, V.P., Lisitsyn, A.P., Polyakova, E.I., Detlef, D., Serova, V.V., Stein, R., 2002. Distribution and composition of insoluble particles in the snow cover of Arctic drift ice (Fram Strait). Doklady Earth Sciences, 383 (3), 385–389.

Shevchenko, V.P., Lisitsyn, A.P., Stein, R., Goryunova, N.I., Kuvichkin, A.A., Kravchishina, M.D., Crews, M., Novigatsky, A.N., Sokolov, V.T., Filippov, A.S., Haas, H., 2007. Distribution and composition of insoluble particles in Arctic snow. Problems of the Arctic and Antarctic, No. 75, 106–118.

Shevchenko, V.P., Pokrovsky, O.S., Vorobyev, S.N., 2017. Impact of snow deposition on major and trace element concentrations. Hydrol. Earth Syst. Sci., vol. 21, 5725–5746.

Talovskaya, A.V., Filimonenko, E.A., Yazikov, E.G., 2014a. Dynamics in the elemental composition of snow cover in the north-eastern zone of influence of Tomsk-Seversk industrial agglomeration. Optics of the Atmosphere and Ocean, No. 6, 491–495.

Talovskaya, A.V., Yazikov, E.G., Filimonenko, E.A., 2014b. Assessment of the atmosphere pollution in urbanized areas of Tomsk region by the results of snow cover study. Geoecology. Engineering Geology. Hydrogeology. Geocryology, No. 5, 408–417.

Talovskaya, A.V., Yazikov, E.G., Filimonenko, E.A., 2018a. Element composition of solid airborne particles deposited in the

snow in the vicinity of boilers using different types of fuel (on the example of Tomsk region). In: Proc. of the II Baikal International Scientific and Practical Conference: Snow cover, precipitation, aerosols: technology, climate and ecology (Irkutsk, June 25–30, 2018). IRNITU, Irkutsk, pp. 55–59 (in Russian).

Talovskaya, A.V., Yazikov, E.G., Filimonenko, E.A., Lata, J.-C., 2018b. Characterization of solid airborne particles deposited in snow in the vicinity of urban fossil fuel thermal power plant (Western Siberia). Environmental Technology (U.K.), 39 (18), 2288–2303.

Vasilenko, V.N., Nazarov, I.M., Fridman, Sh.D., 1985. Snow Cover Pollution Monitoring. Gidrometeoizdat, Leningrad, 185 pp. (in Russian).

Vetrov, V.A., Kuzovkin, V.V., Manzon, D.A., 2014. Acidity of atmospheric precipitation and atmospheric deposition of sulfur and nitrogen in the Arctic Zone of the Russian Federation according to the monitoring of the snow cover chemical composition. Arctic: Ecology and Economy, No. 3 (15), 46–51.

Walker, T.R., Young, S.D., Crittenden, P.D., Zhang, H., 2003. Anthropogenic metal enrichment of snow and soil in northeastern. Environmental Pollution, vol. 121, 11–21.

Wu, G., Li, P., Zhang, X., Zhang, Ch., 2018. Using a geochemical method of dissolved and insoluble fractions to characterize surface snow melting and major element elution. J. Glaciology 64 (248), 1003–1013.

Xue, H., Chen, W., Li, M., Liu, B., Li, G., Han, X., 2020. Assessment of major ions and trace elements in snow: A case study across northeastern China, 2017–2018. Chemosphere, vol. 251, 1–7.

Yanchenko, N.I., Baranov, A.N., Chebykin, E.P., Kolesnikov, S.S., Vodneva, E.N., 2013. Specific features and factors affecting distribution of metals, rare earth elements, carbon and fluorine in snow cover filtrate and solid sediment in Bratsk. Bulletin of Irkutsk State Technical University, No. 10 (81), 141–148.

Zverev, V.P., Rubeikin, V.Z., 1973. The role of atmospheric precipitations in circulation of chemical elements between the atmosphere, lithosphere and hydrosphere. Universities Herald. Geology and Exploration Series, No. 12, 54–60.

Received June 21, 2020
Revised June 28, 2021
Accepted September 10, 2021

Translated by N.N. Mzhelskaya

EARTH'S CRYOSPHERE
SCIENTIFIC JOURNAL

Earth's Cryosphere, 2021, vol. XXV, No. 6, pp. 23–33 http://earthcryosphere.ru/

GEOTHERMAL FIELDS AND THERMAL PROCESSES IN CRYOSPHERE

THERMAL REGIME OF CRYOLITHOZONE AT YTYMDZHA DEPRESSION, ALDAN SHIELD

R.G. Sysolyatin, M.N. Zheleznyak

Melnikov Permafrost Institute SB RAS,
Merzlotnaya str. 36, Yakutsk, 677010, Russia; robertseesaw@gmail.com, fe1956@mail.ru

The results of geocryological studies in the Ytymdzha Depression of the Aldan Shield have been presented. From 1999 to 2001, several exploration boreholes were drilled in the central part of the depression, which made it possible for the first time to obtain information on the geotemperature field, the thermophysical properties of rocks and the thickness of the permafrost stratum. The long-term series of monitoring of the temperature regime of the active layer obtained for the bogged floodplain terrace, the river terrace, and the south-facing slope have been adduced. The temperature of rocks at a depth of 1 m varies from 4.8 to –11.7 °C, with average annual temperature ranging from –1.0 to –4.9 °C. The work has resulted in the sublongitudinal permafrost-geothermal section along the central part of the Ytymdzha Depression, within which the thickness of permafrost varies from 106 to 251 m.

Keywords: *ground temperature, geothermal gradient, permafrost thickness, Ytymdzha Depression.*

INTRODUCTION

The superposed, sublatitudinal depressions of the Aldan Shield (Chulman, Tokarikan, Guvilgra, Ytymdzha and Toko) composed by Mesozoic deposits are the main sources of coal for industrial development. Presently there is active field development within the Chulman Depression (Neryungri, Kabaktinsky and Denisovsky mining and processing plants) and within the Toko Depression (Elga mining and processing plant)). But, according to data from geological prospecting [*Chereposcky, 2004*], all Mesozoic-age depressions are promising for coal mining.

The coal-bearing regions of Southern Yakutia vary greatly in the extent of study of their permafrost conditions. Owing to coal field development and an abundance of factual material, the eastern part of the Chulman Depression and the western part of the Toko Depression are among the most studied regions of the modern cryolithozone distribution [*Belokrylov, Efimov, 1960; Kudryavtsev, 1975; Zheleznyak et al., 1996*].

At the same time, the Ytymdzha, Guvilgra, Toko depressions and a series of smaller structures have no clear characterization of permafrost conditions, they are mapped and described analogously to the Chulman Depression [*Ershov, 1989*]. The impact of surface air temperature inversion presents a deciding factor that determines the discontinuous distribution of permafrost within the Chulman Depression [*Belokrylov, Efimov, 1960*; *Alekseyev, Filosofov, 1970*], while a normal altitudinal zonation is more characteristic of the Toko Depression [*Zheleznyak et al., 1996*; *Zheleznyak, 2005*]. For almost the entire territory of Southern Yakutia (beyond regions of industrial field development) the type and depth of freezing, as well as the permafrost temperature regime, are not reliably determined owing to the absence of factual material.

On the example of the Ytymdzha Depression, specific features of permafrost conditions are considered in comparison with those of larger geological divisions similar in structure and developmental conditions. Data on the temperature regime of permafrost are presented for the first time. For the further expansion of the western Southern Yakutian coal mine surplus and the development of gold-placer deposits it is necessary to consider permafrost parameters. Specifically, in the Ytymdzha Depression, this is owing to the presence of large coal horizons which are potentially suitable for industrial development [*Zhelinsky et al., 1976; Cherepovsky, 2004*].

Permafrost conditions influence the conservation of gas content in coal basins and affect the emission of greenhouse gases [*Gresov et al., 2014*], which makes this research more relevant.

MATERIALS AND METHODS

The work is based on the results of field permafrost-geothermal research conducted from 2001 to 2019 by the staff of the Laboratory of Geothermal Energy of the Permafrost Institute SB RAS. The opportunity to complete the first geothermal measurements in the region arose owing to the geological prospecting works of OJSC Uzhyakutgeologiya

(1999–2001), which consisted of drilling exploratory boreholes 500 m deep in the central part of the Ytymdzha Depression.

During this work, the staff of "Uzhyakutgeologiya" tried to identify the depth of the permafrost base using indirect signs, such as the appearance of water in the borehole, loss of drilling fluid, drilling out of ice plugs, etc. The archive materials provide a brief description of permafrost conditions, according to which the permafrost thickness varies from 30 to 140 m. Beginning in 2001, researchers of the Permafrost Institute SB RAS conducted work to obtain thermometric borehole logging immediately after drilling. Later (2006, 2012, 2016), geothermic measurements were conducted in the boreholes returned to thermal equilibrium. As a result, geothermic measurements were conducted in six boreholes up to a maximum depth of 240 m. Thermistor installations, which were used to determine temperature, were manufactured and calibrated in the Laboratory of Geothermal Energy of the Permafrost Institute SB RAS, with observational error up to 0.05 °C [*Balobaev et al., 1985a*].

Overall, the depth of the permafrost base was identified in 12 boreholes within the Ytymdzha Depression using various methods (calculations, direct measurements, thermal logging analysis, etc.). Direct geothermal measurements were carried out within six boreholes after a long period of recovery of the thermal state of the rocks after drilling. In addition, data from geothermal research and permafrost distribution peculiarities of the nearby Guvigra, Tokarikan and Toko depressions were used to build the permafrost-geothermal section [*Zheleznyak, 2005*].

Calculating the parameters of deep freezing is impossible without information about the thermal physical properties of the rocks composing the section. A typical feature of Mesozoic Age depressions is the persistence of the stratigraphic composition of the deposits [*Zhelinskiy, 1980*]. Single measurements of the thermophysical properties of rocks (Durai and Kabakta formations) performed for the Ytymdzha Depression (6 samples) showed a high convergence of the results with samples from the Chulman and Toka depressions [*Gavriliev, 2013*]. Based on the similar genesis of the depressions, the thermal conductivity of rocks is considered to be the same as in the samples obtained in the Chulmakan and Elga areas [*Gavriliev, 2013*] and is shown in Table 1. The standard thermal conductivity of individual samples has increased values relating to the effective thermal conductivity of the entire strata. This is explained by the presence of cracks, heterogeneity of the section and a difference in structure and texture on stratigraphic boundaries. Effective thermal conductivity of the studied horizons is determined by the material composition, and the similarity in values with the Jurassic series of the Viluy sedimentary basin is established [*Semenov et al., 2018*]. Owing to the dominance of fine-grain sandstone we assume that the Durai Suite is characterized by a large value of effective thermal conductivity. The distribution of rocks of a different lithology (in percentages) was obtained based on deep drilling data (Table 1).

To determine the thermal regime of the active layer in 2013, three observation points were equipped within the landscapes typical for the Ytymdzha Depression (bogged floodplain terrace, river terrace, south-facing slope). Logging stations HOBO U-22 and HOBO U-23 with TMC50-HD sensors, which are widely utilized to conduct geothermal monitoring, were used [*Konstantinov et al., 2011*]. The sensors were located in a thin plastic pipe and planted into soil pits. Vegetation was not removed and suffered minimum possible disruptions. A continuous series of observations was obtained in two of three points owing to disruption by wild animals, as well as challenges in reaching the object for annual maintenance.

In 2019, an automatic APIK-008 soil measuring complex was installed on the first river terrace. It is a portable weather station with broad possibilities for monitoring meteorological parameters, but in the present article only average air temperature values are provided.

Table 1. **Distribution of the main types of rocks (%) in the Ytymdzha Depression based on drilling and thermal conductivity data**

Series	Sandstones			Siltstones	Charcoal	Effective thermal conductivity, W/(m·°C)
	fine-grained	medium-grained	coarse-grained			
Kabakta	27	38	4	25	4	1.7–1.9
Duray	43	9	5	40	2.5	1.9–2.1
Area	Standard thermal conductivity*, W/(m·°C)					
Chulmakan	2.99 (12)			–	0.9–1.1	
Elga	2.57 (4)			2.57 (1)	–	

* Ground thermal conductivity in the frozen condition according to R.I. Gavrilov. Parenthetical text shows the number of samples.

BRIEF DESCRIPTION OF THE ENVIRONMENT OF THE STUDIED AREA

The Ytymdzha Depression is located in the central part of the Aldan Shield (Fig. 1). The boundaries of the depression are determined by the boundary of Mesozoic and Archean rocks. From the south, the depression is bordered by the Gonam Range and the Koltan-Dzhur Range, with maximum altitudes of up to 1848 and 1831 m, respectively. From the north, the Ytymdzha Depression is limited by the area of distribution of Proterozoic rocks of the Aldan Highlands (Fig. 2). Flexure folds on gentle monocline stratum bedding serve as evidence of a block structure of the basement, which is typical for the whole series of Mesozoic depressions [*Imaev et al., 2000*]. Due to the block structure of the basement distribution, the structure and composition of the cover can change abruptly within a small area [*Zhelinskiy, 1980*].

The Ytymdzha Depression is a regional sublatitudinal depression, 130 × 30 km in size. The total thickness of the Mesozoic deposits reaches 1100 m, which is established by geophysical work and confirmed by drilling data [*Rukovich, 2018*]. The thickness of the Quaternary deposits is determined to be 5–15 m and decreases as the altitude decreases. Based on geological survey data with a scale of 1:200 000, Quaternary deposits are predominantly of alluvial, colluvial-solifluctional, lake and bog origin. In a geomorphological respect, the depression is characterized by an undulating topography with watersheds located 200–300 m on average above the valleys. In the central part of the depression, ground temperature monitoring up to the depth of zero annual amplitude was conducted in:

1. A bogged floodplain terrace (peat bog, *mari* (in Yakutia – bogs with rare larches)) with a depleted larch forest or its absence; the elevation range is 550–650 m (Fig. 3, *a*).

2. The erosional river terrace with a pine-larch forest and a *Ledum*-lichen cover with rare birches, alders; the elevation range is 600–700 m (Fig. 3, *b*).

3. The south-facing slope with diluvial grus-sandy loam deposits and vegetation of larch, alder with a forb-blueberry-*Ledum* cover; elevation range 700–1000 m (Fig. 3, *c*).

The water content of the loose deposits of the active layer was not determined and is provided according to monograph data [*Kudryavtsev, 1975, p. 86*].

Permafrost processes include solifluction, frost sorting, the formation of patterned ground, the formation of aufeis, rock glaciers and frost heaving.

According to the results of annual observations, the air temperature in the Ytymdzha Depression for the period from 01.08.2019 to 31.07.2020 was –7.0 °C, which is the average value in respect to the weather stations in the Chulman (–5.2 °C) and Toko (–8.5 °C) depressions (Table 2). This agrees with the prevailing westerlies that increase the severity of climatic conditions in the eastern direction. The temperature inver-

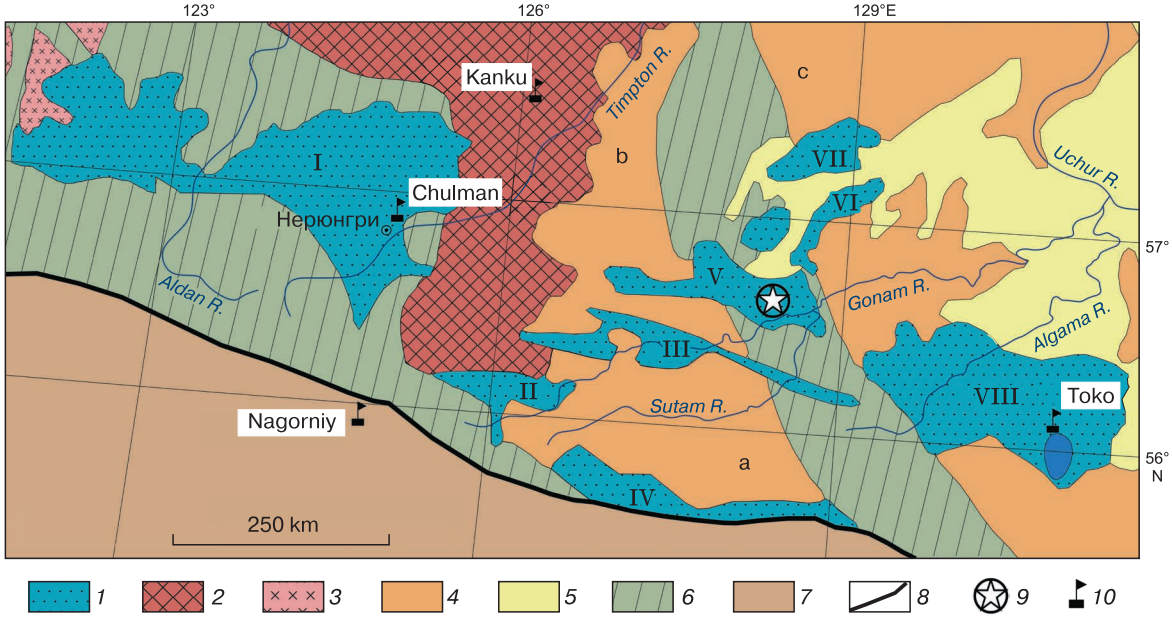

Fig. 1. Geological structures of the central part of the Aldan Shield.

1 – superimposed depressions with Mesozoic rocks (I – Chulman, II – Tokarikan, III – Guviglra and Atugey-Nuyam, IV – Sutam, V – Ytymdzha, VI – Gynam-Cemdzhyn, VII – Kuranakh-Gynym, VIII – Toko); 2–5 – superterraines: 2 – Nimnyr, granulite-orthogneiss (V–Є); 3 – West-Aldan, granite-greenstone (V–Є); 4 – Sutam (a), Seym (b), Uchur (c), granulite-paragneiss (V–Є); 5 – Vendian–Cambrian platform cover; 6 – tectonic mélange zones; 7 – Stanovoy belt; 8 – Stanovoy fault; 9 – study area; 10 – weather stations.

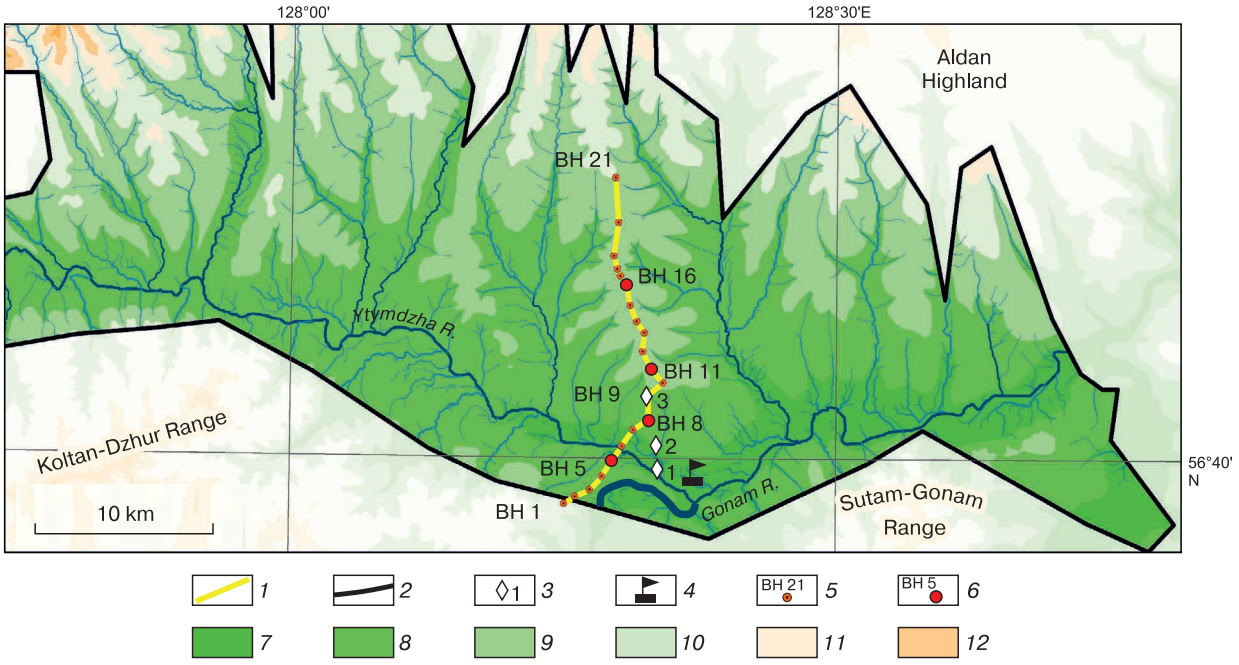

Fig. 2. Study area in the eastern part of the Ytymdzha Depression.

1 – drilling profile; 2 – Ytymdzha Depression boundary; 3 – areas of geothermal monitoring and their numbers; 4 – APIK location; 5 – deep boreholes; 6 – boreholes with geothermal measurements; 7–12 – surface elevation, m: 7 – less than 600; 8 – 600–800; 9 – 800–1000; 10 – 1000–2000; 11 – 1200–1400; 12 – 1400–1600.

Fig. 3. Areas of temperature monitoring:

a – floodplain terrace; b – river terrace; c – south-facing slope, borehole 9. Photo by R.G. Sysolyatin.

Table 2. **Main climate parameters at weather stations in the region for the period 01.08.2019–31.07.2020**

Weather station	Elevation, m	Air temperature, °C				Sum of winter temperatures*, °C·month
		average	maximum	minimum	Amplitude	
Ytymdzha (APIK-008)	568	–7.0	35.0	–49.0	84.0	–134.3
Chulman	858	–5.2	32.7	–41.4	74.1	–110.4
Toko	825	–8.5	32.3	–50.6	82.9	–137.0
Nagorniy	842	–5.4	32.0	–38.0	70.0	–110.0
Kanku	1218	–7.3	30.1	–40.9	71.0	–129.7

* October–April.

sion observed in the Chulman Depression [*Alekseyev, Filosofov, 1970*] can occur as in Ytymdzha Depression with similar topography as in the eastern part of the Toko Depression. The weather stations Toko and APIK-008, located in local topographic lows of the Ytymdzha Depression, are characterized by minimum mean annual temperatures and maximum annual air temperature amplitudes.

ACTIVE LAYER TEMPERATURE

The temperature regime of the active layer was studied on the bogged floodplain terrace, the drained river terrace and the south-facing slope at a depth of 1 m (Fig. 4). The minimum values of the mean annual ground temperature were obtained at the floodplain terrace and vary from –1.2 °C (2015) to –4.9 °C (2017). During the observation period the ground temperature at a depth of 1 m did not exceed –0.1 °C, falling as low as –14 °C (February 2015). The thermal inertia at sites with water content exceeding 60 % is quite high, minimum temperatures are noted in February–March, maximum temperatures in December.

Compared to highly moist areas, more drained landscapes differ significantly in temperature regime. Average annual temperature from –1.0 °C (2015) to –2.7 °C (2017) and maximum values of active layer temperature up to 4.8 °C (August 2015) make terraces with pine-larch forest and an abundance of brush the warmest areas.

The temperature in the active layer on the south-facing slope was measured with an interruption from January 2015 to June 2016, and in May 2019 the measuring equipment was destroyed by a forest fire. The ground did not warm to temperatures higher than +1.3 °C (01.09.2014) in the observation area, and sometimes it cooled to –11.7 °C (March 2018). The mean annual ground temperature values varied from –3.0 °C (2014) to –3.9 °C (2018).

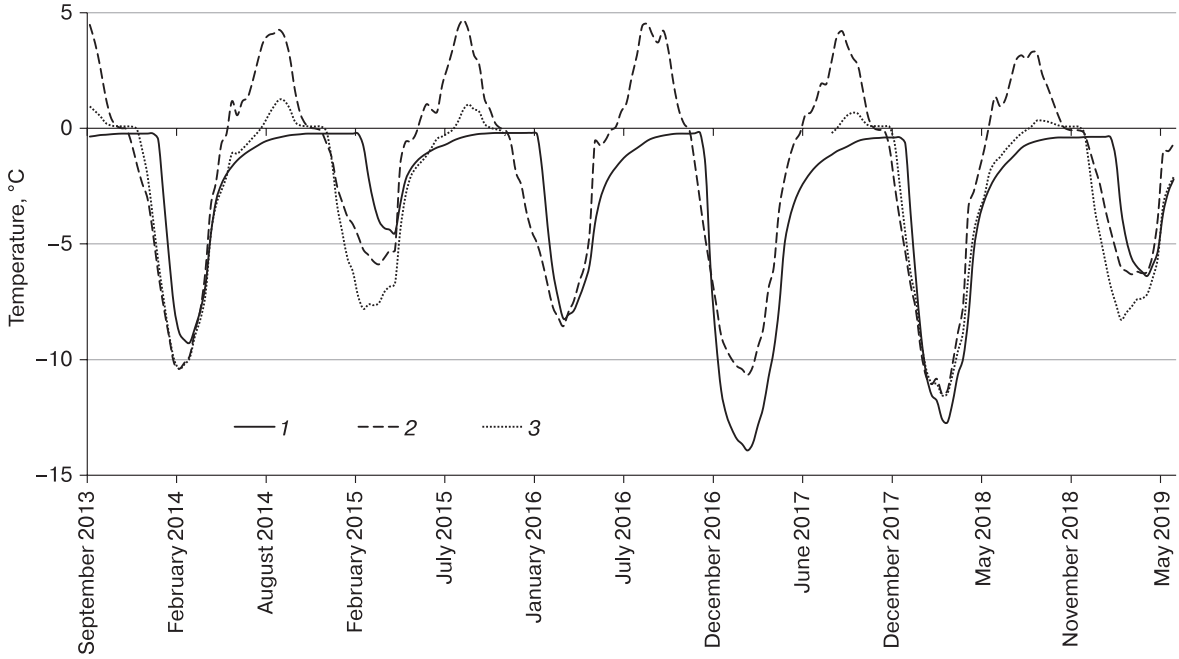

Fig. 4. Variation of ten-day ground temperature at depth 1 m.

1 – floodplain terrace; 2 – river terrace; 3 – south-facing slope.

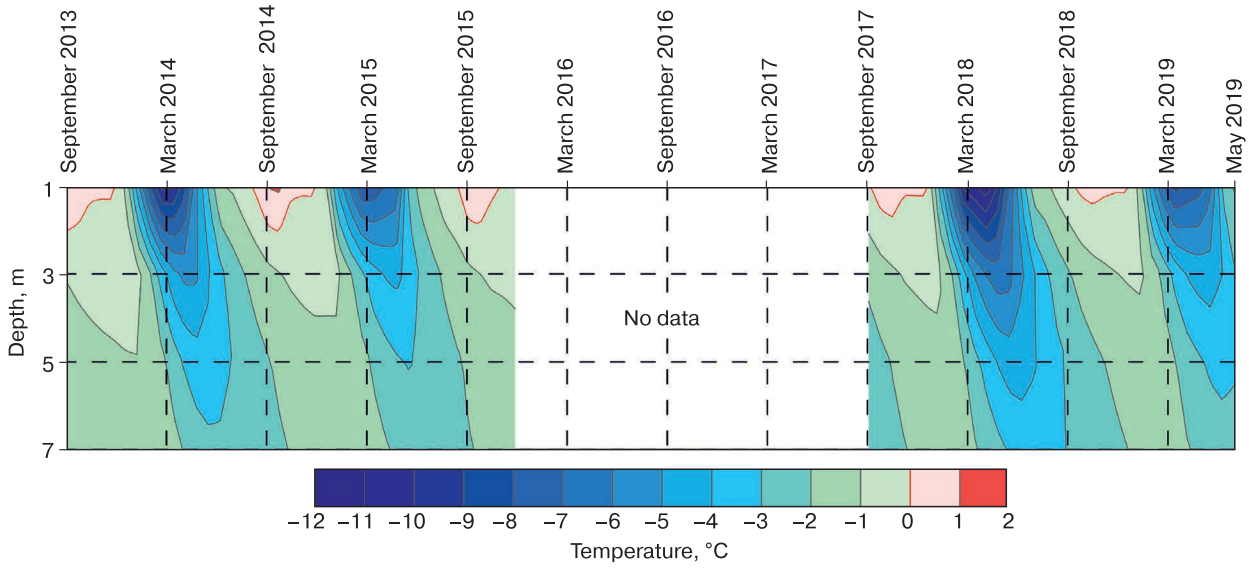

Fig. 5. Rock temperature variation in the layer of annual temperature fluctuations in borehole 9.

The depth of the active layer of the floodplain terrace does not exceed 1 m, which agrees with the calculation data. For the south-facing slope seasonal thawing can reach depths of 2.1–2.2 m under kriging interpolation (Fig. 5), which exceeds the values shown in the work [*Kudryavtsev, 1975, p. 86*]. On the river terrace, at a depth of 1 m, positive temperature is noted from June to mid-November. On the south-facing slope it is positive for no more than two months per year. On the floodplain terrace the active layer does not exceed 1 m.

A steady tendency toward active layer temperature changes is not observed. From 2014 to 2018, a decrease in temperature was noted at a depth of 1 m from −10.3 to −14.7 °C on the floodplain and river terraces, respectively. But the ground temperature in the winter period of 2019 differs by one of the highest values during the entire observation period. An analysis of the processes determining the temperature regime in the active layer requires a more detailed study of all affecting factors, which is not possible in our case owing to the absence even of snow cover data. The latter is highlighted as the main factor which determines the ground temperature regime in Siberia [*Sherstyukov, 2008*].

TEMPERATURE OF DEEP PERMAFROST HORIZONS

During geothermal measurements we were able to determine ground temperature up to depths of 95, 35 and 240 m in boreholes 5, 8 and 16, respectively (Table 3). The ground temperature regime is quasi-stationary, but below a depth of 40 m boreholes 5 and 16 show a stationary temperature distribution (Fig. 6). The geothermal gradient is negative in the zone up to 20–40 m depths and positive below, with average values from 1.0 to 1.8 °C/100 m. According to archive data, thermal logging measurements were taken in boreholes 7 and 13, and a geothermal gradient was identified. But all these measurements were taken in the unfrozen (subpermafrost) zone, 100–150 m below the calculated permafrost base. The gradient value was used when calculating the thickness of the permafrost (see below). For boreholes in which logging was not performed, an average geothermal gradient value of 1.6 °C/100 m was used.

On the flattened watershed (borehole 16), the minimum values of ground temperatures (−1.5 °C) are seen at 35–40 m deep, i.e. lower than the depth of zero annual amplitude indicated in [*Kudryavtsev, 1975, p. 75*]. Below, up to the permafrost base at a depth of 190 m, the temperature is rising with an average gradient of 1.0 °C/100 m. In unfrozen ground the geothermal gradient rises to 1.4 °C/100 m, and at a depth of 240 m the temperature reaches +0.7 °C. The average density of the heat flux in the frozen zone was 0.020 W/m^2, 0.028 W/m^2 in the unfrozen (subpermafrost) zone, the overall value was 0.022 W/m^2 for the 200 m (Table 4). The thermal conductivity in each specific depth range was estimated by the composition and homogeneity of the rocks.

Within the steep north-facing slope, borehole 5, owing to its proximity to a cliff, is impacted by side freezing, so at a depth of 40 m the ground temperature falls to −3.1 °C. To a maximum measured depth of 95 m, in direct proximity to a large coal horizon, it increases with a gradient of 1.8 °C/100 m and reaches −2.1 °C.

In the middle part of the south-facing slope (borehole 8) the minimum temperature (−2.1 °C) is seen at depths of 30 and 35 m.

Table 3. **Borehole (BH) location, temperature parameters and calculated permafrost thickness**

BH	Elevation, m	Topographic feature	Slope aspect	Slope, grad.	Temperature* at depth. 40 m, °C	Temperature gradient, °C/100 m		Effective thermal conductivity, W/(m·°C)	Permafrost thickness*, m	Heat flux, W/m²	Permafrost thickness, m		
						average	by borehole logging				by equation (1)	by BH logging gradient	By gradient *
5	670	Slope	North	25	**–3.1**	**1.8**	1.6	1.8	251	0.021	308	234	221
6	580	Floodplain	None	0	–1.9	1.45	1.6	1.8	173	0.023	189	159	171
7	590	Terrace	»	0	–1.8	1.45	**1.1**	1.8	183	0.023	181	204	164
8	720	Slope	South	25	**–2.1****	1.45	**1.83**	1.8	187	0.021	221	155	185
9	750	»	»	10	–2.0	1.45	**1.26**	1.8	192	0.023	199	199	178
10	815	»	»	15	–1.7	1.45	**1.98**	1.8	154	0.022	178	126	157
11	840	Watershed	»	15	–1.1	1.45	**3.26**	1.8	106	0.022	129	74	116
12	870	»	»	10	–1.2	1.45	**1.29**	1.8	130	0.023	135	133	123
13	930	»	»	15	–1.3	1.45	**1.45**	1.8	135	0.022	145	130	130
14	950	»	»	5	–1.4	1.45	1.6	1.8	138	0.023	150	128	137
15	900	»	North	10	–1.5	1.45	1.6	2.8	145	0.023	159	134	143
16	880	»	»	15	**–1.5**	**1.1**	1.6	2.0	**190**	0.022	175	134	176

Notes. Bold text highlights measured (actual) values.
* Measured or calculated indicator.
** Temperature from depth 35 m.

We were able to measure the temperature in boreholes 7, 9 and 11 only in the layer of annual ground temperature fluctuations, and at the beginning of August 2006, at the deepest point possible for measuring, it was –1.2, –2.0 and –0.9 °C, respectively (Fig. 7). According to the temperature graphs obtained in deep boreholes (5, 8 and 16), minimum temperature values are attributed to depths of 35–40 m. The difference in temperatures between depths 10 and 35–40 m can range from 0.1 to 0.5 °C, which in addition to the topographic features can also be explained by the reaction to changes in the climate conditions in the region [*Zavadskij, 2013*]. This difference was taken into consideration when calculating ground temperatures at a depth of 40 m to draw a permafrost-geothermal section and is reflected in Fig. 8 and in Table 3.

DISCUSSION OF RESULTS

The result of the research is a sublongitudinal permafrost-geothermal profile through the central part of the Ytymdzha Depression (Fig. 8). To calculate the average depth of the permafrost base (Table 3) we used:

– the temperature gradient, obtained during thermal logging in boreholes;

– the average gradient obtained using direct measurements in the permafrost (boreholes 5, 16);

– the expression reflecting the stationary distribution of ground temperature in permafrost:

$$Z = T\frac{\lambda}{q} + 40, \qquad (1)$$

where Z is the calculated thickness of the permafrost, m; T is the temperature at a depth of 40 m, °C; λ is the effective ground thermal conductivity, W/(m·°C); q is the density of the inner heat flux, W/m² [*Carlsaw, Jaeger, 1964*].

The density of the heat flux for each borehole was determined using the formula

$$q = q_0 \cos \alpha, \qquad (2)$$

where q_0 is the starting value of the in-ground heat flux for the area, W/(m·°C); α is the surface slope angle.

Expression (2) reflects the impact of the relief on the heat flux density in the given area [*Balobaev, Levchenko, 1978*]. The starting value of the heat flux in the Ytymdzha Depression was not determined owing to the absence of deep geothermal boreholes. The measurement of the heat flux in the Chulman and Toko depressions allowed us to establish increased values of the in-ground heat flux relative to the rest of the Aldan Shield [*Zheleznyak, 2005*]. To calculate the thickness of the permafrost in the Ytymdzha Depression, we used the initial intensity of the in-ground heat flux q_0 at borehole 16 equal to 0.023 W/m² (Table 4).

Effective thermal conductivity of the strata was determined using material composition of rocks, percentages of rocks in suites and in the section. Thick coal horizons, which can decrease the thermal conductivity of the entire thickness owing to their own low thermal conductivity, have the biggest impact.

All calculated values of the permafrost thickness in borehole locations were used as reference points

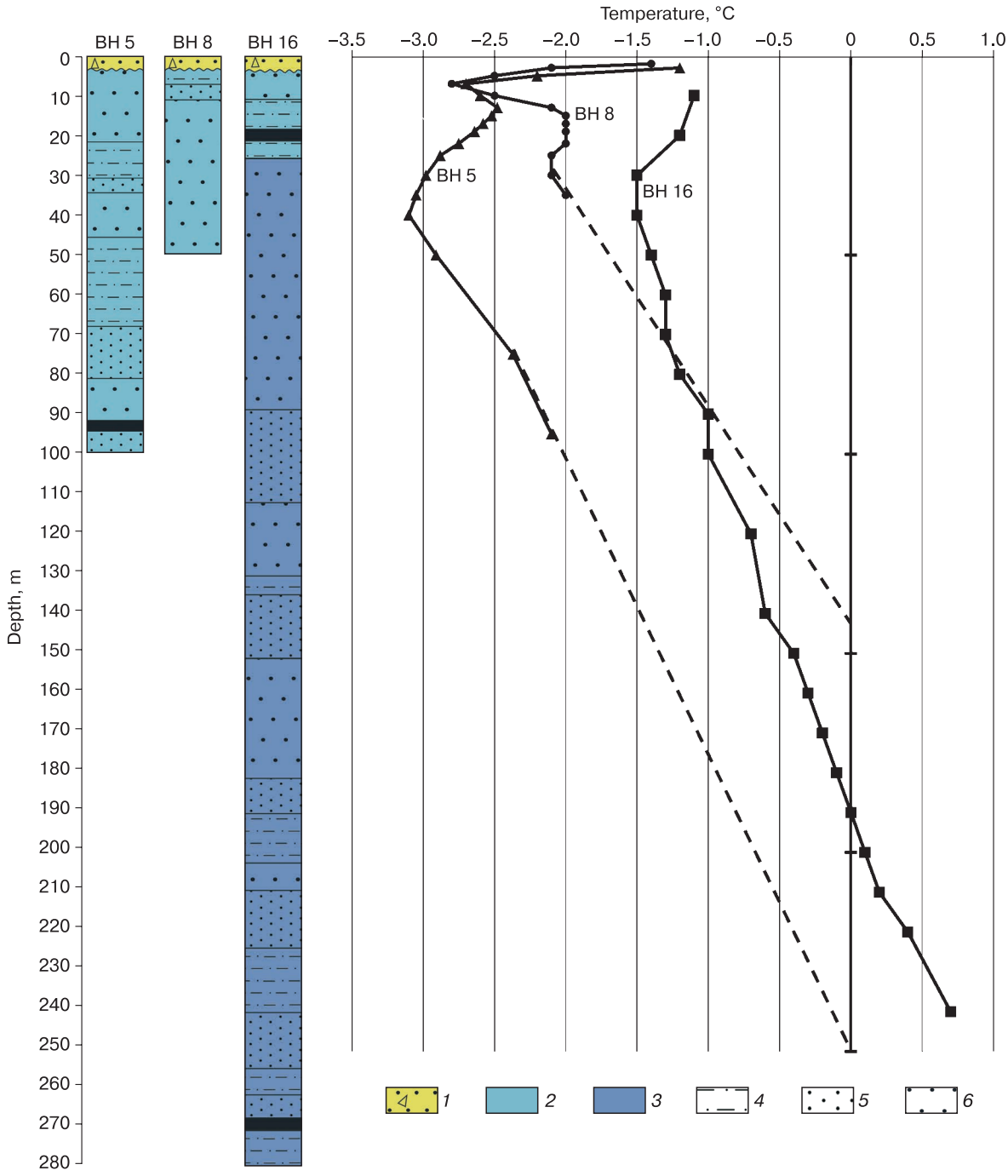

Fig. 6. Rock temperature variation in deep boreholes.

1 – Quaternary deposits; 2 – Kabakta series (J_3kb); 3 – Duray series (J_2dr); 4 – siltstones; 5 – fine-grained sandstone; 6 – medium-grained sandstone. The dashed line corresponds to the gradient temperature increase.

when establishing the permafrost base (Table 3). The permafrost base shown in Fig. 8 is found at minimum depth at the sites of boreholes 9–11. The given area belongs to the south-facing slope and has a thick coal horizon. Such an impact of coal layers on the ground temperature regime has been noted before [*Balobaev et al., 1985b; Gresov et al., 2014; Gao et al., 2017*]. The maximum permafrost thickness is seen in borehole 5, where the steep slope increases the surface area which is involved in heat exchange with the atmosphere, and the north-facing slope decreases the incoming solar radiation.

Table 4. **Temperature and thermophysical rock parameters of borehole 16**

Depth range, m	Rock temperature difference, °C	Gradient*, °C/m	Ground thermal conductivity, W/(m·°C)	Heat flux**, W/m^2
40–50	0.10	0.010	2	0.020
50–60	0.10	0.010	2	0.020
60–70	0.00	0.000	2	0.000
70–80	0.10	0.010	2	0.020
80–90	0.20	0.020	2	0.040
90–100	0.00	0.000	2.1	0.000
100–120	0.30	0.015	2.1	0.032
120–140	0.10	0.005	2	0.010
140–150	0.20	0.020	2	0.040
150–160	0.10	0.010	1.9	0.019
160–170	0.10	0.010	2	0.020
170–180	0.10	0.010	2.2	0.022
180–190	0.10	0.010	2	0.020
190–200	0.10	0.010	2	0.020
200–210	0.10	0.010	2	0.020
210–220	0.20	0.020	2	0.040
220–240	0.30	0.015	2	0.030

* Average value 0.011.
** Average value: 0.02 in permafrost, 0.028 in unfrozen ground, 0.022 in general.

The depth of the permafrost base in the central part of the Ytymdzha Depression provided in archive materials differs from the results obtained by the authors 50–100 m toward the increasing permafrost thickness. This is particularly prominent in borehole 16, where we were able to perform instrumental measurements up to the permafrost base. Here the difference is up to 100 m. According to measurement results, borehole 5 also shows a discrepancy in the current depth of the permafrost base, but the exact difference was not established. Compared to the Chulman and Toko depressions, the studied area has no thawed zones (aside from possible river taliks of the Ytymdzha and Gonam rivers) (Fig. 9). On flat watersheds and south- and west-facing slopes, there are thawed zones in the Chulman Depression [*Belokrylov, Efimov, 1960; Kudryavtsev, 1975*], while a decrease in permafrost thickness is seen in the Ytymdzha Depression under the same landforms. There is no significant difference in permafrost thickness (like in the Toko Depression [*Zheleznyak, 2005*], owing to the undulating terrain of the Ytymdzha Depression not contributing to the change in permafrost base depth.

A temperature inversion of surface air [*Alekseyev, Filosofov, 1970*] which creates a special kind of freezing, presented in the Chulman Depression [*Belokrylov, Efimov, 1960*], is not observed. However, the increase of the permafrost thickness in depressed areas (boreholes 6, 7) indicates a possible effect from the concentration of cold air masses in valleys.

In accordance with the relief, landscape conditions and the measured ground temperature in deep boreholes and the active layer, permafrost distribution in the Ytymdzha Depression is continuous (Fig. 8). Taliks in the Ytymdzha Depression can exist under the riverbeds of the Ytymdzha and Gonam rivers. Islands of *Chosenia* – a regional indicator of thawed ground [*Tyrtikov, 1969*] – are also attributed to them. Icing fields attributed to main rivers' tributaries can locally form zones of discontinuous freezing. A small amount of icing in such a tectonically active

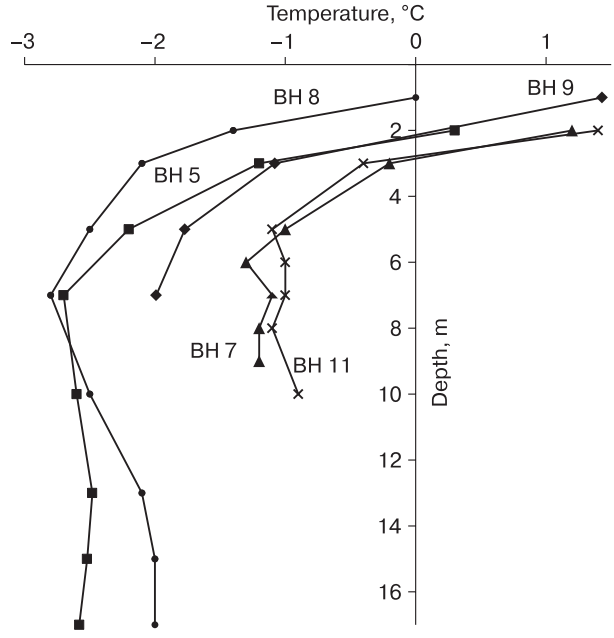

Fig. 7. Ground temperature in the layer of annual temperature fluctuations on 10.08.2006.

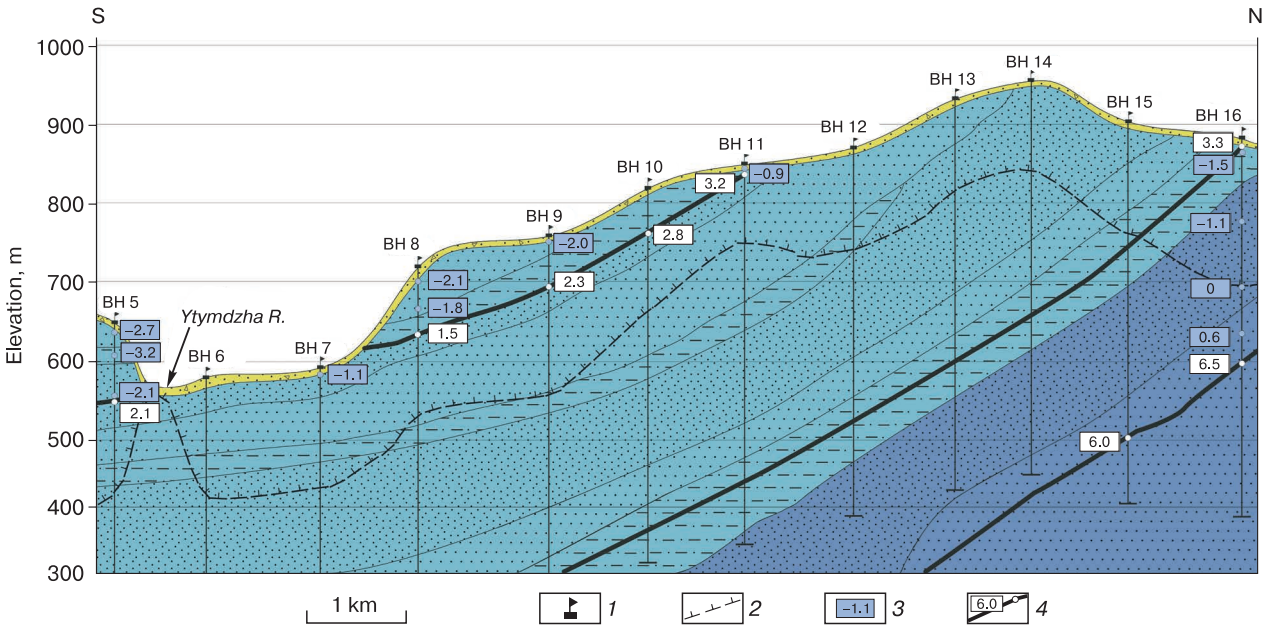

Fig. 8. Sublongitudinal permafrost-geological profile through the central part of the Ytymdzha Depression.

1 – location and number of deep boreholes; 2 – permafrost base according to the results of direct measurements and calculations; 3 – the ground temperature in the borehole, °C; 4 – large coal horizon and its thickness, m. For other symbols see Fig. 6.

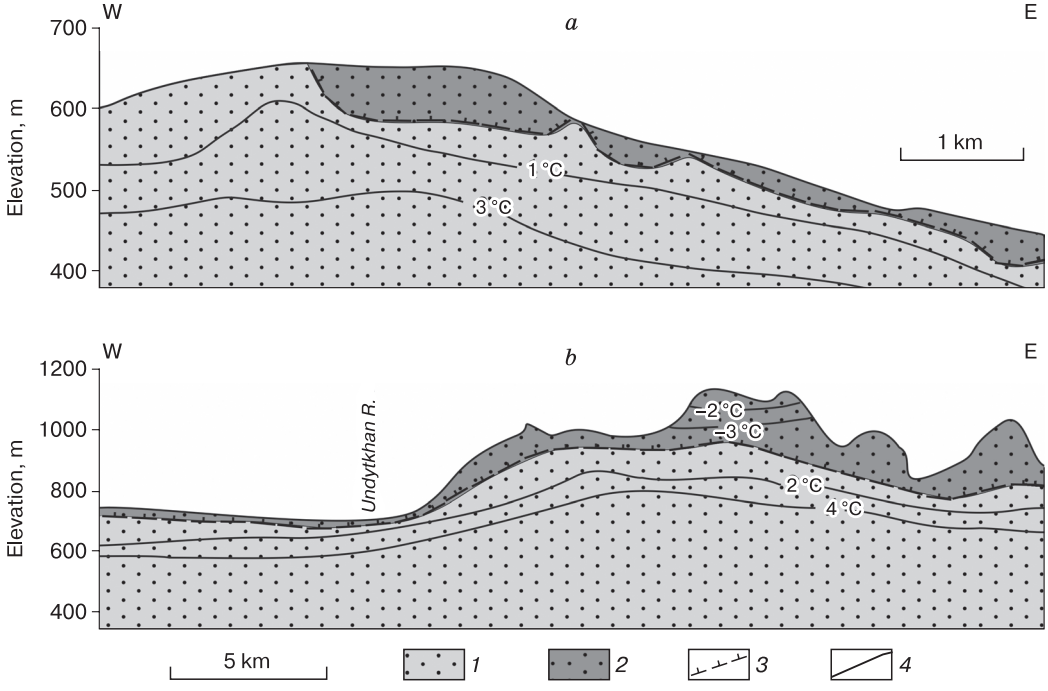

Fig. 9. Permafrost-geothermal sections on the areas of the Chulman (*a*) and Toko (*b*) depressions [Zheleznyak, 2005].

a – Ungra site; b – Elga site; 1 – unfrozen ground; 2 – frozen ground; 3 – permafrost base; 4 – isotherms.

structure indicates backfilling of the majority of cracks, through which underground water unloading can occur [*Fotiev, 1965*].

CONCLUSION

1. Floodplain terraces are characterized by the smallest thickness of the active layer, and within river

terraces (and, possibly, flat watersheds) the ground temperature is maximal.

2. The mean annual ground temperature at a depth of 1 m varies from –1.0 to –4.9 °C. Bogged river terraces are characterized by minimum values, while within river terraces the values are maximal with an average ground temperature rise of up to 4.0 °C per year.

3. Minimum ground temperature below the depth of zero annual amplitude varies from –1.5 to –3.1 °C. The measured geothermal gradient in permafrost equals 1.45 °C/100 m on average. According to a single measurement, the heat flux density in permafrost is 0.02 W/m^2, while in the unfrozen (subpermafrost) zone it increases to 0.028 W/m^2.

4. Based on the performed drilling and geothermal permafrost research, it was determined that the Ytymdzha Depression area has the most severe permafrost conditions among the Mesozoic depressions of the Aldan Shield. Permafrost has a continuous distribution, and its thickness varies from 106 to 251 m, according to calculations.

5. The relief and thermophysical properties of the ground affect the permafrost thickness. In the central part of the Ytymdzha Depression, the minimum depth of freezing is typical for south-facing slopes with a linked large coal horizon.

Acknowledgments. *The authors are grateful to Sergei Ivanovich Serikov for his valuable advice and assistance during the fieldwork.*

The work was carried out within the framework of the budget project AAAA-A20-120111690010-2 "Geothermal field and permafrost strata of the North-East of Russia. Peculiarities of Formation and Dynamics".

References

Alekseyev, V.R., Filosofov, G.N., 1970. Orographic air temperature inversion in Eastern Siberia and its role in the formation of permanently frozen ground. In: Thermal and Water Regime of Some Siberian Regions. Nauka, Leningrad, pp. 102–107 (in Russian).

Balobaev, V.T., Volod'ko, B.V., Devyatkin, V.N. et al., 1985a. Handbook on the application of semiconductor thermocouple thermistors for geocryological measurements. IMZ SO AN SSSR, Yakutsk, p. 48 (in Russian).

Balobaev, V.T., Devyatkin, V.N., Gavriliev, R.I., Rusakov, V.G., 1985b. On geothermophysical studies of minerals in the Northeast. Geologiya i geologorazvedka [Geology and Geological Exploration], No. 1, 36–37.

Balobaev, V.T., Levchenko, A.I., 1978. Geotermicheskie osobennosti i merzlaya zona hr. Suntar Hayata (na primere Nezhdaninskogo mestorozhdeniya). In: Geophysical Research in Siberia. A.V. Pavlova (Ed.). Nauka, Novosibirsk, pp. 129–142 (in Russian).

Belokrylov, I.D., Efimov, A.I., 1960. Permafrost rocks of the zone of iron-ore and coal deposits of South Yakutia. Izd-vo AN SSSR, Moscow, p. 74 (in Russian).

Carlsaw, H.S., Jaeger, J.C., 1959. Conduction of Heat in Solids. Oxford University Press, New York, 510 pp.

Cherepovsky V.F. (Ed.), 2004. Coal Base of Russia. Geoinformmark, Moscow, vol. VI, pp. 419–453 (in Russian).

Ershova, E.D. (Ed.), 1989. Geocryology of the USSR. Central Siberia. Moscow University Press, Moscow, 413 pp. (in Russian).

Fotiev, S.M., 1965. Groundwater and Permafrost of the South Yakutia Coal Basin. Moscow University Press, Moscow, 230 pp. (in Russian).

Gao, S., He, R., Jin, H. et al., 2017. Thermal recovery process of a backfilled open-pit in permafrost area at the Gulian strip coal mine in Northeast China. J. Mountain Science 14 (11), 2212–2229.

Gavriliev, R.I., 2013. Catalogue to Thermal Physical Properties of Mountain Rocks of the North-East of Russia. M.N. Zheleznyak, V.I. Zhizhin (Eds.). IMZ SO RAN, Yakutsk, 172 pp. (in Russian).

Gresov, A.I., Obzhirov, A.I., Yatsuk, A.V., 2014. Geostructural regularities of the distributklns of permafrost in gas- and coal-bearing basins in the North-East of Russia. Kriosfera Zemli [Earth's Cryosphere], XVIII (1), 3–11.

Imaev, V.S., Imaeva, L.P., Koz'min, B.M., 2000. Seismotectonics of Yakutia. GEOS, Moscow, 227 pp. (in Russian).

Konstantinov, P.Ya., Fedorov, A.N., Machimura, T., Iwahana, G., Yabuki, H., Iijima, Y., Costard, F., 2011. Use of automated recorders (data loggers) in permafrost temperature monitoring. Kriosfera Zemli [Earth's Cryosphere], XV (1), 23–33.

Kudryavtsev V.A. (Ed.), 1975. Southern Yakutia. Moscow University Press, Moscow, 443 pp. (in Russian).

Rukovich, A.V., 2018. Geological structure and coal content of the Ytymdzha Depression of the Gonamsky coal-bearing region of the Southern Yakutia coal basin. Uspekhi sovremennogo estestvoznaniya [Advances in Modern Natural Science], No. 12, 200–205.

Semenov, V.P., Zheleznyak, M.N., Kirillin, A.R., Zhizhin, V.I., 2018. Thermal conductivity of sedimentary rocks in the Leno-Viluy oil-and-gas bearing province. Earth's Cryosphere XXII (5), 26–34.

Sherstyukov, A.B., 2008. Correlation of soil temperature with air temperature and snow cover depth in Russia. Kriosfera Zemli [Earth's Cryosphere] XII (1), 79–87.

Tyrtikov, A.P., 1969. Influence of Vegetation Cover on Freezing and Thawing of Soils. Moscow University Press, Moscow, 192 pp. (in Russian).

Zavadskij, F.R., 2013. Evolution of geocryological and hydrological conditions in South Yakutia under the influence of climate change. Diss. ... kand. geol.-min. nauk. Yakutsk, 151 pp. (in Russian).

Zheleznyak, M.N., 2005. Geotemperature field and cryolithozone of the Southeast Siberian platform. Nauka, Novosibirsk, 227 pp. (in Russian).

Zheleznyak, M.N., Lyubomirov, A.S., Pozdnyakov, I.V., 1996. Geocryological conditions of the Toka Depression. In: Proc. of the First Conference of Russian Geocryologists. Moscow University Press, Moscow, book 1, pp. 522–528 (in Russian).

Zhelinsky, V.M., 1980. Mesozoic Coal Formation of Southern Yakutia. Nauka, Novosibirsk, 120 pp. (in Russian).

Zhelinsky, V.M., Korobitsyna, V.N., Karimova, S.S., 1976. Mesozoic Deposits and Genetic Types of Coal Seams of South Yakutia. Nauka, Novosibirsk, 124 pp. (in Russian).

Received February 28, 2021
Revised June 15, 2021,
Accepted September 7, 2021

Translated by M.A. Korkka

EARTH'S CRYOSPHERE
SCIENTIFIC JOURNAL

Earth's Cryosphere, 2021, vol. XXV, No. 6, pp. 34–41 http://earthcryosphere.ru/

GEOLOGICAL CRYOGENIC PROCESSES AND FORMATIONS

THE INVENTORY OF RETROGRESSIVE THAW SLUMPS (THERMOCIRQUES) IN THE NORTH OF WEST SIBERIA BASED ON 2016–2018 SATELLITE IMAGERY MOSAIC

N.B. Nesterova[1], A.V. Khomutov[1,2], M.O. Leibman[1,2], T.A. Safonov[1], N.G. Belova[2,3]

[1] *Tyumen State University, Volodarskogo str. 6, Tyumen, 625003, Russia; n.b.nesterova@utmn.ru*
[2] *Earth Cryosphere Institute, Tyumen Scientific Centre SB RAS, Malygina str. 86, Tyumen, 625026, Russia; akhomutov@gmail.com*
[3] *Lomonosov Moscow State University, Faculty of Geography, Leninskiye Gory 1, Moscow, 119991, Russia; belova@geogr.msu.ru*

Remote sensing methods of retrogressive thaw slumps (RTS) – also called thermocirques (TC) – study include identification of them on vast territories. The satellite imagery mosaics from the Yandex.Maps service covering the Yamal and Gydan peninsulas was innovatively used for this purpose. All RTS (TC) that occurred at the lake coasts were classified as either active or stabilized, the orientation of each RTS (TC) was determined. We identified 86 active and 20 stabilized RTS in the Yamal peninsula and 224 active and 109 stabilized RTS in Gydan. The distribution of RTS orientation was found to be not random. Multiple comparisons of RTS orientation over cardinal compass points showed a statistically significant predominance of the Northern RTS orientation over the Eastern, as well as the Western orientation over the Eastern. At the same time, none of the orientations showed statistically significant predominance over the others. No statistically significant relationship between RTS orientation and RTS activity was found.

Keywords: *thermodenudation, thermocirques, retrogressive thaw slumps, remote sensing, statistics, Yamal, Gydan, Yandex.Maps.*

INTRODUCTION

Thermodenudation is a complex of slope and erosion processes associated with the thawing of exposed permafrost or ground ice [*Kizyakov, 2005*].

Continuous distribution of permafrost and the presence of tabular ground ice [*Baulin et al., 1967; Romanenko et al., 2001*], in combination with the dynamics of the active layer [*Leibman, Egorov, 1996*], contribute to the development of thermodenudation and formation of specific negative landforms [*Voskresensky, 2001; French, 2017*]. In English-language literature, thermodenudation landforms, as well as the process contributing to their development, are described by the term *retrogressive thaw slump* (RTS) [*Burn, Friele, 1989; French, 2017*]. Thermodenudation developing inland differs from that on the seashores by coastal thermoerosion added [*Khomutov, Leibman, 2008*]. In this work, the subject of this study is thermodenudation landforms located inland and confined to lakeshores: thermocirques (TC) or in other words retrogressive thaw slumps (RTS), which, according to the classification of M.O. Leibman and A.I. Kizyakov [*2007*], formed by a complex of cryogenic earth flows of different ages.

RTS or TC have the shape of a crescent depression in the slope, developing polycyclically through activation and stabilization stages, and becoming more active at intervals of several years [*Burn, 2000*]. A characteristic element of the active RTS morphology is the presence of a sub-vertical headwall with ice or ice-rich permafrost exposure, as well as flows of wet material [*Lewkowicz, 1987; Lantuit, Pollard, 2005*]. During the stabilization stage, RTS (TC) stabilize and overgrow [*Burn, Friele, 1989*], while the outline of the headwall of once active RTS is visible in the relief [*Brooker et al., 2014*].

RTS (TC) are under study by both field and remote-sensing methods. Due to their polycyclic nature, it is important to study the long-term dynamics of RTS [*Lewkowicz, Way, 2019*].

An important area of RTS (TC) research method using remote sensing is their inventory: identification of all RTS found in the imagery and the parameters such as orientation, activity status, size, polycyclicity, etc. Multispectral satellite imagery [*Kokelj et al., 2013; Lacelle et al., 2015*], as well as aerial photographs, are used to look for RTS [*Segal et al., 2016*]. Among the methods of direct identification of RTS using imagery, the following can be highlighted:

– visual manual digitization based on characteristic features [*Kokelj et al., 2013; Ramage et al., 2017; Lewkowicz, Way, 2019*];

– automated interpretation of satellite imagery (tasselled cap) [*Brooker et al., 2014*];

– deep learning method [*Huang et al., 2020*].

For further study of identified RTS, regression analysis is often used [*Lacelle et al., 2015; Segal et al., 2016; Ramage et al., 2017*] as well as correlation analysis [*Balser et al., 2014*] testing the influence of various environmental controls on the formation and polycyclic behaviour of RTS. In some works, different activity stages are also considered [*Balser et al., 2014; Ramage et al., 2017*]. A limited number of studies provide data on the RTS orientation or the orientation of the slope with RTS [*Kokelj et al., 2009; Lacelle et al., 2015; Wang et al., 2016*].

There is no database of RTS (TC) distribution in the Arctic, and there are no large-scale maps of the tabular ground ice distribution in the north of West Siberia, while tabular ground ice is a key factor in RTS occurrence in West Siberia. Satellite imagery makes it possible to cover vast areas, identify a large number of RTS and perform statistical processing of their distribution and various parameters. At the same time, the application of satellite imagery not only as commonly used raster files but also as a mosaic of satellite imagery in the background of available online cartographic services has great potential.

This study is aimed at making an inventory of RTS located inland of the peninsulas (RTS on the seacoasts were not considered here) and occurring at lake catchments. It is based on the only freely available mosaic of high-resolution satellite imagery of 2016–2018, presented on the Yandex.Maps online service (http://yandex.ru/maps). Additionally, primary statistical analysis of the relationship between the number of RTS, their activity and orientation was performed. The Yamal and Gydan peninsulas were selected as the study area, field observations of RTS being undertaken at the key sites, while their large-scale inventory was never performed.

STUDY AREA

The study covers the north of West Siberia within an area between 68–72° N and 66–83° E. The study area is an accumulation plain. Further from the coasts in the north of the peninsulas elevations of 35 m above sea level are observed. A significant part of central Yamal is a flat and rolling hills surface with elevations up to 67 m above sea level. The Yuribey Upland along the Gydan coast has elevations up to 87 m above sea level. The Gydan ridge stretches in its central part from southwest to northeast, with elevations up to 127 m above sea level [*Ecological atlas..., 2018*]. The peninsulas are characterized by ravine-gully and small river networks complicated by thermoerosion and thermokarst landforms [*Romanenko, 1997; Gubarkov, Leibman, 2010*]. There are plenty of bogs and lakes. The majority of the lakes are classified as thermokarst and oxbow [*Romanenko, 1997*]. Recent studies have stated the possibility that some lakes result from intense gas emissions [*Dvornikov et al., 2019*].

The territory is characterized by continuous permafrost distribution, permafrost thickness reaches 450 m [*Ershov, 1989*]. The specificity of the studied peninsulas is the widespread tabular ground ice [*Streletskaya et al., 2002*] and its shallow occurrence, which determines the presence of numerous RTS [*Khomutov et al., 2012*].

MATERIALS AND METHODS OF RTS (TC) IDENTIFICATION

The work includes identification of RTS (TC), the status of their activity, RTS orientation, and statistical analysis.

Identification of RTS (TC) and their activity status

The identification of the RTS (TC) located inland and occurring at the lake coasts on the Yamal and Gydan peninsulas was done manually on the Yandex.Maps online service (http://yandex.ru/maps) by creating a point with a spatial reference. We used visual interpretation signs. For each point, information on RTS activity status and orientation was added.

Satellite data for imagery mosaics, available at the online service Yandex.Maps were processed by the SCANEX company using databases: WorldView-2 Data (DigitalGlobe, Inc.), IKONOS Data (Geo Eye, Inc.), TerraColor Data (Earthstar Geographics), IRS Data (ANTRIX Corporation Ltd.), European Space Imaging GmBH data, DigitalGlobe, Inc. and Airbus DS. These databases contain imagery from WorldView-2, IKONOS, Landsat-7, Sentinel, SPOT-1-5 and many others.

The Yandex.Maps service does not provide information on the time and date of the survey, as well as on the satellite model used for specific satellite imagery from the mosaics. This limits the possibilities of detailed analysis, as well as the study of the spectral characteristics of objects, but did not exclude the possibility of identifying RTS by visual interpretation signs. Therefore, the lack of detailed information about the time and date of the survey and satellite model does not seem crucial. At the same time, the People's Yandex.Maps service, which shows the same mosaic of satellite imagery as on the Yandex.Maps service, provides information on the month and year of the survey. Satellite imagery of the study area was taken mainly in July 2017, partially in July 2016, September 2016, June 2017 and September 2017. Our work was carried out after updating the mosaic of satellite imagery presented in the database covering the study area in 2018.

It should be highlighted that objects identified as RTS, were retrieved using imagery presented in the Yandex.Maps service with different spatial resolution ranging from 0.4 to 15 m, mainly up to 2 m. In this regard, only relatively large RTS (with a length

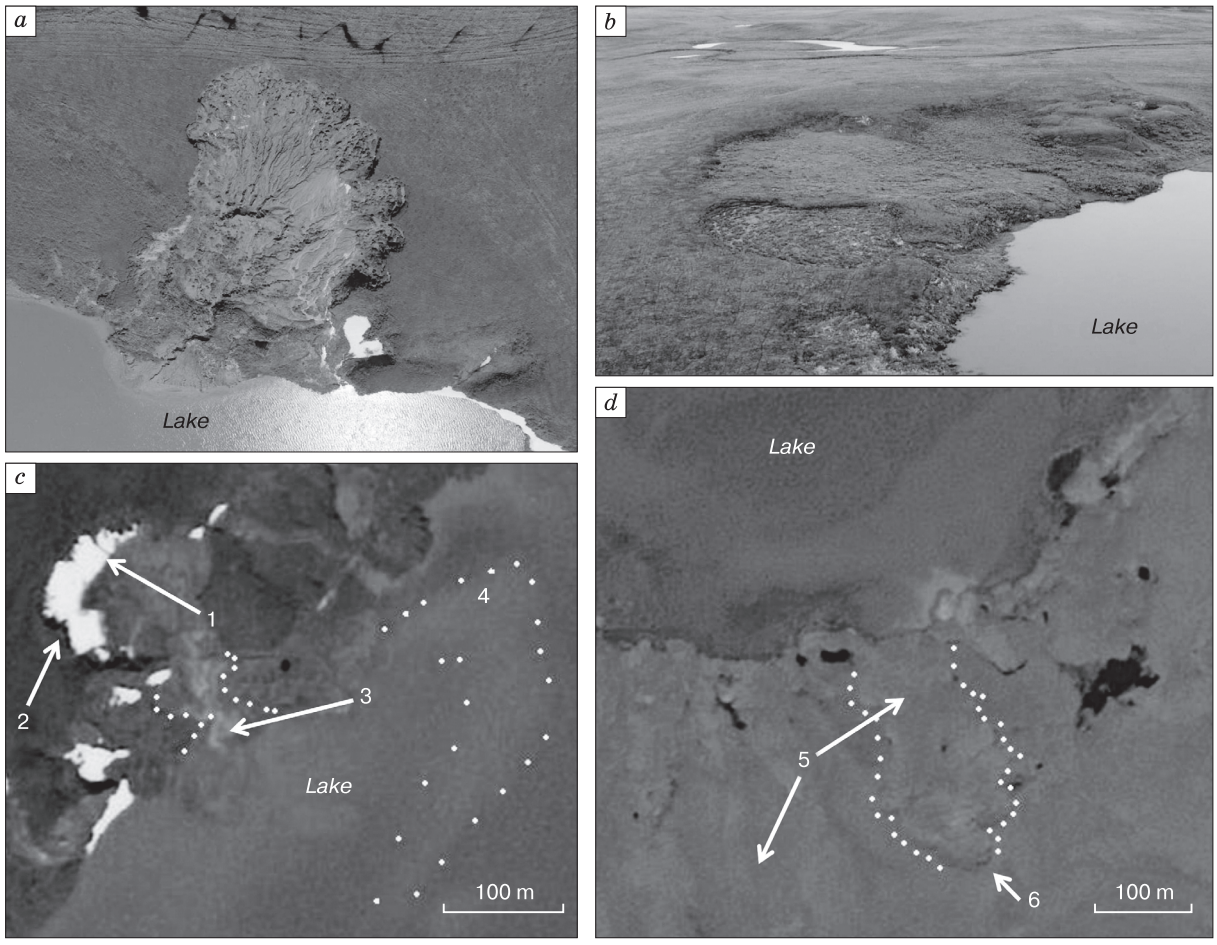

Fig. 1. Examples of RTS (TC) and their visual interpretation signs:

a – an active RTS, a photo taken from an unmanned aerial vehicle (photo by A.V. Khomutov); *b* – stabilized RTS, a photo taken from an unmanned aerial vehicle (photo by A.V. Khomutov); *c* – an active RTS in a mosaic of satellite imagery from Yandex.Maps; visual interpretation signs: *1* – a specific crescent shape, *2* – snow and (or) shadow, outlining RTS headwall, *3* – a flow of thawed grey material (outlined by a dotted line) [*Segal et al., 2016*], *4* – increased water turbidity and a tail of thawed grey material (outlined by a dotted line); *d* – a stabilized RTS in a mosaic of satellite imagery from Yandex.Maps; visual interpretation signs: *5* – RTS colour similar to the colour of the surrounding tundra vegetation; *6* – a noticeable edge of the former headwall (outlined by a dotted line).

and width of at least 20 m) were considered, their identification was doubtless.

RTS (TC) were divided into two groups according to their activity: active and stabilized. Examples of an active and stabilized RTS (TC) on the photos taken from an unmanned aerial vehicle are shown in Fig. 1. Typical visual interpretation signs of active RTS (TC) on satellite imagery are: a crescent shape of a pronounced edge, the presence of a headwall with exposures of permafrost and tabular ground ice, a snowpack or shadow that outlines headwall, flows of thawed material, and the absence of vegetation [*Balser et al., 2014; Brooker et al., 2014; Segal et al., 2016*]. Stabilized RTS (TC) are visually characterized by the absence of a headwall with exposures of permafrost and tabular ground ice (shadow from the scarp), the absence of flows of thawed material (grey colour), the presence of vegetation (green colour), while the relief of the former exposure is noticeable [*Balser et al., 2014; Brooker et al., 2014*]. The interpretation signs of active and stabilized RTS on the mosaic of satellite imagery of the Yandex.Maps service are shown in Fig. 1, *c*, *d*. Partially stabilized RTS with some signs of activity (for example, flows) are classified as active.

To assess the effectiveness of the use of visual interpretation signs, the authors superimposed RTS marked on very-high-resolution satellite imagery available for some areas to RTS on Yandex.Maps service image and received a satisfactory result (Fig. 2).

Further visualization and analysis of the obtained georeferenced point data were performed in the ArcGIS 10.3 program.

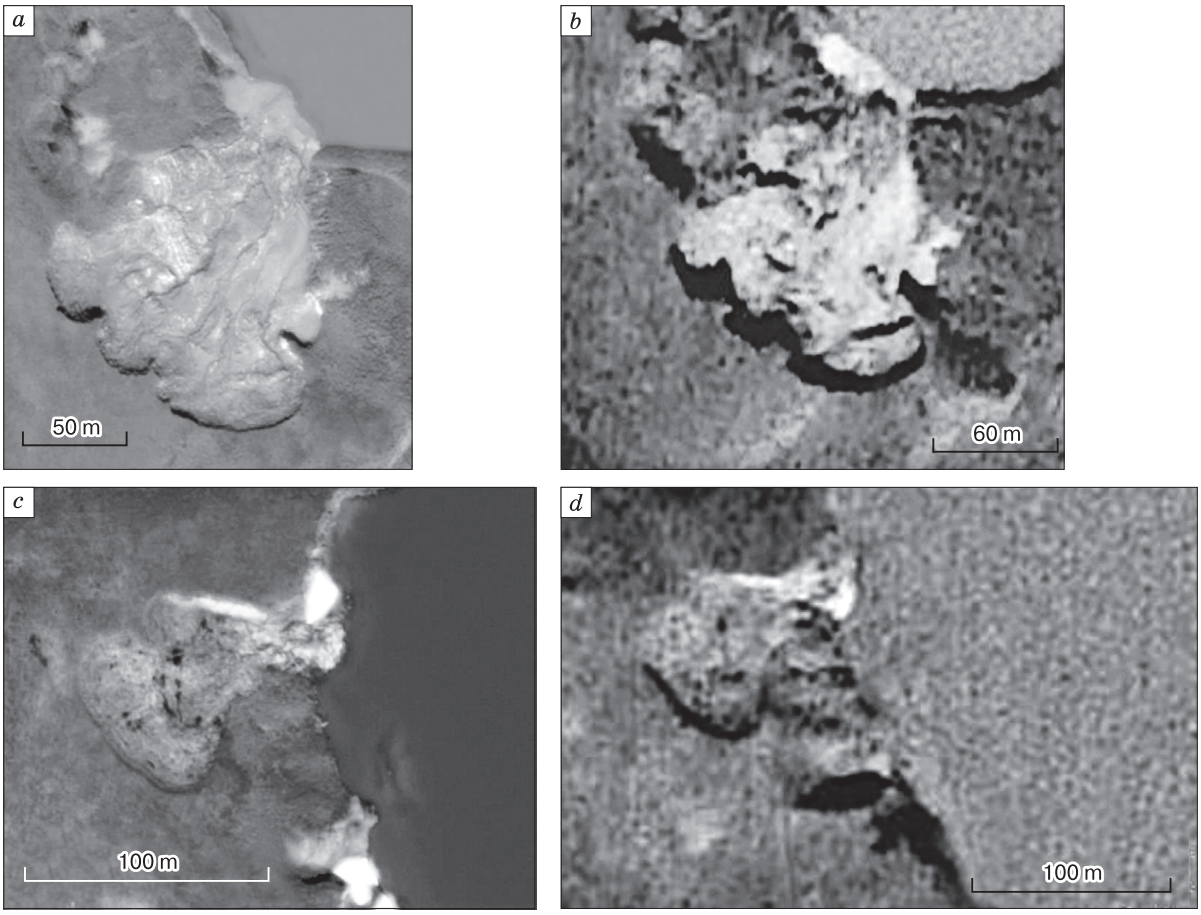

Fig. 2. Examples of an active RTS (*a*, *b*) and a stabilized RTS (*c*, *d*) in the WorldView-2 satellite imagery dated July 10, 2018 (*a*, *c*) and a mosaic of satellite imagery from the Yandex.Maps service, 2018 (*b*, *d*).

RTS orientation and statistical analysis

There is no generally accepted idea of what is RTS orientation. In some studies, RTS orientation is defined as the slope orientation [*Lacelle et al., 2015*], the orientation of the headwall [*Wang et al., 2016*], or as the direction of the normal to the line between two points of intersection of RTS edges with the shoreline of the lake [*Kokelj et al., 2009*]. The authors accepted the last one from [*Kokelj et al., 2009*]. The chosen method allows us to compare our results with the results obtained in the north of Canada (Fig. 3).

RTS orientation initially was determined along 16 points of the compass. For further comparison of the obtained results with the data in [*Kokelj et al., 2009*], orientations were combined into cardinal compass points: N, S, W, and E.

To determine whether the distribution of RTS orientation is random, we used the Pearson's goodness-of-fit test (chi-squared test for equal proportions), which was also applied in [*Kokelj et al., 2009*]. Pearson's goodness-of-fit test is used to assess the correspondence of an empirical distribution to a theo-

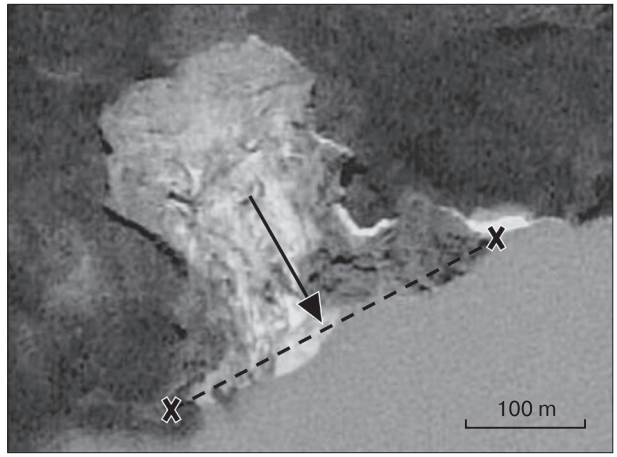

Fig. 3. Visualization of the method for determining RTS orientation [*Kokelj et al., 2009*].

The "X" symbol denotes the point of intersection of RTS edges with the shoreline of the lake, the dashed line connects the two points of intersection, and the arrow is perpendicular to this line (the direction of the arrow is accepted for the RTS orientation).

retical one [*Stepanov, Shavrin, 2005*]. In our case, the theoretical is a uniform distribution. Any statistically significant deviation of the distribution of RTS orientations from the theoretical one is considered uneven, thus, not random.

To determine the regularity of the distribution of RTS orientations over cardinal compass points, and to detect the predominance of one of them over the others, a multiple (pairwise) comparison of exposures with each other was carried out using a test for equal proportions. As a result, Fisher's *z*-test was calculated. This allowed us to calculate the *p*-value with a threshold value of 5 %.

To determine the relationship between activity status and RTS orientation, Pearson's goodness-of-fit test was applied as well.

All statistical tests were performed using RStudio v.1.2.5001 software.

RESULTS AND DISCUSSION

On the Yamal and Gydan peninsulas, 439 RTS were identified on a total area of ~88 thousand km^2, i.e., about 5 RTS per 1000 km^2. On Yamal with a total area of 122 thousand km^2, 106 RTS are located on an area of ~40.8 thousand km^2, i.e., less than 3 per 1000 km^2. On Gydan with a total area of 160 thousand km^2, 333 RTS are found on an area of ~47.2 thousand km^2, i.e., more than 7 per 1000 km^2.

On Yamal, we have identified 86 active and 20 stabilized RTS. On Gydan, 224 RTS active and 109 stabilized RTS were found (Fig. 4).

Since only relatively large RTS were identified, we initially underestimated the total number of RTS of different sizes on both peninsulas. Other researchers also note the likelihood of underestimating the number of RTS during the manual procedure on the imagery of medium spatial resolution [*Lewkowicz, Way, 2019*].

The northernmost RTS on Yamal is located at 70°56′14″ N, the southernmost – at 68°00′55″ N. On Gydan, the northernmost RTS is located at 71°56′25″ N, the southernmost at 69°25′09″ N. The area of RTS distribution is located within the zone where tabular ground ice was observed and described (Fig. 4) [*Streletskaya et al., 2002*], which, along with ice-rich permafrost and ice wedges, determines the occurrence of thermodenudation landforms in this

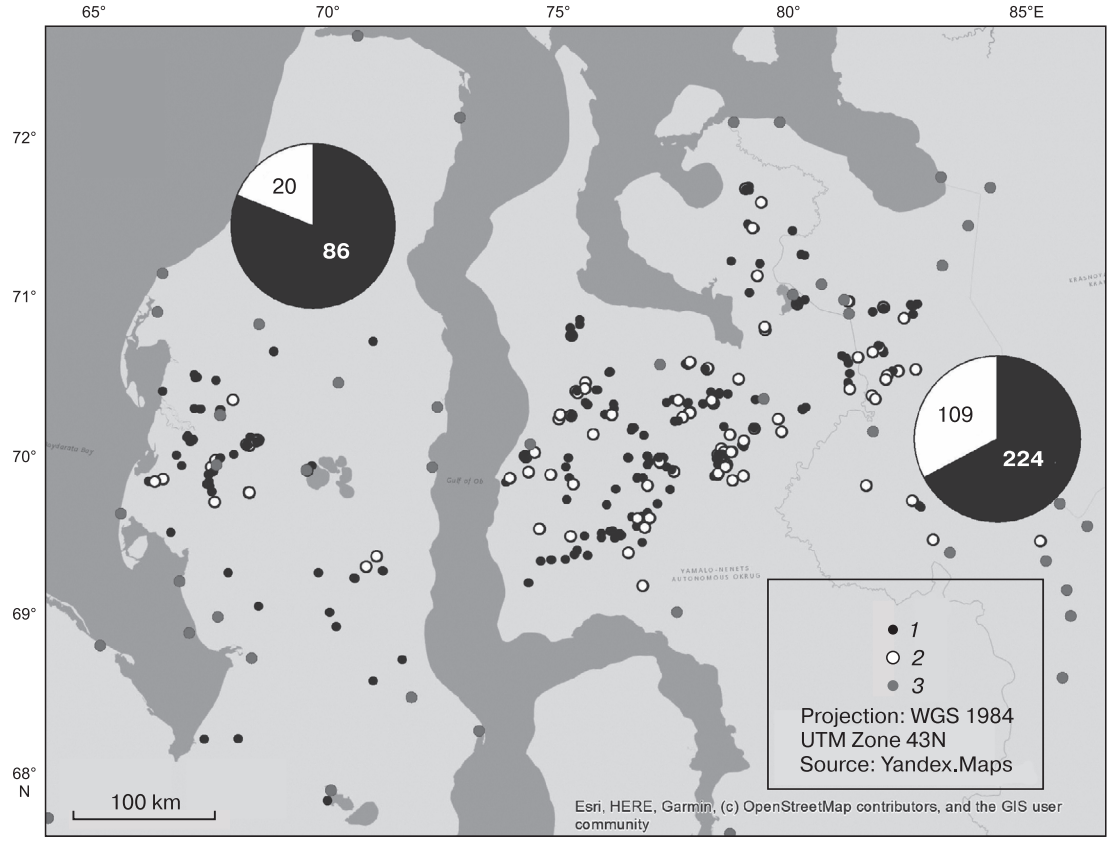

Fig. 4. Distribution of the identified RTS on the Yamal and Gydan peninsulas.

1 – active RTS; *2* – stabilized RTS; *3* – sites of tabular ground ice occurrence, indicated in the publications of the "Massive ice" database [*Streletskaya et al., 2002*]. The pie charts show the number of identified RTS of the different activity statuses on the Yamal and Gydan peninsulas.

region. The presence of tabular ground ice in the north of the Yamal Peninsula does not lead to the development of RTS due to a significant decrease in the terrain elevations there.

The predominance of active RTS on both peninsulas shows that in 2016–2018 thermodenudation processes were actively progressing in the study area (Fig. 4). This is consistent with the results of field studies in this area [*Khomutov et al., 2017*].

The distribution of RTS orientation for Yamal and Gydan is shown in Fig. 5.

In general, for both peninsulas, the statistical test showed that at the 5 % significance level, the distribution of RTS orientations over cardinal compass points is not random. This conclusion is consistent with the results obtained in the study by S. Kokelj et al. [*2009*] discussing the distribution of 530 RTS (both active and stabilized) in the highlands east of the Mackenzie River (northern Canada). In our study, none of the RTS orientations was determined as statistically predominant over all the others. It should be highlighted that multiple comparisons of RTS orientations showed a statistically significant predominance of northern orientation over eastern, as well as a western orientation over eastern. There is also no correlation at the 5 % level of significance between the RTS orientation in total on both peninsulas and the status of RTS activity.

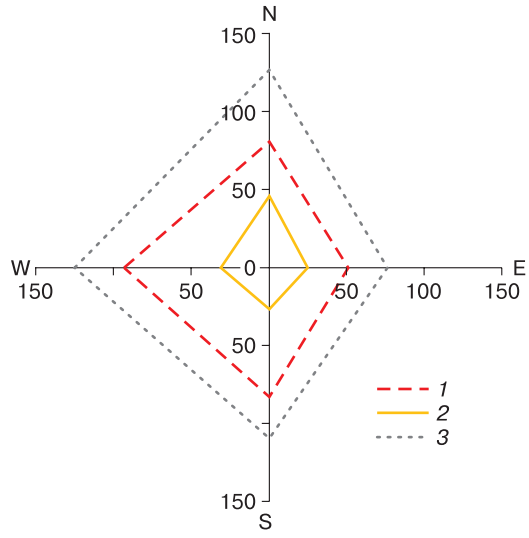

Fig. 5. Distribution of RTS orientation by cardinal compass points in Yamal and Gydan.

Number of RTS: *1* – active, *2* – stabilized, *3* – total active and stabilized.

From the given sample on each of the peninsulas, differences in the distribution of orientations of active and stabilized RTS were revealed. Despite the

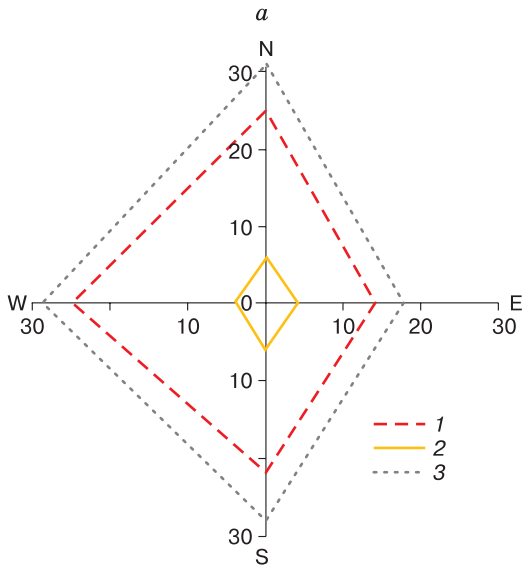

Yamal

Cardinal direction	Number of RTS		
	1	*2*	*3*
N	25	6	31
E	14	4	18
S	22	6	28
W	25	4	29

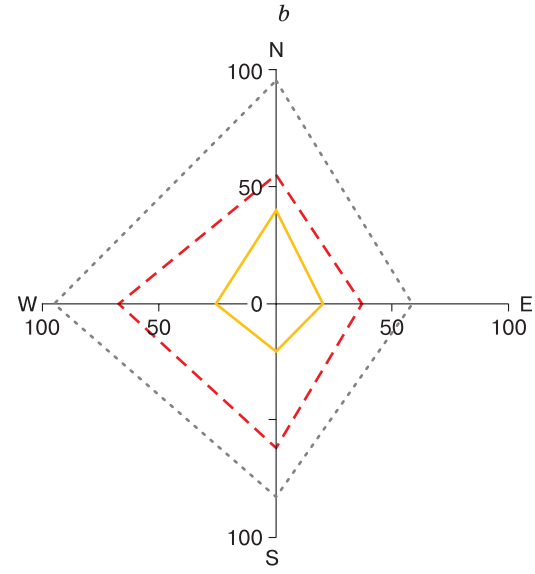

Gydan

Cardinal direction	Number of RTS		
	1	*2*	*3*
N	56	40	96
E	38	21	59
S	62	21	83
W	68	27	95

Fig. 6. Distribution of RTS orientation by cardinal compass points in Yamal (*a*) and Gydan (*b*).

For legend see Fig. 5.

similar distribution of orientations of all RTS on both peninsulas (Fig. 6), active RTS on Yamal have predominant northern, western, and southern orientations, and on the Gydan Peninsula – southern and western. For the stabilized RTS on Yamal, there is no prevailing orientation, and for Gydan, it is clearly defined to face the north.

Similar studies showed that in northwestern Canada (Richardson Ridge and Peel Plateau), eastern orientations prevail for 212 RTS observed [*Lacelle et al., 2015*]. In northwestern Canada (the Mackenzie River delta), the prevailing orientation of RTS was identified as northern [*Kokelj et al., 2009*], and a study of 18 RTS located in northern Canada demonstrated that RTS development was not related to slope orientation [*Wang et al., 2016*].

Such ambiguous results concerning the prevalence of any RTS orientation with different activity statuses are probably related to the presence of other driving factors that were not considered in this paper. Such factors can be geological and geocryological features (ice content in permafrost, depth to the tabular ground ice, distribution of active layer thickness on slopes of different orientations); climatic controls (thickness of snow on slopes of different orientations, duration of sunshine, wind direction); geomorphology (predominance in the particular orientation of slopes in the study area); biogeographic characteristics (shrub height) of RTS sites. All these factors are to be considered in a further much more detailed study of the RTS distribution in the north of West Siberia.

CONCLUSION

In this work, the method of visual identification of RTS (TC) based on a mosaic of publicly available satellite imagery of the Yandex.Maps cartographic service was successfully applied for the first time to the area of the Yamal and Gydan peninsulas.

As a result, 439 RTS were discovered: 106 RTS located on Yamal (86 active and 20 stabilized), and 333 RTS located on Gydan (224 active and 109 stabilized).

The northernmost and southernmost RTS identified on the Yamal Peninsula are located at 70°56′14″ N, and 68°00′55″ N, respectively, and identified on the Gydan Peninsula, at 71°56′25″ N, and 69°25′09″ N, respectively.

The revealed predominance of active RTS is consistent with the results of the field studies of the authors who reported the intensification of thermodenudation in recent years in connection with the extreme climatic events of 2012 and 2016.

The primary statistical analysis of RTS orientation showed: 1) non-random distribution of RTS orientations with a significance level of 5 %, while none of the directions was noted as prevailing over all the others, in other words, there was no dominant RTS orientation found; 2) the absence of a statistically significant relationship between RTS orientation and the status of their activity.

The results are partially consistent with the results of studies in the north and northwest of Canada, where thermodenudation processes are widespread, and the differences are probably related to the regional geological-geomorphological, geocryological, cryolithological, environmental and climatic characteristics of the study area.

The results obtained demonstrate the widespread distribution of RTS in the study area, and their successful inventory based on publicly available remote sensing materials provides a basis for their further multifactorial research.

Acknowledgements. *This work was carried out with partial financial support from the Russian Foundation for Basic Research within the framework of scientific project No. 18-05-60222. Methodological approaches were developed when performing work on state assignment No. 121041600042-7.*

References

Balser, A.W., Jones, J.B., Gens, R., 2014. Timing of retrogressive thaw slump initiation in the Noatak Basin, northwest Alaska, USA. J. Geophys. Research: Earth Surface, CXIX (5), 1106–1120.

Baulin, V.V., Belopukhova, E.B., Dubikov, G.I., Shmelev, L.M., 1967. Geocryological Conditions of Western Siberia Lowland. Nauka, Moscow, 214 pp. (in Russian).

Brooker, A., Fraser, R.H., Olthof, I. et al., 2014. Mapping the activity and evolution of retrogressive thaw slumps by tasselled cap trend analysis of a Landsat satellite image stack. Permafrost and Periglacial Processes XXV (4), 243–256.

Burn, C.R., 2000. The thermal regime of a retrogressive thaw slump near Mayo, Yukon Territory. Can. J. Earth Sciences, XXXVII (7), 967–981.

Burn, C.R., Friele, P.A., 1989. Geomorphology, vegetation succession, soil characteristics and permafrost in retrogressive thaw slumps near Mayo, Yukon Territory. Arctic, XLII (1), 31–40.

Dvornikov, Y.A., Leibman, M.O., Khomutov, A.V. et al., 2019. Gas emission craters of the Yamal and Gydan peninsulas: A proposed mechanism for lake genesis and development of permafrost landscapes. Permafrost and Periglacial Processes XXX (3), 146–162.

Ecological Atlas of the Yamalo-Nenets Autonomous Okrug: results of scientific research, state, dynamics, forecast, 2018. E.V. Aghbalyan, R.I. Idrisov, A.V. Dobryakova (Eds.). Tyumen University Press, Tyumen, 116 pp. (in Russian).

Yershov E.D. (Ed.), 1989. Geocryology of the USSR. Western Siberia. Nedra, Moscow, 454 pp. (in Russian).

French, H.M., 2017. The periglacial environment. John Wiley & Sons, Hoboken, NJ, 544 pp.

Gubarkov, A.A., Leibman, M.O., 2010. Bead-shaped channel forms as evidence of paragenesis of cryogenic and hydrological processes in the small-river valleys of Central Yamal. Kriosfera Zemli [Earth's Cryosphere], XIV (1), 41–49.

Huang, L., Luo, J., Lin, Z. et al., 2020. Using deep learning to map retrogressive thaw slumps in the Beiluhe region (Tibetan Plateau) from CubeSat images. Remote Sensing of Environ. CCXXXVII, p. 111534.

Khomutov, A.V., Leibman, M.O., 2008. Landscape controls of Thermodenudation rate change on Yugorsky peninsula coast. Kriosfera Zemli [Earth's Cryosphere], XII (4), 24–35.

Khomutov, A.V., Leibman, M.O., Andreeva, M.V., 2012. Mapping of ground ice in Central Yamal. Vestnik Tumenskogo gosudarstvennogo universiteta [Tyumen State University Herald], No. 7, 76–84.

Khomutov, A., Leibman, M., Dvornikov, Y. et al., 2017. Activation of cryogenic earth flows and formation of thermocirques on central Yamal as a result of climate fluctuations. In: Workshop on World Landslide Forum. Cham, Springer, pp. 209–216.

Kizyakov, A.I., 2005. The dynamics of thermodenudation processes at the Yugorsky Peninsula coast. Kriosfera Zemli [Earth's Cryosphere], IX (1), 63–67.

Kokelj, S.V., Lacelle, D., Lantz, T.C. et al., 2013. Thawing of massive ground ice in mega slumps drives increases in stream sediment and solute flux across a range of watershed scales. J. Geophys. Research: Earth Surface, CXVIII (2), 681–692.

Kokelj, S.V., Lantz, T.C., Kanigan, J. et al., 2009. Origin and polycyclic behaviour of tundra thaw slumps, Mackenzie Delta region, Northwest Territories, Canada. Permafrost and Periglacial Processes XX (2), 173–184.

Lacelle, D., Brooker, A., Fraser, R.H., Kokelj, S.V., 2015. Distribution and growth of thaw slumps in the Richardson Mountains–Peel Plateau region, northwestern Canada. Geomorphology CCXXXV, 40–51.

Lantuit, H., Pollard, W.H., 2005. Temporal stereophotogrammetric analysis of retrogressive thaw slumps on Herschel Island, Yukon Territory. Natural Hazards and Earth System Sciences, V (3), 413–423.

Leibman, M.O., Egorov, I.P., 1996. Climatic and environmental controls of cryogenic landslides, Yamal, Russia. In: International Symposium on landslides terrain (Trondheim, June 17, 1996), Trondheim, Norway, pp. 1941–1946.

Leibman, M.O., Kizyakov, A.I., 2007. Cryogenic landslides of the Yamal and Yugorsky Peninsulas. IKZ SO RAN, Moscow, 206 pp. (in Russian).

Lewkowicz, A.G., 1987. Headwall retreat of ground-ice slumps, Banks Island, Northwest Territories. Can. J. Earth Sciences, 1987, 24 (6), 1077–1085.

Lewkowicz, A.G., Way, R.G., 2019. Extremes of summer climate trigger thousands of thermokarst landslides in a High Arctic environment. Nature Communication, X (1), 1–11.

Ramage, J.L., Irrgang, A.M., Herzschuh, U. et al., 2017. Terrain controls on the occurrence of coastal retrogressive thaw slumps along the Yukon Coast, Canada. J. Geophys. Research: Earth Surface, CXXII (9), 1619–1634.

Romanenko, F.A., 1997. Formation of lake basins on the plains of Arctic Siberia: Abstract of PhD thesis, Moscow, 25 pp. (in Russian).

Romanenko, F.A., Voskresensky, K.S., Tarasov, P.E. et al., 2001. Peculiarities of formation of relief and sediments West Yamal and Baidaratskaya Bay cost (Kara Sea). In: Problems of General and Applied Geoecology of the North. Moscow University Press, Moscow, pp. 41–68 (in Russian).

Segal, R.A., Lantz, T.C., Kokelj, S.V., 2016. Acceleration of thaw slump activity in glaciated landscapes of the Western Canadian Arctic. Environ. Res. Letters, XI (3), 034025.

Stepanov, M.N., Shavrin, A.V., 2005. Statistical Methods of Processing Mechanical Test Results. Mashinostroenie, Moscow, 399 pp. (in Russian).

Streletskaya, I.D., Ukraintseva, N.G., Drozdov, I.D., 2002. Tabular ground ice of the Arctic. A digital database. Vestnik Moskovskogo Universiteta. Seria 5. Geografia [Moscow University Bulletin. Series 5. Geography], No. 3, 7–13.

Voskresenskij, K.S., 2001. The Modern Relief-Forming Processes on Plains of the Northern Russia. Moscow University Press, Moscow, 262 pp. (in Russian).

Wang, B., Paudel, B., Li, H., 2016. Behaviour of retrogressive thaw slumps in northern Canada–three-year monitoring results from 18 sites. Landslides XIII (1), 1–8.

URL: http://yandex.ru/maps (last visited: 18.08.2019).

Received December 28, 2020
Revised September 15, 2021
Accepted October 14, 2021

Translated by N.B. Nesterova

EARTH'S CRYOSPHERE
SCIENTIFIC JOURNAL

Earth's Cryosphere, 2021, vol. XXV, No. 6, pp. 42–51 http://earthcryosphere.ru/

SURFACE AND GROUND WATERS IN TERRESTRIAL PERMAFROST REGION

ASSESSMENT OF THE AMOUNT OF WINTER PRECIPITATION IN MOUNTAIN BASINS AND THEIR INFLUENCE ON FLOOD FORMATION (CHARYSH AND ANUY RIVER BASINS, ALTAE AS A CASE STUDY)

V.P. Galakhov[1], S.Yu. Samoilova[1], E.V. Mardasova[2]

[1]*Institute for Water and Environmental Problems, SB RAS, Molodezhnaya str. 1, Barnaul, 656038, Russia*
[2] *Altai State University, Lenina ave. 61, Barnaul, 656049, Russia; galahov@iwep.ru*

The paper presents an estimate of the annual precipitation amount for the winter period (1967–2006) in the basins of the Charysh and Anuy mountain rivers. A kinematic model for air mass movement when crossing orographic barriers is used for calculations. The initial data are monthly precipitation totals (November–March) obtained from meteorological stations and gauges located within the basins and at the adjacent territory. Based on the single-factor dependencies and multiple correlation/regression analysis, we assess the dependences of melt runoff depth on total precipitation for winter and flood (April–June) time periods in the gaging stations "Charyshsky state farm" on Charysh River and "Anuysky state farm" – on Anuy.

Keywords: *Altai, Charysh River, Anuy River, winter precipitation, high water, runoff depth.*

INTRODUCTION

Climatic changes in the last decade have had a significant impact on the water regime of high and middle-latitude rivers, especially during high water. This is primarily due to a change in the amount of solid sediments, a shifting of the periods and a decrease in the duration of snow cover [*Barnett et al., 2005; DeWalle, Rango, 2008; Shiklomanov, 2008*]. An increase in temperatures during the cold period and, as a consequence, a decrease in the depth of seasonal soil freezing cause an increase in water content in the low season and a decrease in melt runoff in spring due to infiltration losses [*Shiklomanov, 2008; Kalyuzhny, Lavrov, 2012*].

There has been a decrease in the annual flow rate of rivers up to 5–22 % in the rivers of the Ob basin since the 1970s [*Shiklomanov, 2008*]. At the same time, the frequency of unfavorable hydrological processes associated with flooding of the settlements during high water and rain floods [*Puzanov et al., 2018*].

The main task for hydrological forecasts is to estimate snow reserves in the catchment basin since up to 70 % of the flood runoff is formed by the meltwater [*Apollov et al., 1974*]. Traditionally, in hydrological studies, the amount of precipitation in mountainous areas is linked to the absolute height of observation points [*Kharshan, 1970; Revyakin, Kravtsova, 1977; Mukhin, 2013*]. In recent decades, snow storage distribution models have been used, including a number of terrain characteristics (height, slope aspect, slope gradient, distance to the orographic barrier, etc.) [*Li et al., 2015; Samoilova, Galakhov, 2020*], as well as landscapes [*Gensiorovsky, 2007*], or combination of these parameters [*Lubenets, Chernykh, 2019*]. This approach is successful when the data from snow-amount surveys are used.

Remote sensing methods are widely used, but in mountainous areas, they give satisfactory results only together with field observations [*Iglovskaya, Narozhny, 2010; Romasko, Burakov, 2017; Churyulin et al., 2018*].

A network of instrumental observations in Altai does not cover the watershed areas and slopes of mountain ranges where maximum snow reserves form.

This work is part of a study on the assessment of snow reserves and forecasting of flood runoff in mountain rivers of the Upper Ob basin. The previously developed methodology [*Galakhov, 2003*] makes it possible to estimate the amount of winter precipitation in mountain basins under the lack of hydrometeorological information. The technique has been successfully used in hydrological calculations and medium-term forecasts of water levels in the Charysh River [*Galakhov et al., 2016, 2018*]. In spite of the fact that the volume of the flood and the maximum water levels depend on the same factors (water reserves in the snow cover, liquid precipitation of the flood and the water absorption capacity of the basin) [*Popov, 1979*], their relationship is not always unambiguous. The intensity and course of snowmelt in the basin have a substantial influence on the formation of levels, and, as a result, the rate of the meltwater flow into the river network, as well as congestions.

In this paper, we assess winter precipitation in the basins of the Charysh and Anuy rivers using the author's model of the snow reserve distribution in complex orography conditions. To verify the simulation results, the relationship between the amount of winter precipitation and the flood volume expressed in the runoff layer is analyzed.

STUDY OBJECTS

Two basins of the Charysh and Anuy rivers (Fig. 1), the 1st order left tributaries of the Ob River, which are located within the Altai Mountainous region, were selected as study objects. Both basins are located on the northern macro slope of the Altai Mountainous region and have absolute heights of 150–200 m in the lower course, up to 2000–2300 m and more in the upper course (Fig. 1).

The basin of the Charysh River. The source of the Charysh River is located at the junction of the Korogonsky and Seminsky ridges at an altitude of 1800 m. From the north, the basin is bounded by the Bashchelak ridge, from the south by the Tigiretsky and the Korgonsky ranges of the northern Altai (1800–2300 m). The basin area is 22 000 km^2, the length of the river is 547 km, and the average slope is 3 ‰. Conventionally, the basin can be divided into two parts: mountainous down to the village of Karpovo (13 900 km^2) and foothill part (smaller in the area). Close to the gaging station "Charyshsky state farm", the Charysh River basin has an area of 20 700 km^2, and its average height is 750 m. The woodiness of the basin is 15 %. The average long-term flow rate is 193 m^3/s, the maximum is 2650 m^3/s (1958). The flood is multi-peak. As a rule, it lasts from the end of March to the second decade of July with a maximum in late May-early June. The share of flood runoff in annual runoff is 51–84 % [*Surface, 1975*].

The Anuy River basin is bounded by the Baschelaksky ridge to the west and by the Anuy ridge to the east. The length of the river is 327 km, and the total area of the basin is 6930 km^2. The catchment area up to the gaging station "Anuysky state farm" is 4870 km^2, the average height of the catchment is 790 m, and the average slope of the river is 5.1 ‰. The woodiness of the basin is 20 %. The average long-term flow rate is 31.1 m^3/s, the maximum is 462 m^3/s (1966). The flood is multi-peak, lasts from the end of March to the end of June, and reaches its maximum in the third decade of April. On average, 42 to 73 % of

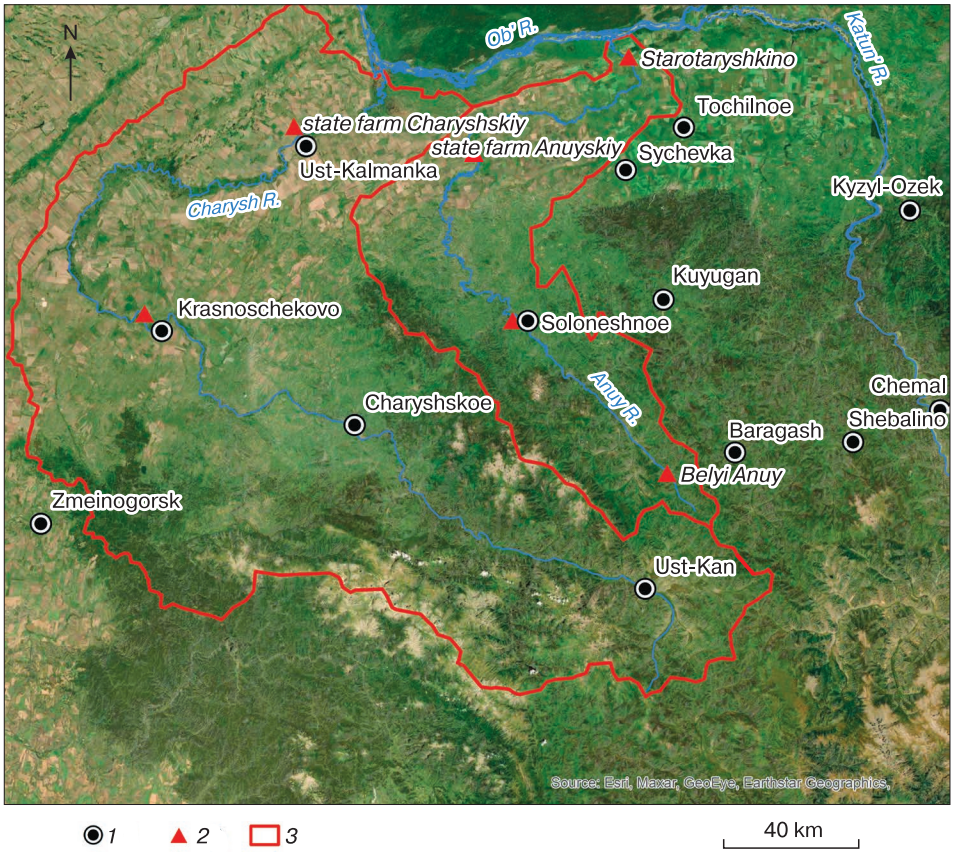

Fig. 1. Basins of the Charysh and Anuy rivers.

1 – hydrometeorological stations and posts; *2* – hydrological posts; *3* – borders of the Charysh and Anuy river basins.

the annual runoff passes during the flood [*Suface, 1975*]. In contrast to the basin of Charysh river, the catchment area of the Anuy River to the gaging station "Anuysky state farm" is entirely comprised by low mountains and middle mountains, there is a foothill plain downstream with an area of about 2,000 km^2.

RESEARCH METHODS AND INITIAL DATA

Traditionally in hydrological studies, the amount of precipitation is linked to the absolute height of observation points [*Kharshan, 1970; Revyakin, Kravtsova, 1977; Mukhin, 2013*]. The verification of this pattern in the basins of the Charysh and Anuy rivers has revealed the absence of a statistically significant relationship between winter precipitation and an absolute altitude in most years [*Galakhov et al., 2020*]. In addition, the highest weather station in the Charysh River basin is Ust-Kan (1037.4 m), in the Anuy River basin the highest is Kuyagan post (560 m), and the maximum absolute heights in the basins reach 2000 m or more. Thus, it is impossible to interpolate annual winter precipitation in the studied basins based on their dependence on absolute height.

Estimation of precipitation amounts for the cold period using an orographic additive to the speed of the air-mass vertical movements. The influence of mountains on atmospheric fronts is diverse. It is manifested through the detention of atmospheric fronts, the change in the speed of a particular front section movement, the aggravation of fronts, formation of frontal waves in the front of the windward side of the ridge and the erosion of frontal zones when they pass over the ridges. Quite a peculiar is a process associated with the circumference of the frontal zone of an orographic obstacle [*Shakina, 1985; Galakhov, 2003*].

It is known that the intensity of precipitation depends on the speed of the air flow vertical movements [*Rogers, 1979*]. It is very difficult to determine the speed of vertical movements due to the processes occurring in the cloud mass itself. But it is possible to determine the addition to the speed of vertical movements of air masses (i.e., the change in the speed of vertical movements of air masses due to the orography) during the formation of solid precipitation using fairly simple kinematic models.

Earlier the authors have developed a simplified kinematic model of the distribution of solid precipitation in the complex orography based on the principles of the movement of air flows skirting an obstacle or passing over it, described in [*Barry, 1964; Rogers, 1979; Skorer, 1980; Matveev, 1981, 1984*]. It requires a minimum set of input data, including the absolute height of the underlying surface, taken from the topographic base map with a certain grid spacing, the speed and direction of the upcoming atmospheric fronts, as well as the temperature of the surface air layer taken from the aerological station records. The algorithm and a detailed description of the model are published in [*Galakhov, 2003*]. This method of calculation is applicable only to winter conditions when the temperature of the underlying surface is negative and more or less uniform, additionally, in the conditions of low and medium-height mountains (elevations no more than 2 km). In the studied basins, this condition is generally satisfied.

Based on this model, a territory matrix with a grid spacing of 25 × 25 km is created for the basins of the Anuy and Charysh rivers. In the lower-left corner of each grid cell, average orographic additives to the speed of air-mass vertical movements during the formation of solid precipitation were calculated (Fig. 2), and for the rest of the area they were determined by interpolation. The values of the orographic additive for the research area vary from −1 m/s (Ust-Kansk basin) to 0.75 m/s or more (the area of Zmeinogorsk) and depend, first of all, on the slopes of the surface, the absolute height of the terrain, as well as the speed and direction of the flows of the prevailing air masses [*Galakhov, 2003*]. This matrix allows to interpolate precipitation data from weather stations and posts for the entire territory of the basin, taking into account the orographic additive.

The calculation of the average amounts of winter precipitation in the basin was carried out as follows. At the initial stage, the amount of winter precipitation X was determined for each year at meteorological stations and posts located within the studied basins and on the adjacent territory. The sum of winter precipitation is taken as the sum of precipitation from November 1 to March 31. Data sources are meteorological monthly and materials of the websites of Roshydromet (http://aisori.meteo.ru/) and "Weather and Climate" (http://www.pogodaiklimat.ru). The research period was determined by the availability of meteorological monthly reports and data on surface runoff, which were later used for "hydrological control".

Further, based on the obtained values of X and the orographic additive to the speed of vertical movements of V_z in the area of weather stations, a dependence of $X = f(V_z)$ was constructed.

Then, the average amount of winter precipitation in the cells was estimated using the obtained regression equations $X = f(V_z)$ and the orographic addition of V_z in each grid cell of the matrix (Fig. 2).

For the Charysh River basin, the period 1967–1981 was analyzed, including years with extreme water content: 1969 was close to a maximum, 1974 was close to a minimum, as well as the period 1993–2001 and 2006. The list of meteorological stations, their absolute heights, as well as the values of the orographic additive and the average long-term precipitation for the winter months are presented in Table 1.

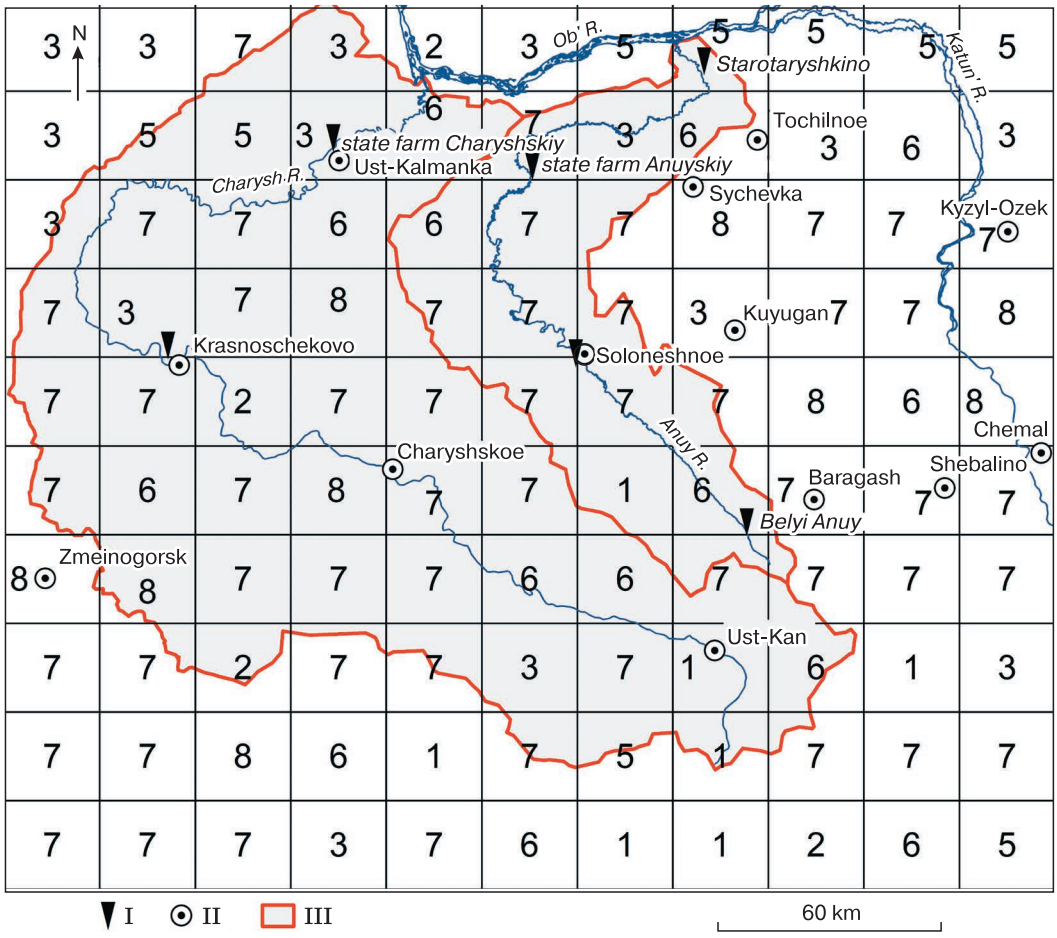

Fig. 2. Matrix of orographic additive to the speed of vertical movements of air masses in the basins of the Charysh and Anuy rivers.

1 – from −1.0 to −0.5 m/s; 2 – from −0.5 to −0.1 m/s; 3 – from −0.1 to −0.01 m/s; 4 – from −0.01 to 0 m/s; 5 – from 0 to 0.01 m/s; 6 – from 0.01 to 0.1 m/s; 7 – from 0.1 to 0.5 m/s; 8 – from 0.5 to 1.0 m/s m/s. The orographic additive value refers to the lower left corner of the cell. Meteorological stations and posts within the studied basins are shown: I – hydrological, II – meteorological; III – basin boundaries.

For calculations on the Anuy River basin, a shorter period was chosen: from 1967 to 1974 and from 1981 to 1988, as there are meteorological monthlies only for these years, which makes it possible to include data on meteorological posts in the calculation of precipitation fields. Also, by analogy with the Charysh River basin, calculations were additionally performed (without data on posts) according to weather station data for the period from 1993 to 2001 and 2006. The list of weather stations and posts which data were used to calculate precipitation fields in the Anuy River basin is given in Table 2.

When determining the amount of winter precipitation for each weather station, the need for a correction for the blizzard transfer was assessed on the basis of the ratio of snow reserves according to landscape snow-amount surveys and the precipitation meter (the coefficient of blizzard transfer). Most

Table 1. **Weather stations used to calculate the amount of winter precipitation (November–March) in the Charysh River basin**

Weather station or post	Absolute height*, m	Average long-term amount of precipitation*	V_z, m/s
Zmeinogorsk	354.6	164	0.75
Krasnoshchekovo	240	116	0.30
Charyshskoe	400	103	0.41
Soloneshnoe	400	150	0.25
Chemal	410	60	0.27
Shebalino	870	63	0.30
Ust-Kan	1037.4	35	−0.03

Note: V_z – orographic additive. Weather stations are given in italics.

* According to [*Directory..., 1969*].

Table 2. **Weather stations used to calculate the amount of winter precipitation (November–March) in the Anuy River basin**

Weather station or post	Absolute height*, m	Average long-term amount of precipitation*, mm*	V_z, m/s
Ust-Kalmanka	149	–	0.0
Krasnoschekovo	240	116	0.3
Charyzhskoe	400	103	0.41
Soloneshnoe	400	150	0.25
Starotyryshkino	167	108	0.05
Tochilnoe	200	148	0.055
State farm Anuysky	–	–	0.1
Sychevka	225	113	0.2
Kuyagan	560	140	0.2

Note: V_z – orographic additive. Weather stations are given in italics.

* According to [*Directory..., 1969*].

Table 3. **Dependence of the blizzard transfer oefficient on the maximum snow cover height, Ust-Kalmanka weather station**

Year	Date of accumulation of maximum snow reserves	Maximum snow reserves, mm	The amount of winter precipitation, mm	The coefficient of blizzard transfer
1968/69	20 March	76	178.7	0.43
1972/73	20 March	71	132.7	0.54
1974/75	10 February	24	31.7	0.76
1975/76	20 March	81	119.0	0.68
1978/79	15 March	82	173.2	0.47

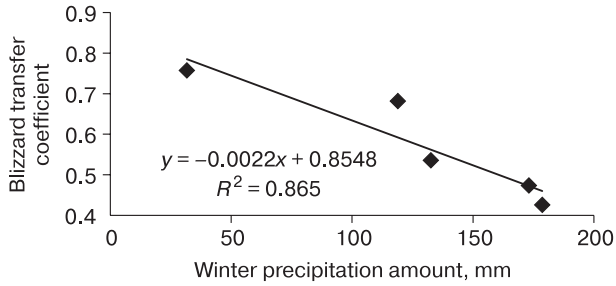

Fig. 3. Dependence of the blizzard transfer coefficient on the amount of winter precipitation measured by snow gauge (weather station Ust-Kalmanka).

weather stations have either a blizzard transfer coefficient close to 1.0 or is constant from year to year, which indicates the absence of a blizzard concentration. According to the Ust-Kalmanka state meteorological station, the coefficient varies in different years from 0.43 to 0.76 (Table 3).

At the same time, a statistically significant dependence of the blizzard transfer coefficient on the amount of winter precipitation was found (Fig. 3). This dependence was used to account for the influence of the snowstorm concentration at this meteorological station, as well as at the posts of the foothill plain located in similar conditions: Starotyryshkino, Tochilnoe, state farm Anuysky and Sychevka, because there are no enough snow-survey data in these points.

Thus, the calculation of the annual amount of winter precipitation was carried out for all meteorological stations (posts) taking into account the correction for blizzard transport. Regression equations in the form $X = f(V_z)$ were obtained.

An example of the dependence $X = f(V_z)$ for the winter of 1973/74 in the basin of the Charysh River and the basin of the Anuy River is shown in Fig. 4.

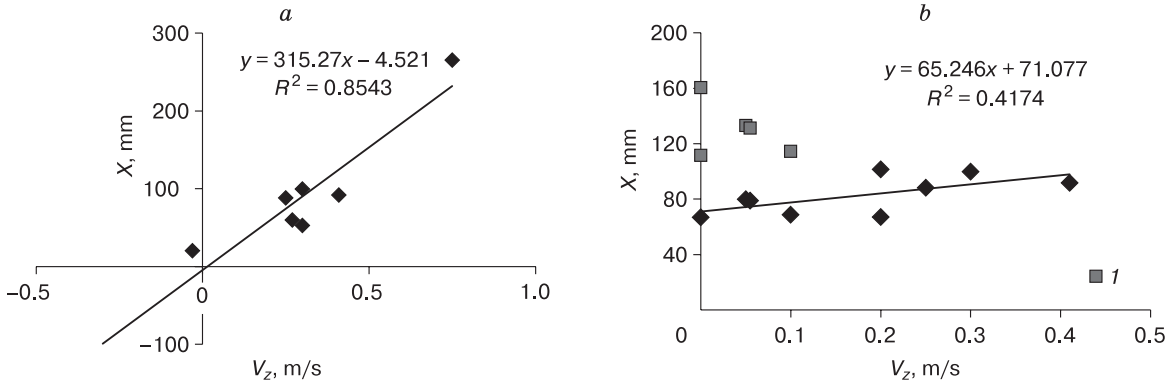

Fig. 4. Dependence of the amount of winter precipitation (X) in the winter of 1973/74 in the Charysh River basin (a) and the Anuy River basin (b) on the orographic additive to the speed of vertical movements of air masses (V_z).

The squares (*1*) show the sum of winter precipitation for meteorological stations and posts without taking into account the blizzard concentration (Ust-Kalmanka, Starotyryshkino, Tochilnoye, state farm Anuysky, Sychevka).

Table 4. **The determination coefficients between the amount of winter precipitation and orographic additive, Charysh River basin**

Winter	R^2	F	Winter	R^2	F
1967/68	0.66	15.75	1968/69	0.85	40.22
1969/70	0.91	70.87	1970/71	0.79	15.0
1971/72	0.63	13.69	1972/73	0.72	22.65
1973/74	0.85	29.3	1974/75	0.44	5.45
1975/76	0.57	10.81	1976/77	0.55	17.4
1977/78	0.62	11.28	1978/79	0.60	7.58
1979/80	0.84	43.03	1980/81	0.70	9.26
1993/94	0.75	11.77	1994/95	0.85	23.0
1995/96	0.76	12.3	1996/97	0.73	10.69
1997/98	0.80	16.0	1998/99	0.64	7.14
1999/00	0.87	32.27	2000/01	0.69	8.79
2005/06	0.66	9.7	2005/06	0.66	9.7

Table 5. **The determination coefficients between the amount of winter precipitation and orographic additive, Anuy River basin**

Winter	R^2	F	Winter	R^2	F
1967/68	0.63	15.8	1968/69	0.37	4.06
1969/70	0.26	2.50	1970/71	0.01	0.06
1971/72	0.75	18.25	1972/73	0.37	3.54
1973/74	0.42	5.02	–		
1980/81	0.52	7.65	1981/82	0.59	10.14
1982/83	0.52	7.68	1983/84	0.18	1.56
1984/85	0.30	2.51	1985/86	0.34	3.10
1986/87	0.05	0.30	1987/88	0.20	0.98
1993/94	0.78	6.99	1994/95	0.97	62.01
1995/96	0.45	1.64	1996/97	0.98	138
1997/98	0.92	25.77	1998/99	0.38	1.25
1999/00	0.52	2.20	2000/01	0.50	1.96
2005/06	0.89	16.53	2005/06	0.89	16.55

The quality control of each equation was carried out by standard methods using the coefficient of determination R^2 and Fisher's F-criterion, determined as

$$F = \frac{R^2}{1-R^2}(n-2), \qquad (1)$$

where n is the number of observations.

The determination coefficients and criterion F for each winter season are presented in Tables 4 and 5.

At meteorological stations in the basin of the Anuy River, the amount of winter precipitation for a single year do not have such a high amplitude as in the basin Charysh (Fig. 4). Therefore, in most cases, the statistical relationship with the orographic additive is much weaker (Table 5).

After calculating the amount of precipitation in each cell of the matrix, the basin average value of the amount of winter precipitation for each year was estimated (Tables 6, 7).

Assessment of the impact of precipitation on flood runoff. The evaluation of the calculation results for winter precipitation was carried out according to the principle of "hydrological control" based on the analysis of their relationship with the volume of high water expressed as the runoff layer.

The data on the flood runoff layer before 1980 were taken from the reference books of the state water cadaster [*Surface, 1969; Surface, 1975; Surface, 1984*], later was calculated by the authors using daily water flow rate data from hydrological yearbooks and the website of the Information and Analytical Center of the Register and Cadaster (http://gis.vodinfo.ru/).

The relationship between the runoff layer and the precipitation of the cold period was estimated using one-factor dependencies and by means of multiple correlation and regression analysis. The amounts of winter precipitation in the basin, calculated using an orographic additive, as well as the amount of precipitation for the flood period, calculated from monthly precipitation data, accounting for the average flood periods, are taken as predictors.

Table 6. **Precipitation amount during winter (November–March) and flood period (April–June) and the flood runoff layer, the Charysh River – gaging station "Charyshsky state farm"**

Hydrological year	Precipitation amount, mm		Flood runoff layer, mm	High water period
	November–March	April–June		
1967/68	113	152	193	16.03–08.07
1968/69	174	233	387	11.04–19.07
1969/70	81	230	248	25.03–06.08
1970/71	99	251	309	25.03–03.08
1971/72	96	225	229	03.04–07.08
1972/73	101	228	305	28.03–19.07
1973/74	88	121	119	29.03–10.06
1974/75	54	176	232	29.03–19.07
1975/76	88	137	144	14.04–22.06
1976/77	110	161	182	31.03–21.06
1977/78	74	192	171	18.03–23.07
1978/79	77	221	208	15.04–08.07
1979/80	64	190	142	09.04–13.07
1980/81	82	112	118	18.03–14.07
1993/94	74	235	190	26.03–20.06
1994/95	110	276	223	26.03–06.07
1995/96	58	197	184	09.04–05.08
1996/97	80	103	160	26.03–12.06
1997/98	71	252	–	–
1998/99	63	236	156	03.04–21.07
1999/00	66	272	172	28.03–21.07
2000/01	94	263	259	22.03–31.07
2005/06	106	152	231	27.03–23.07

Table 7. **Precipitation amounts for winter (November–March) and flood period (April–June) and the flood runoff layer, the Anuy River – gaging station "Anuysky state farm"**

Hydrological year	Precipitation amount, mm		Runoff layer, mm		Floods	High water period
	Novermber–March	April–June	with rain floods	without rain floods		
1967/68	112	147	113	107	15–23.05	14.03–21.06
1968/69	158	231	225	225	–	06.04–06.07
1969/70	75	213	118	79	13.05–05.06	21.03–04.07
1970/71	87	173	126	115	09–15.05; 18–30.05	25.03–18.06
1971/72	94	203	90	90	–	05.04–29.06
1972/73	101	261	161	140	16.05–08.06	23.03–20.06
1973/74	76	125	62	62	–	28.03–9.06
1980/81	88	121	63.3	63	–	21.03–24.06
1981/82	70	265	63.2	61	06–13.05	01.04–01.06
1982/83	66	244	82.3	78	24.05–06.06	22.03–12.06
1983/84	65	240	56.7	49	19.05–05.06	16.04–26.06
1984/85	80	191	92.2	92	–	28.03–15.06
1985/86	79	175	93.7	91	07–11.05; 03–10.06	05.04–21.06
1986/87	71	175	97.2	96	17–21.05; 24–28.05	03.04–18.06
1987/88	81	197	109.7	98	15.05–10.06	22.03–24.06
1993/94	74	201	97	80	27.04–01.05;11–20.05;22–30.05	11.03–01.07
1994/95	121	263	155.9	139	19–29.05; 02–24.06	20.03–01.07
1995/96	69	192	72	70	27–28.04; 04–06.05; 23–27.05	11.04–11.06
1996/97	78	159	90.5	87	09–21.05	18.03–10.06
1997/98	80	233	79	73	02–06.05; 18–23.05; 11–13.06	09.04–21.06
1998/99	69	201	67	65	07–15.06	28.03–25.06
1999/00	84	234	106	101	05–07.05; 13–16.05; 06–08.06	25.03–01.07
2000/01	102	245	124	121	01–02.05; 19–22.05	19.03–29.06
2005/06	112	282	171.2	160	28.04–06.05; 17–22.05; 27.05–01.06	29.03–14.06

runoff, since the conditions during this runoff are generally similar [*Burakov, Ivanova, 2010*]. The end of snowmelt was determined according to a complex graph as the moment of violation of the correspondence between the course of temperatures and water flow rate, when an increase in temperatures does not cause an increase in flow rate [*Kharshan, 1970*]. On the decline of the flood, rain floods formed by liquid precipitation that had fallen after the end of snowmelt were distinguished. The allocation of rain runoff on the hydrograph was done by "cutting off" individual peaks (floods) with subsequent exclusion when calculating the flood runoff layer.

On the Charysh River, the flood is multi-peak and more extended in time, which is associated with a wide variety of landscapes and climates, so it is often impossible to identify rain floods on the hydrograph. The flood runoff layer for the Charysh River is calculated taking into account rain floods.

RESULTS AND DISCUSSION

Tables 6 and 7 present calculations of winter precipitation amount, precipitation from April to June period, and the flood runoff layer for each year.

The results of the calculation of winter precipitation amount and the flood runoff layer (Tables 6, 7) were analyzed using statistical methods of correlation and regression analysis. At the first stage, correlation matrices and graphs of the dependence of the flood runoff layer on the amount of winter precipitation for the Anuy and Charysh rivers were constructed (Fig. 5).

Correlation analysis showed that the amount of winter precipitation is the main factor in the formation of flood runoff: in general, the Anuy River basin is characterized by a closer relationship between winter precipitation and runoff (r = 0.87) than the Charysh River basin (r = 0.64). The "cut off" of rain floods on the decline of the flood for the Anuy River has increased, as expected, the closeness of the relation (r increased to 0.91). Liquid precipitation during the decline of the flood period, which forms rain floods, is second in importance. Moreover, according to the results of correlation analysis, both for Anuy and Charysh rivers, the highest correlation coefficient of flood runoff is observed with summarized monthly precipitation from April to June (inclusive). The inclusion of liquid precipitation in July for the Charysh River reduces the correlation with the flood runoff.

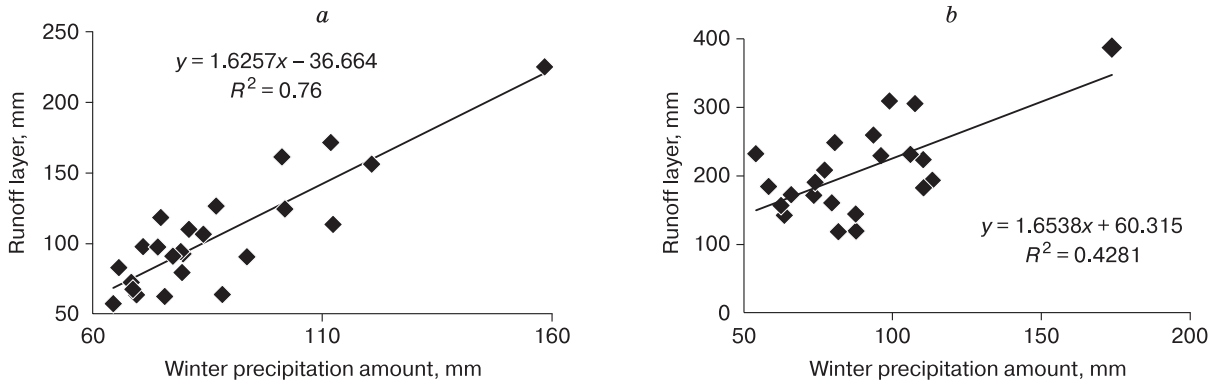

Fig. 5. Dependence of the flood runoff layer of the Anuy River (*a*) and the Charysh River (*b*) on the amount of winter precipitation (November–March).

Obviously, this may be due to more significant losses for the evaporation, the transpiration, wetting of vegetation and the filtration into soils in July (compared to May–June). It is noted that for the Anuy River, liquid precipitation contributes significantly less to the formation of high water ($r = 0.37$) than for the Charysh River ($r = 0.58$).

At the second stage, the results of correlation analysis were used to develop multiple linear regression equations based on two significant predictors: the amount of winter precipitation (from November to March) calculated using an orographic additive, and the amount of precipitation during the high water period (April to June) at a representative meteorological station. The parameters of the equations for the Anuy and Charysh rivers are given in Table 8.

In general, for the Anuy River equation is as follows:

$$h = 1.53P_1 + 0.21P_2 - 72.1 \quad (2)$$

and for the Charysh River is:

$$h = 1.47P_1 + 0.64P_2 - 49.3, \quad (3)$$

where h is the layer of runoff for the flood (mm), P_1 is the amount of winter precipitation (mm), P_2 is the rainfall period, floods (mm).

The values of the coefficients of determination $R^2 = 0.81$ $\left(R^2_{\text{norm}} = 0.79\right)$ and the Fisher criterion $F = 45.05$ (critical value $F = 3.47$ at a significance level of 5 %) in the equation for Anuy River (2), indicate a high level of reliability. For the Charysh River, the quality of equation (3) is somewhat worse: $R^2 = 0.67$, $R^2_{\text{norm}} = 0.63$, $F = 18.4$ (critical value 3.55), but it also explains the dependence of the runoff layer on precipitation quite well. Both equations can be used as a predictive model. The less close relationship of the main predictor with the runoff and the worse quality of the multiple regression model for the Charysh River are associated with a significant influence on the flood runoff of the factors determining the water absorption capacity of the river basin, which are not taken into account in the model.

Previous works of the authors have shown that the initial period of snow accumulation plays an important role in the formation of maximum flood levels in the Charysh River basin. If the thickness of the

Table 8. **Regression statistics and coefficients of the multiple linear regression equation**

Parameter	Coefficient value	Coefficient standard error	Multiple R	R^2	Normalized R^2	*F*-test	Number of years
	Flood runoff of Anuy River (accounting rain floods)						
Free term	–72.1	21.75	0.90	0.81	0.79	45.05	24
P_1, mm	1.53	0.18					
P_2, mm	0.21	0.09					
	Flood runoff of Charysh River (with account of rain floods)						
Free term	–49.28	44.09	0.82	0.67	0.63	18.14	21
P_1, mm	1.47	0.35					
P_2, mm	0.64	0.17					

Note: P_1 is the sum of winter precipitation (November–March); P_2 is precipitation during the high water period (April–June).

snow cover before the onset of significant frosts (below −10 °C) is more than 20–25 cm, and there is no significant seasonal freezing of rocks in the basin, then in the spring period in the gaging station of the state farm Charyshsky maximum levels observed are 1 meter lower compared to years when meteorological conditions contribute to seasonal freezing [*Galakhov et al., 2018*].

Studies of the conditions for the formation of snow cover in the Anuy River basin, carried out using similar methods, indicate no influence of seasonal freezing on the flood runoff [*Galakhov et al., 2020*]. According to the authors, such significant differences in the processes of melt runoff formation in two neighboring basins are associated with their geomorphological features. The basin of the Anuy River to the state farm Anuysky gaging station is represented by middle and low mountains only, which, as a rule, are distinguished by higher and constant coefficients of melt runoff [*Apollov et al., 1974; Burakov, 1986*]. About 40 % of the Charysh River basin is a foothill plain, which is characterized by a large variability of melt runoff coefficients depending on the state of soils in the basin (rock composition, moisture content, depth of seasonal freezing) and, as a consequence, melt runoff losses for infiltration.

CONCLUSION

1. As shown earlier [*Galakhov et al., 2020*], in the basins of the Anuy and Charysh rivers, in most cases there is no statistically significant dependence of the amounts of winter (November–March) precipitation according to hydrometeorological stations and posts on their absolute height. The use of an orthographic additive to the speed of air mass vertical movements for calculating the amount of winter precipitation is preferable. For the Charysh River basin, there is a close relationship between the amount of winter precipitation and the orographic addition to the speed of air mass vertical movements both on a multi-year scale and in individual years. Statistically insignificant coefficients of determination between the amount of winter precipitation and an orographic additive in the Anuy River basin in some cases are associated with a more uniform distribution of precipitation fields within the basin.

2. The analysis of the dependence of the winter precipitation amounts obtained using an orographic additive and the flood runoff layer performed by the authors earlier [*Galakhov et al., 2020*] has shown their close ($R^2 = 0.76$) relationship in the Anuy River basin. The accounting of rain floods on the decline of the flood was carried out in two ways: by the method of their "cut-off", and the introduction of an additional predictor into the regression equation, the amount of precipitation from April to June on the Soloneshnoye Station, that has allowed increasing the determination coefficients to 0.83 and 0.81, respectively. All this, firstly, confirms the reliability of calculations of precipitation amounts. Secondly, it allows us to conclude that winter precipitation is the main factor affecting the volume of flood runoff in the Anuy River basin.

3. In the Charysh River basin, the relationship between the amounts of winter precipitation and the volume of runoff is much weaker ($R^2 = 0.43$). Correlation analysis has shown that for the Charysh River, liquid precipitation from April to June has a greater effect on the volume of high water than for the Anuy River. The introduction of high-water precipitation (April to June) into the regression equation significantly improved the quality of the model ($R^2 = 0.67$, $R^2_{\text{norm}} = 0.63$). In general, in comparison with the Anuy River basin, the relationship between runoff volume and precipitation is less significant. This is due to the fact that about 40% of the basin is located on the foothill plain, which is characterized by a large variability of melt runoff coefficients depending on the condition of the soils (their composition, degree of moisture, freezing). This hypothesis requires confirmation and further research.

4. The obtained multiple regression equations confirm the reliability of winter precipitation calculations and can be used for medium-term forecasts of flood volume on the Anuy and Charysh rivers. At the same time, in a mountain basin with relatively homogeneous landscape and climatic conditions (the Anuy River), it is acceptable to use a one-factor correlation dependence of the flood runoff on the amount of winter precipitation. For the Charysh River basin, which has a complex geomorphological structure, it is necessary to introduce additional predictors into the model that characterize the precipitation of the flood period and the condition of soils that determine their infiltration ability.

References

Apollov, B.A., Kalinin, G.P, Komarov, V.D., 1974. Course of hydrological forecasts. Gidrometeoizdat, Leningrad, 420 pp. (in Russian).

Barnett, T.P., Adam, J.C., Lettenmaier, D.P., 2005. Potential impacts of a warming climate on water availability in snow-dominated regions. Nature, 438, 303–309.

Barry, R.G., 1964. Weather and climate in the mountains. Gidrometeoizdat, Leningrad, 263 pp. (in Russian).

Burakov, D.A. (Ed.), 1986. Snow-water-glacial resources of the Upper Ob basin and forecasts of spring flood runoff. Izd-vo TGU, Tomsk, 254 pp. (in Russian).

Burakov, D.A., Ivanova, O.I., 2010. Analysis of formation and forecast of spring snowmelt flood runoff in forest and forest-steppe basins of Siberian rivers. Russian Meteorology and Hydrology, 35 (6), 421–431.

Churyulin, E.V., Kopeikin, V.V., Rozinkina, I.A., Frolova, N.L., Churyulin, A.G., 2018. Analysis of the characteristics of the snow cover from satellite and model data for different catchments in the European territory of the Russian Federation. Hydrometeorological Research and Forecasting, No. 2 (368), 120–143.

DeWalle, D.R., Rango, A., 2008. Principles of Snow Hydrology. Cambridge University Press, Cambridge, 410 pp.

Directory on the climate of the USSR, 1969. Issue 20. Air humidity, precipitation, snow cover. Gidrometeoizdat, Leningrad, 333 pp. (in Russian).

Galakhov, V.P., 2003. Conditions for maximum mountain snow reserves accumulation and their calculations. Nauka, Novosibirsk, 104 pp. (in Russian).

Galakhov, V.P., Popov, E.S., Mardasova, E.V., Plekhova, A.V., 2016. Forecast of maximum water levels in river Charysh during snowmelting. Bulletin of the Altai Branch of the Russian Geographical Society, No. 3 (42), 38–44 (in Russian).

Galakhov, V.P., Mardasova, E.V., Lyutsiger, N.V., Samoilova, S.Yu., 2018. Influence of fall freezing on maximum levels of Charysh river basin. Bulletin of the Altai Branch of the Russian Geographical Society, No. 1 (48), 54–57 (in Russian).

Galakhov, V.P., Samoilova, S.Yu., Mardasova, E.V., 2020. Effect of snow cover formation on snowmelt runoff (the Anuy River basin as case study). Bulletin of the Altai Branch of the Russian Geographical Society, No. 1 (56), 24–33 (in Russian).

Gensiorovsky, Yu.V., 2007. Calculation of maximum snow reserves on the basis of landscape-indicative properties of snow cover. Data of Glaciological Studies, No. 102, 73–79 (in Russian).

Guide to hydrological forecasts, 1989. Issue 1. Long-term forecast. Elements of the water regime of rivers and reservoirs]. Gidrometeoizdat, Leningrad, 357 pp. (in Russian).

Iglovskaya, N.V., Narozhny, Yu.K., 2010. Determination of Altai snow reserves with the use of satellite information. Tomsk State University Journal, No. 334, 160–165 (in Russian).

Kalyuzhny, I.L., Lavrov, S.A., 2012. Basic physical processes and regularities of winter and spring river runoff formation under climate warming conditions. Russian Meteorology and hydrology, 37 (1), 68–81.

Kharshan, Sh.A., 1970. Long-term forecasts of mountain river runoff in Siberia. Gidrometeoizdat, Leningrad, 211 pp. (in Russian).

Li, D., Durand, M., Margulis, S., 2015. Quantifying spatiotemporal variability of controls on microwave emission from snow covered mountainous regions. IEEE Journal of Selected Topics in Applied Earth Observations and Remote Sensing, June 2015, DOI: 10.1109/JSTARS.2015.2440332.

Lubenets, L.F., Chernykh, D.V., 2019. Intra-landscape distribution of snow storage in the Mayma river basin (low-mountain area of the Russian Altai). Led i Sneg [Ice and Snow], No. 59 (3), 319–332.

Matveev, L.T., 1981. Dynamics of clouds. Gidrometeoizdat, Leningrad, 311 pp. (in Russian).

Matveev, L.T., 1984. A course in general meteorology. Atmospheric physics. Gidrometeoizdat, Leningrad, 751 pp. (in Russian).

Mukhin, V.M., 2013. Methodological basis of physical-statistical kinds of short-range forecasts of mountain river runoff. In: Proceedings of the Hydrometcentre of Russia. vol. 349, pp. 5–46 (in Russian).

Popov, E.G., 1979. Hydrological forecasts. Gidrometeoizdat, Leningrad, 257 pp. (in Russian).

Puzanov, A.V., Zinovyev, A.T., Bezmaternykh, D.M., Reznikov, V.F., Troshkin, D.N., 2018. Hazardous hydrological phenomena in the upper Ob basin: current trends and forecasting. Water sector of Russia, No. 4, 69–77 (in Russian).

Revyakin, V.S., Kravtsova, V.I., 1977. Snow cover and avalanches in Altai. TGU Publ., Tomsk, 214 pp. (in Russian).

Rogers, R.R., 1979. A short course in cloud physics. Gidrometeoizdat, Tomsk, 232 pp. (in Russian).

Romasko, V.Yu., Burakov, D.A., 2017. Space monitoring of snow-covered areas of river basins. Journal of the Siberian Federal University. Series: Engineering and technologies, 10 (6), 704–713 (in Russian).

Samoilova, S.Yu., Galakhov, V.P., 2020. Estimation of mean annual solid precipitation (snow cover water equivalent) at the high mountain areas (Katun river basin, Altai). In: IV Vinogradov conference. Hydrology: from learning to worldview. Collection of reports of the International scientific conference in Memory of the outstanding Russian scientist Yuri Borisovich Vinogradov. (St. Petersburg, 2020). Izd-vo VVM, St. Petersburg, pp. 760–764 (in Russian).

Shakina, N.P., 1985. Dynamics of atmospheric fronts and cyclones. Gidrometeoizdat, Leningrad, 263 pp. (in Russian).

Shiklomanov, I.A. (Ed.), 2008. Water resources of Russia and their use. State Hydrological Institute, St. Petersburg, 598 pp. (in Russian).

Skorer, R., 1980. Aerohydrodynamics of the environment. Mir, Moscow, 549 pp. (in Russian).

Surface water resources of the USSR, 1969. Hydrological studies. Vol. 15. Altai and Western Siberia. Issue 1. Mountain Altai and Upper Irtysh. V.A. Semenov (Ed.). Gidrometeoizdat, Leningrad, 216 pp. (in Russian).

Surface water resources, 1975. The main hydrological characteristics. Vol. 15. Altai, Western Siberia and Northern Kazakhstan. Issue 1. Upper and Middle Ob. J.S. Popov (Ed.). Gidrometeoizdat, Leningrad, 542 pp. (in Russian).

Surface water resources, 1979. Многолетние данные о режиме и ресурсах поверхностных вод суши. Ч. 1. Реки и каналы. Т. 1. РСФСР, Вып. 10. Бассейны Оби (без бассейна Иртыша), Надым, Пура, Таза. Popov, J.S. (Ed.). Gidrometeoizdat, Leningrad, 487 pp. (in Russian).

URL: http://aisori.meteo.ru/ClimateR (last visited: 02.02.2020).

URL: http://gis.vodinfo.ru/ (last visited: 01.06.2020).

URL: http://www.pogodaiklimat.ru (last visited: 01.07.2020).

Received August 3, 2020
Revised June 13, 2021
Accepted August 19, 2021

Translated by S.B. Sokolov

SUBPERMAFROST WATERS IN THE EAST CHUKOTKA'S UPLAND

V.E. Glotov

Shilo North-East Interdisciplinary Scientific Research Institute, Far East Branch, Russian Academy of Sciences (NEISRI FEB RAS), Portovaya str. 16, Magadan, 685000, Russia, geoecol@neisri.ru

The purpose of the article is to reveal the conditions of occurrence and formation of subpermafrost waters, which have been encountered by wells in the Paleozoic, Triassic terrigenous rocks and in the Lower Cretaceous granitoids of the Chukotka Upland. In the Paleozoic sequence, confined subpermafrost waters were encountered at depths from 223 to 340 m. The specific flow rates vary from 0.01 to 0.5 L/(s·m), the composition of the waters is predominantly chloride, and mineralization ranges from 0.2 to 1.3 g/dm^3. In the Triassic rocks, at depths from 100 to 300 m, the piezometric surface of waters is higher than wellhead levels by 3–4 m and up to 58.4 m. The specific yield varies from 0.00001 to 0.25 L/(s·m). The waters are chloride, hydrocarbonate and sulphate, salinity ranges from 0.1 to 3.1 g/dm^3. In the granitoid massifs, the thickness of permafrost near the sea coast is about 100 m; within the watersheds, it is about 450 m. The specific yield varies from 0.0001 to 0.013 L/(s·m). The obtained data, confirmed by magnetotelluric sounding, indicate the development of hydrogeological massifs composed of igneous and metamorphosed rocks in the upland. Structures with quasi-stratum fracture reservoirs, associated with overthrusts and faults, were formed in the terrigenous Triassic sequences. The impermeable fault planes divide the quasi-strata into sections, which are poorly interconnected hydraulically. For this reason, in the Triassic subpermafrost strata, the stagnant or extremely impeded water exchange predominates persisting for more than 400 thousand years; while in the hydrogeological massifs, the water exchange is more active.

Keywords: *Chukotka Upland, permafrost zone, subpermafrost waters, active and extremely impeded water exchange, cryogenic pressure, magnetotelluric sounding.*

INTRODUCTION

The Chukotka Upland is located north of the Arctic Circle and is divided by the meridian 180° into parts: the eastern part drained by the rivers of the East Siberian Sea basin and the western part drained by the Chukchi Sea basin (Fig. 1). During the Second World War, the Valkumey tin ore deposit, located near the seaport of Pevek in the eastern part of the upland, had strategic importance. In subsequent years, the Pervonachalnoye tin ore deposit, Mayskoye gold ore deposit, and gold placers in the basins of the Ichuveem, Pegtymel and other rivers were revealed in this area. Hydrogeological materials were obtained during the prospecting, exploration and mining of the deposits. These data were partially summarized in collective works [*Tolstikhin, 1972; Efimova et al., 1977; Afanasenko et al., 1989*]. These and subsequent publications have focused on groundwaters of suprapermafrost and open taliks as the main sources of freshwater [*Shumikhina, 1999; Glotov and Glotova, 2015; Glotov, 2020*]. The main drawback of the published works is that the specific features of the distribution, occurrence, and formation of subpermafrost waters were not described. The purpose of the present study is to eliminate these disadvantages.

The scientific and practical relevance of this work is determined by the important role of hydrogeological features of subpermafrost strata to provide stability of underground engineering structures, to evaluate the prospects of using these strata as storages for fresh water and other fluids, and to solve a number of geoecological and geophysical problems.

Materials and methods. The analysis and synthesis of the handwritten geological reports and publications, including the author's ones, were used. Data were obtained by drilling and hydrogeological sampling of wells, and underground mining. To obtain geocryological and hydrogeological data, the results of deep magnetotelluric sounding (MTS) on the 2-DV-A reference profile were used for the first time in this area.

The object of the study is the main natural factors of the formation and distribution of groundwater in the eastern part of the Chukotka Upland. The western part is distinct from the eastern one by tectonics and geological history in the Middle Pleistocene–Holocene time. Therefore, the modern permafrost-hydrogeological characteristics of these areas have their own specifics, which we do not consider in this paper.

The subject of the study is the subpermafrost waters, which generally occur in the Paleozoic-Early Mesozoic terrigenous sedimentary rocks and in the Lower Cretaceous intrusive massifs. Groundwaters of volcanogenic covers: seasonally thawed layer, suprapermafrost and open taliks require separate study and have been partially studied previously [*Glotov and Glotova, 2013; Glotov, 2020*].

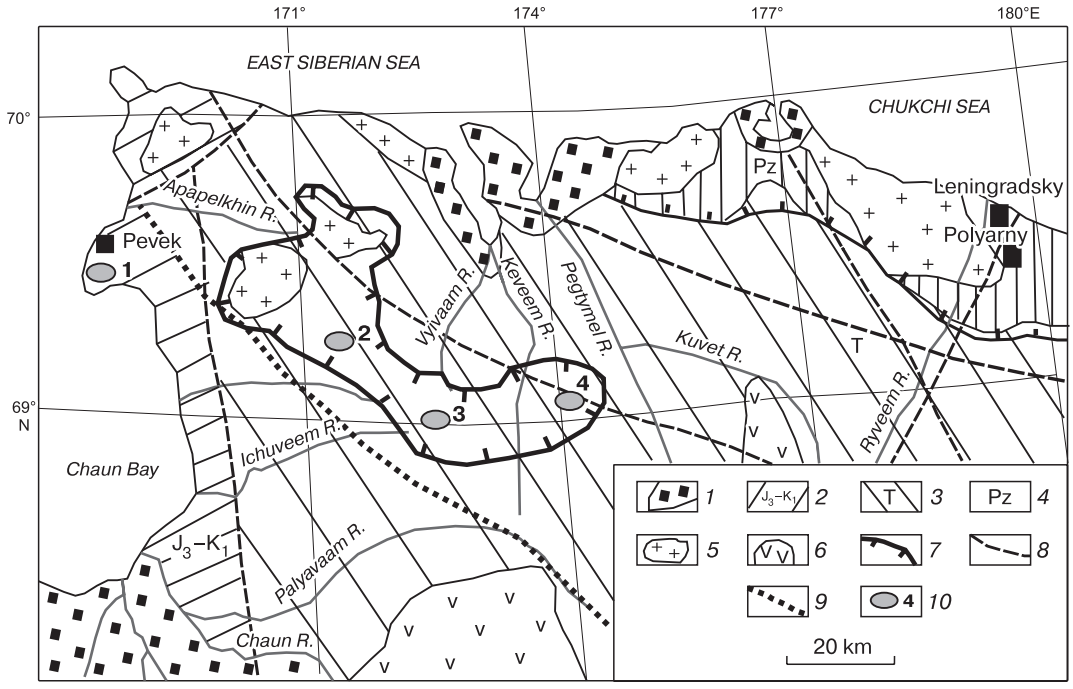

Fig. 1. The geographic and geological scheme of the Chukotka terrane, the fragment of the passive continental margin (east of the Chukotka Upland) [*Zhuravlev and Kalinin, 1999*]:

1 – Cenozoic sediments of the modern depressions; *2* – Upper Jurassic–Lower Cretaceous sedimentary rocks of the Anyuy subterrane; *3* – Triassic and *4* – Paleozoic sedimentary rocks of the Chaun subterrane; *5* – Lower Cretaceous granitoid massifs; *6* – Cretaceous volcanogenic covers; *7* – boundaries of arched uplifts; *8* – deep faults; *9* – geophysical profile 2-DB-V-A; *10* – sites of hydrogeological works, including: Valkumey (1) and Pervonachalnoye (2) tin-ore deposits, Ichuveem area of placer gold deposits (3), and Mayskoye gold-ore deposit (4).

BRIEF DESCRIPTION OF THE STUDY OBJECT

The main natural factors that determine the features of the hydrogeological conditions are relief, rivers, climate, geological structure, and permafrost features [*Pinnecker, 1977*].

The relief of the eastern part of the Chukotka Upland is characterized by subdued watersheds with absolute elevations of 500–800 m. Within this area, there are distinctly dissected ridges and mountain ranges, composed of magmatic rocks, with elevations up to 1500 m, and some tops are up to 1837 m in height. Traces of the Middle and Late Pleistocene mountain-valley glaciations are widespread [*Glushkova and Smirnov, 2020*].

The Palyavaam and Pegtymel rivers are *mountain rivers* with the largest catchment area (up to 17 thousand km^2). Open runoff exists in the period from late May to early November, in small streams – until the end of September. In winter, icings are formed in river channels [*Tolstikhin, 1974; Alekseev et al., 2011*].

The climate is characterized by the mean annual air temperature of around –10 °C; the maximum warm period lasts 100–110 days; the long-term mean annual amount of precipitation is 220–260 mm. About 60 % of precipitation falls in the form of rainfall [*Belikovich et al., 1997*].

In terms of geology, the eastern part of the Chukotka Upland belongs entirely to the Chaun subterrane – the part of the larger Chukotka terrane*, which is a fragment of the Late Paleozoic – Early Cretaceous passive continental margin [*Byalobzhesky et al., 2006*]. The subterrane is composed of the Cambrian (?) regionally metamorphosed chlorite shales and the Devonian sandstones, shales, and limestones; the Lower and Middle Carboniferous sandstones with carbonate cement and conglomerates; the Upper Carboniferous-Permian carbonaceous shales and sandstones, which compose the Velitkenay dome on the coast of the East Siberian Sea. The Lower–Middle Triassic graywackes and clayey shales, the Upper Triassic sandstones, siltstones, and clayey shales are distributed throughout the area. These sedimentary rocks were formed on the continental shelf. In the

* Terrane is a block of the earth's crust of regional sizes, separated from the surrounding area by faults [*Byalobzhesky et al., 2006*].

Lower Cretaceous, they were intruded by granitoids [*Polzunenkov, 2018*].

A specific feature of the Chaun subterrane is the development of arch-thrust structures (uplifts) modifying the folded bedding of the Triassic sequence. The largest of these structures is the Ichuveem structure, up to 100 km long and up to 30 km wide. The dip angles on the structure flanks range from 10 to 50°. Thrust faults with an amplitude of up to first kilometers, faults, and thrust faults are widely developed [*Zhuravlev and Kalinin*, 1999]. Ore deposits are located within such stressed areas [*Volkov et al., 2006*].

In terms of geocryology, the studied region belongs to the area of the continuous permafrost zone, considered as a cryogenic aquiclude [*Fotiev, 2013*]. The permafrost thickness on the tops of watersheds reaches 450 m (Valkumey granitoid massif); in the river valleys, it is up to 340 m. In the watersheds, the temperature of permafrost at the depth of zero annual amplitude (15–20 m) ranges from –9 to –11 °C [*Afanasenko et al., 1989*], in river valleys, it varies from –4.5 to –6.0 °C [*Efimova et al., 1977*].

RESULTS OF HYDROGEOLOGICAL WORKS

Following the structural-stratigraphic principle of distinguishing hydrogeological taxa [*Basic provisions..., 2001*], we consider the hydrogeological stages composed of the Paleozoic regionally metamorphosed and the Triassic sedimentary rocks, which are widespread in the east of the upland, and a group of the Lower Cretaceous granitoid intrusions.

Watering of rocks of all stages is associated with the development of zones of superimposed fracturing, which is diverse in origin.

Paleozoic rocks

Subpermafrost waters of Paleozoic rocks were studied in the coastal zone while searching for water supply sources for Leningradsky and Polyarny settlements. Table 1 demonstrates the established hydrogeological characteristics.

Subpermafrost waters in the Upper Paleozoic rocks in the valley of the Ryveem River are confined and characterized by the self-discharge up to 0.8 L/s, the specific flow rate g = 0.12–0.4 L/(s·m), and the transmissivity coefficient k_p = 4–12 m^2/day.

The pumping with 32 m lowering gave 1.35 L/s, g = 0.042 L/(s·m) in the valley of the Pilhinkuul River, 20–25 km to the south of the sea coast. In line with this well, in the river valley, the base of the cryogenic aquiclude was found at the depth of 320 m by drilling in November 1971. The aquifer is 40 m thick. Subpermafrost waters are confined. A static level is higher than the daylight surface by 58.4 m; the self-discharge flow rate at the maximum groundwater head is 1.17 L/s, g = 0.02 L/(s·m), k_p = 1 m^2/day.

By a predominant anion, subpermafrost waters belong to the hydrocarbonate, sulfate and chloride classes; by the total salinity, they vary from fresh (0.2–0.8 g/dm^3) to slightly saline (1.3 g/dm^3).

Waters of the chloride class are widespread in the lower reaches of the Ryveem River. Their total mineralization ranges from 0.6 to 1.1 g/dm^3 with the chlorine-ion content ranging from 189 to 497 g/dm^3.

Waters of the bicarbonate class are fresh; they are common for both coastal and inland areas. The content of bicarbonate ion is up to 445 g/dm^3 with a weak-alkaline reaction. The distribution of these waters is controlled by the presence of aquiferous black clayey shales saturated with organic matter.

Waters of the sulfate class are found in the vicinity of Polyarny settlement. Their mineralization is 0.6–0.8 g/dm^3, and the sulfate-ion content is up to 280 mg/dm^3. Magnesium predominates among cations, which indicates possible ore mineralization associated with basalt or andesite dikes.

Table 1. **Parameters of the water-bearing capacity of the Paleozoic rocks**

Area	Depths of wells, m	Thickness of the cryogenic aquiclude, m	Specific flow rate of wells, L/(s·m)	Mineralization of water, g/dm^3	Content of ions, mg/dm^3
Sea coast (3–5 km from the sea), abs. elevations of wellheads are 10–20 m; the valley of the Ryveem River	$\frac{293-390}{330}$	$\frac{223-335}{228}$	$\frac{0.12-0.49}{0.25}$	M $\frac{0.6-1.1}{0.9}$	Cl $\frac{189-197}{215}$; HCO_3 $\frac{102-464}{305}$
Coastal zone (20–25 km from the sea), abs. elevations 20–55.9 m; the valleys of the Pilkhinkuul River and its tributaries	$\frac{330-410}{362.6}$	$\frac{275-340}{301}$	$\frac{0.01-0.3}{0.13}$	M $\frac{0.2-1.3}{0.73}$	Cl $\frac{51-117}{72}$; HCO_3 $\frac{97-445}{251}$; SO_4 $\frac{35-715}{331}$

Note. *Here and below:* the numerator is from the lowest to the highest values, the denominator is arithmetic mean.

We conclude that the arithmetic-mean parameters of the water-bearing capacity of the Paleozoic rocks indicate their relatively high filtration properties in all penetrated intervals. This is associated with the development of regionally metamorphosed sequences of sedimentary rocks, represented by limestones and sandstones with calcareous cement in the dome structure. Thrust faults are not typical for this structure. Under these conditions, watering mostly occurs along the fault zones, where there are traces of carbonate leaching.

Triassic rocks

Data on the subpermafrost waters of these rocks were obtained during the search for fresh groundwater for water supply in the river valleys and during the exploration of the Pervonachalnoye tin ore deposit, the Mayskoye gold ore deposit, and the Ichuveem gold placer cluster. The sites of all deposits are connected with the Ichuveem arch-thrust uplift, stretching from the Pyrkakaiveem River to the valley of the Keveem River. To study the conditions of the mining of the deposits, hydrogeological boreholes were drilled within all topographic features. Taking into consideration the different purposes of the works performed, the results are presented separately.

Results of the work within the arch-thrust uplift

Table 2 demonstrates the basic hydrogeological parameters in the generalized form. All sites are located in subdued low-mountain terrain in the basins of streams of the 4th and lower orders, characterized by similar conditions in terms of geology. It was revealed that the thickness of the cryogenic aquiclude, hydrodynamic and hydrogeochemical parameters in the neighboring blocks are similar under different landforms. To illustrate this statement, the data on the sites of the Pervonachalnoye deposit was considered. In the upper reaches of the Pyrkakaiveem River, two wells, each 250 m deep, were drilled in January–May 1978 in the area, where the river bed intersects the thrust fault zone (Fig. 2, *A*). The thickness of the cryogenic aquiclude is 201 m in the hanging wall, composed of Middle Triassic polymictic sandstones, i.e., almost 46 m thicker than in the footwall of the thrust fault (Fig. 2, *B*).

The impermeable zone of the thrust with a thickness of up to 5 m is composed of crushed host rocks cemented by mylonitized material. The presence of the confining tectonic screen explains differences between the thicknesses of the cryogenic aquiclude, hydrodynamic parameters, and the chemical composition of water. In the footwall, the water composition is expressed by a formula

$$M\ 0.31\ \frac{Cl\ 56\ (HCO_3)\ 38}{Na\ 71\ Ca\ 26}$$

with the chlorine ion content of 112.5 mg/dm^3. In the hanging wall, it is

$$M\ 0.11\ \frac{(HCO_3)\ 67\ Cl\ 29}{Na\ 41\ Ca\ 30\ Mg\ 29}$$

with the chlorine ion content of 21.3 mg/dm^3.

Table 2. **Parameters of the water-bearing capacity within the arch-thrust uplift**

Deposit	Depths of wells, m	Permafrost thickness, m	Specific flow rate of wells, L/(s·m)	Mineralization of water, g/dm^3	Content of ions, mg/dm^3
Pervonachalnoye deposit; abs. elevations of wellheads are 152–301 m; 45 wells	$\frac{134.9-453.5}{235.5}$	$\frac{127-218}{149.3}$	$\frac{0.0001-0.25}{0.04}$	$M\ \frac{0.11-1.6}{0.42}$	$Cl\ \frac{10.6-258.4}{51.7}$ $HCO_3\ \frac{47-1171}{116}$ $SO_4\ \frac{12-1085}{108.6}$
Ichuveem gold placer; abs. elevations of wellheads are 90–240 m; 26 wells	$\frac{210-400}{286}$	$\frac{100-238}{159}$	$\frac{0.00003-0.2}{0.034}$	$M\ \frac{0.6-1.28}{0.84}$	$Cl\ \frac{14.2-250}{53.5}$ $HCO_3\ \frac{134-793}{384.5}$ $SO_4\ \frac{4-730}{271}$
Mayskoye deposit; abs. elevations of wellheads are 208.7–297.4 m; 18 wells	$\frac{210-302}{222}$	$\frac{210-260}{235.6}$	$\frac{0.000008-0.026}{0.005}$	$M\ \frac{0.31-0.98}{0.7}$	$Cl\ \frac{21.3-184}{78}$ $HCO_3\ \frac{171-756}{421}$ $SO_4\ \frac{0-375}{79.8}$

On the basis of the pumping test in the hanging wall, $g = 0.003$ L/(s·m), $k_p = 0.09$ m^2/day; in the footwall, $g = 0.004$ L/(s·m), $k_p = 0.12$ m^2/day. The correspondence of the slope of the piezometric surface to the slope of the river bed points to the presence of a hydrodynamic connection, even though it is impeded.

Figure 2, *B* demonstrates data from two wells drilled on the watershed of the Oleniy stream and the Pyrkakaiveem River (Krutoy stockwork). The borehole with the absolute elevation of the wellhead of 208 m revealed the bottom of the cryogenic aquiclude at the depth of 218 m. Confined groundwaters beneath this bottom rose above the daylight surface by 18.6 m, $g = 0.02$ L/(s·m). A formula of the water composition is:

$$M\ 0.6\frac{SO_4\ 68\ Cl\ 22}{Ca\ 47\ Na\ 29}\ pH\ 6.8;$$

Fe^{2+} content is 4.5 mg/dm^3. The well in the watershed (34 m above) penetrated permafrost 162 m thick, water rose above the wellhead by 54.3 m, $g = 0.008$ L/(s·m). A formula of the water composition is:

$$M\ 0.85\frac{Cl\ 93}{Na\ 89}\ pH\ 7.6.$$

According to geological data, there are normal faults between these wells, the fault planes of which are composed of tectonic mylonitized breccia 0.5 m thick. Such fault planes provide hydrogeological differences between the spatially close blocks and limit their water resources. This fact was highlighted by all hydrogeologists, who studied the hydrogeological conditions of mining the ore deposits in the Chukotka Upland.

Therefore, drilling of wells in different sites of the arch-thrust structure showed that the Triassic fractured aquiferous deposits are widespread. However, their water-bearing capacity, in general, is fragmentary, low and uneven in area. Contacts of the fragments are tectonic (cataclased or mylonitized fault planes) or hydrothermal (veins of quartz, kaolinite). Small values of the transmissivity coefficient (less than 0.01 m^2/day) do not induce large water inflows into the workings during underground mining, but the presence of water in fractures makes barriers of all underground workings unstable. Therefore, during the development of subpermafrost ore zones of the Mayskoye gold ore deposit, all underground workings require sheeting, although water inflows are extremely small and characterized as dripping.

Results of works on the study of subpermafrost waters in the river valleys

In conditions of the continuous cryogenic aquiclude, river valleys are the most promising source of water supply. In mountain areas, the valleys are usually attributed to fault zones, including fault planes of trust faults, strike-slip faults, and normal faults. A generalization of the available material shows that open taliks in the river valleys in the eastern part of the Chukotka Upland are rare and associated with graben valleys, filled by loose glacial or alluvial sediments more than 10–15 m thick [*Glotov, 2020*]. Such

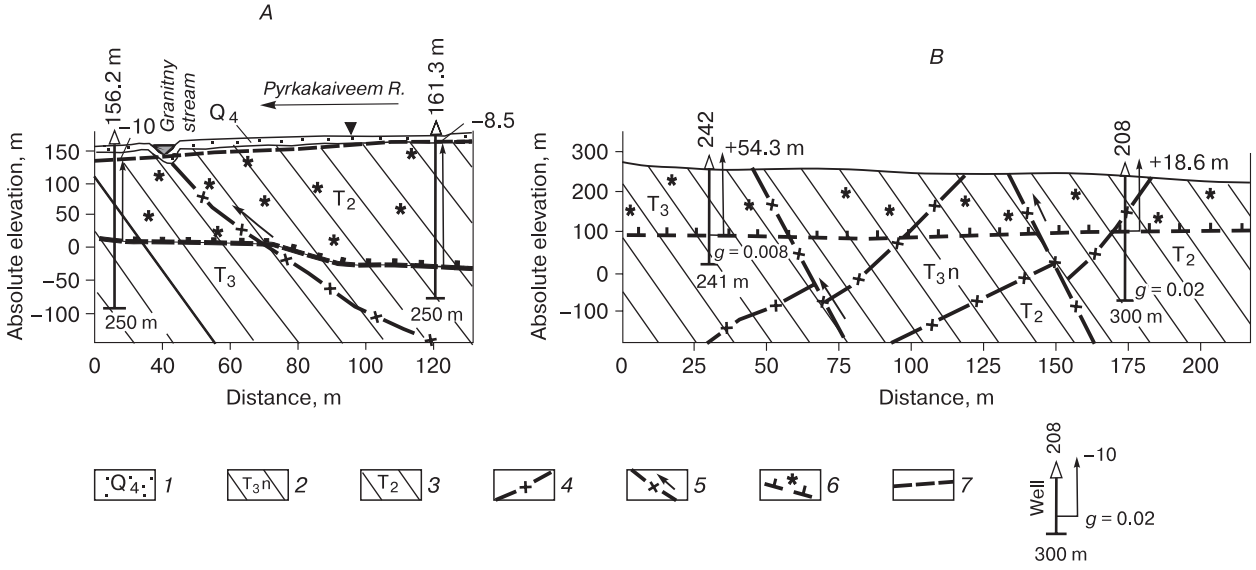

Fig. 2. The schematic hydrogeological cross sections along the valley of the Pyrkakaiveem River near the Granitny stream (*A*) and along the watershed of Oleniy stream – Pyrkakaiveem River (*B*):

1 – Quaternary alluvial sediments; *2* – Upper Triassic, Norian Stage – interbedding of clayey shales, siltstones, and fine-grained sandstones; *3* – Middle Triassic sedimentary rocks, sandstones and siltstones; *4* – thrust faults, hydrothermally transformed mylonites in a thrust plane; *5* – normal faults, cataclasites in a fault plane; *6* – permafrost base; *7* – a level of subpermafrost waters in the river valley. Well: figures below – well depth, m; figures above – an absolute elevation of a wellhead, m; *g* – specific flow rate, L/(s×m); an arrow – a height of subpermafrost water rise, m; plus – above the wellhead, minus – below the wellhead.

Table 3. **Parameters of the water-bearing capacity of the Triassic sedimentary rocks in the river valleys**

Area	Depths of wells, m	Permafrost thickness, m	Specific flow rate of wells, L/(s·m)	Mineralization of water, g/dm^3	Content of ions, mg/dm^3
Coastal area; abs. elevations 5–80 m; up to 9 km from the coast of the Chaum Bay; 20 wells	300–602 / 386	140–250 / 175	0.0007–0.09 / 0.02	M 0.19–3.1 / 1.73	Cl 2.56–445 / 80.6; HCO_3 78–507.5 / 180.4; SO_4 0.1–60 / 31.4
Inland area; abs. elevations 156–302 m; 11 wells	201–300 / 286	120–240 / 191.5	0.0005–0.28 / 0.04	M 0.13–2.6 / 0.66	Cl 2.3–445 / 80.6; HCO_3 97.6–829.5 / 294; SO_4 0.6–44.5 / 23

areas have been revealed only in the basin of the Pegtymel River. Therefore, Table 3 demonstrates the summarized results of drilling and sampling of the wells situated in the areas outside the zones with open taliks.

There are noticeable differences in the hydrogeological parameters of the coastal zone. In terms of geology, it is located on the eastern flank of the Anyuy subterrane. The inland area belongs to the Chaun subterrane (Table 3).

In general, the total mineralization and the chlorine ion content are higher in coastal areas than in inland areas; however, the water transmissivity of rocks in the first one is 2.2 times lower than in the second one.

It should be noted that subpermafrost waters by their composition belong to the hydrocarbonate, chloride, and sulfate classes, typical for the subpermafrost waters of the Paleozoic formations and Triassic deposits in the arch-thrust uplifts.

A group of intrusive massifs

Hydrogeological characteristics of this group were obtained only during the development of Valkumey tin ore deposit attributed to the granitoid massif of the same name. This massif is represented by Pevek Mountain, characterized by subdued relief with the absolute elevation of 616 m. During underground mining at the elevations from +150 to –250 m, it was established that the cryogenic aquiclude is continuous. In the coastal zone, its thickness is about 100 m. The assumed thickness of the cryogenic aquiclude in the upper part of the slope (at the top of the mountain) is about 400–450 m.

The subpermafrost waters, encountered by underground mining, occur in the submeridional zones of the faults that also host the ore bodies. The head in the coastal zone does not exceed 10 m above the mouth. Perhaps, below the watershed, subpermafrost waters do not contact the cryogenic aquiclude and their levels are free.

The long-term observations of water inflows into underground workings show that all aquiferous faults are poorly interconnected hydrodynamically. After opening of the aquiferous zone, the water inflow varies from the first units up to 30 m^3/day. In 10–15 days, the inflow decreases by 2–3 times. In 2–3 weeks, sometimes, up to 5–6 months, it decreases until draining. The water bearing capacity of the fault zones before their uncovering can be estimated on the basis of the pumping data from advance wells, which have been drilled from the bottom of the workings on different horizons (Table 4).

Table 4. **Pumping data from advance wells in underground workings [*Glotov and Glotova, 2003*]**

No.	Abs. elevation, m	Absolute mark of the depth of penetration of aquifers, m	Pumping results		
			Constant flow rate in the first 5 days, L/s	Lowering from static level, m	Specific flow rate, L/(s·m)
1	+10	–167	0.02	48.5	0.0004
2	+10	–90	0.35	90.0	0.0040
3	–50	–75	0.75	60.0	0.0130
4	–100	–130	0.015	110.0	0.0001
5	–100	–180	1.00	110.0	0.0090

The attention should be paid on the existence of the relatively water-rich objects ("pockets") in ore zones. According to the chief geologist of the mine A.D. Kharyutkin, such "pockets" are characterized by abundance of calcite veins in the fractured zone.

The subpermafrost waters are characterized by the sodium-calcium chloride or calcium-sodium composition. By the total mineralization, they are fresh (up to 1 g/dm^3), brackish (1–20 g/dm^3), saline (0–40 g/dm^3), and brine (more than 40 g/dm^3) [*Glotov and Glotova, 2003*].

Freshwaters are encountered by the workings located at a distance of 0.5 km or more from the Chaun Bay. They occur below the bottom of the cryogenic aquiclude as lenses in faults, forming the zone of fresh waters underlain by brackish waters.

Saline waters and brines occur beneath the bottom of the Chaun Bay as isolated lenses with salinity up to 300–320 g/dm^3. One of them with the composition of water

$$M\ 314\frac{Cl\ 100}{Mg\ 73\ Na\ 26}\ pH\ 6.8$$

was encountered during underground mining of an ore vein in the Pribrezhny site on 19.03.1970. The presence of these waters indicates the cryogenic metamorphization at the temperatures from -10 to -15 °C [*Abramov, 2014*]. It is possible that cryopegs were formed near the day surface and then penetrated to deeper horizons.

Study of the tritium content in the samples taken by D.V. Efimova from self-discharging wells on the –100-m horizon on 18.07.1974 [*Efimova et al., 1978*] showed that brackish water, the composition of which is reflected by a formula

$$M\ 37.9\frac{Cl\ 98}{Ca\ 70\ (Na + K)\ 22},$$

contains 83 TU or 9.9 Bq/L; in the water of the Chaun Bay, it is 13.4 Bq/L. These values correspond to natural values of tritium in natural waters of the zone of active water exchange. However, subpermafrost waters, encountered in the Valkumey massif, where there is the continuous cryogenic aquiclude, are distributed in the zone of impeded water exchange, as evidenced by the presence of ions of divalent iron in sulfate brine. It is possible that tritium-containing air of the mine penetrates into the dried zones of faults; and, when air moisture is condensed, tritium-bearing waters are formed, diluting brackish waters. The formation of tritium could also occur during the natural decay of radioactive components.

Concluding the hydrogeological characteristics of the Paleozoic and Triassic sedimentary rocks and a group of intrusive rocks, we will focus on some common features in the Chukotka Upland.

1. Subpermafrost waters in the Triassic sedimentary rocks are confined everywhere, including the watersheds above the possible sources of groundwater feeding. In the group of intrusive massifs, subpermafrost waters may have a free level within the near-watershed areas.

2. Water transmissivity below the cryogenic aquiclude in the Paleozoic regionally metamorphosed formations, studied in the river valleys, is tens of times higher than the same parameter in the Triassic sedimentary rocks and intrusive massifs.

3. In terms of the chemical composition, waters of the hydrocarbonate class, waters of the chloride class in the coastal lowlands, and waters of the sulfate class in the zones of hydrothermal sulfide mineralization are most common. According to the total mineralization, waters of low salinity and fresh waters predominate. However, the high bicarbonate content is possible in waters of any class of both hydrogeological stages.

HYDROGEOLOGICAL FEATURES OF THE SOUTH OF THE CHUKOTKA UPLAND ON THE BASIS OF MAGNETOTELLURIC SOUNDING

Magnetotelluric sounding (MTS) was performed in 2002–2004 by the group from Karpinsky Russian Geological Research Institute (VSEGEI) along the profile 2-DV-A from Pevek Mountain to the Valunistoye mine. Figure 3 illustrates a fragment of the profile, the depth of which is limited to 3000 m, because it is close to the total thickness of the Triassic sedimentary rocks in this site of the works. The profile runs along the southwestern flank of the Ichuveem arch-thrust uplift to the upper reaches of the Palyavaam River. The geoelectric section crosses the Upper Jurassic – Lower Cretaceous sedimentary-volcanogenic sequence at a distance of about 12–15 km from Pevek. This sequence is a part of the Anyuy subterrane. Further up to 40 km, the section crosses the zone of the Pevek submeridional deep fault, dividing the Anyuy and Chaun subterranes.

Up to 150 km, the section of the profile is represented by the Triassic sedimentary rocks, which are underlain by the Paleozoic sedimentary rocks at a depth of more than 3000 m. The sedimentary rocks are ruptured by dikes and massifs of magmatic rocks, broken by numerous normal faults and thrust faults. The complete geoelectric sections are presented online at VSEGEI website: Section-2-DV-A_Geoelec_raz_0-225 km.jpg (https://vsegei.ru/ru/info/gisatlas/dvfo/chukotsky_ao/index.php).

Using results of the MTS in geologically and geocryologically similar areas of the Northeast of Russia [*Khasanov and Sharafutdinov, 2011*], the author distinguished the blocks of monolithic magmatic and metamorphosed rocks with electrical resistivity (ER) > 398 Ohm·m in the studied geoelectric section. Their water-bearing capacity is manifested in the form of narrow sub-vertical bands with an electri-

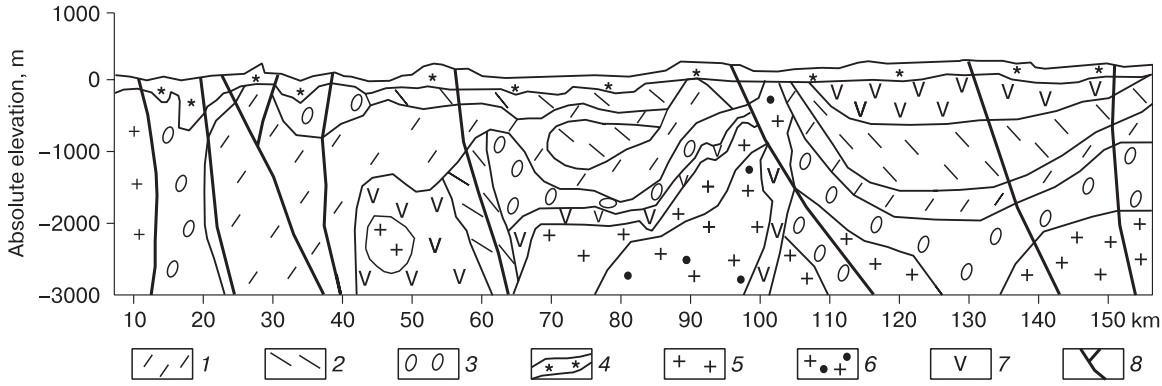

Fig. 3. The geoelectric section of the southern margin of the Chukotka Upland in the segment of 10–150 km from Pevek.

Based on an enlarged fragment of the geoelectric and seismic profile 2-DV-A (*vsegei.ru/ru/info.../2021*). Electrical resistivity of the zones (Ohm·m): *1* – <25.1; *2* – 25.1–32.8; *3* – 32.8–158; *4* – 158–358; *5* – 358–1000; *6* – 1000–10,000; *7* – >10,000; *8* – fault.

cal resistivity of 25.1–39.8 Ohm·m. By conditions of the groundwater occurrence, such blocks are typical hydrogeological massifs.

The near-surface continuous band, which shape partly repeats the topography, is also characterized by high electrical resistivity. Its thickness varies from 200 to 400 m. Two belts with approximately equal thickness are distinguished in the band: the upper belt with ER from 158 to 251 Ohm·m, and the lower belt with ER of 252–398 Ohm·m. The author considers the continuous band as permafrost, which consists of the upper belt – an ice-bearing layer of regionally fractured rocks and the lower belt – frozen rocks lying deeper than the zone of hypergene fracturing.

The cryogenic aquiclude lies on the Triassic subpermafrost sedimentary formations with relatively low resistivity, their ER ranges from less than 25.1 to 158 Ohm·m. The ER value in this case reflects water transmissivity of rocks or specific flow rates of the wells and groundwater mineralization determined by pumping. For example, in the profile interval of 102–105 km in the valley of the Sredny Inchoun River, permafrost lies on the layer with ER less than 25.1 Ohm·m. Earlier, the well 302 m deep was drilled here. Confined subpermafrost waters were encountered at the depth of 217 m and the water level rose above the wellhead by 34.6 m. In pumping on 26.06.1991, a constant flow rate of 12.5 L/s was obtained at 67.4-m lowering, g = 0.19 L/(s·m), k_p = 20 m^2/day. A formula of the water composition is

$$M\ 0.82\ \frac{HCO_3\ 79\ Cl\ 21}{Na\ 72\ Mg\ 19}\ pH\ 6.3.$$

The content of bicarbonate ion is 756 mg/dm^3. The data of this well reflect the hydrogeological features of the most low-resistance zone. Subpermafrost strata are traced along the entire profile up to about 150 km, which is associated with the extensive development of thrust faults. Therefore, the MTS results quite clearly reflect the general hydrogeological and permafrost features of the studied blocks of the earth's crust.

DISCUSSION

On the basis of drilling and sampling of wells, underground mining, and interpretation of MTS results, we can conclude that there are two classes of waters distributed in the subpermafrost setting – local fracture waters and quasi-stratum fracture waters. The local-fracture waters are typical for magmatic rock massifs and for the dome of the Paleozoic regionally metamorphosed sequences. These waters also occur in the Mesozoic lithified sedimentary sequences. Taking into account the fact that the thickness of the cryogenic aquiclude on them exceeds the depth of hypergenic fracturing, these massifs can be considered analogous to the hydrogeological massifs previously identified in Eastern Siberia [*Shepelev et al., 1983*]. While the local fracture waters are sufficiently studied and their relationship with fault zones is quite clear, the quasi-stratum fracture waters are poorly studied. Therefore, we emphasize that the quasi-stratum fracturing develops in monolithic sedimentary rocks, when their blocks move along thrust faults. The tectonophysical consequences of such displacements are actively studied [*Seminsky, 2003; Danielsen and Dahlin, 2009; Seminsky et al., 2016*]. According to the established concepts, at the stage preceding the displacement of blocks (strata), the zones of paragenetically connected ruptures arise due to geological pressure. These are the leading fractures of shear and rupture, which form the fracturing zone. With further growing of pressure, fractures enlarge; main fault planes arise; a layer of tectonically crushed rocks (cataclasites), which are often cemented by clays pro-

duced by friction (mylonites), is formed along a strike of the fault planes. The thickness of this layer in our case does not exceed 10 m. However, because of low water permeability, it can be considered as a confining barrier, which divides the fracturing zone, developed earlier, into two quasi-stratum reservoirs, poorly connected in terms of hydrogeodynamics.

Tectonic activity is also manifested in the formation of sub-vertical faults or fractures, which are filled with hydrothermal quartz, kaolin, ore minerals, etc. These vein formations are also poorly permeable and, together with the fault planes, form a network of relatively impermeable screens, which divide the quasi-stratum fracture reservoirs into fragments or sections. These screens generally impede water exchange, but do not prevent transmission of hydrostatic pressure. This fact is confirmed by the connection of the field of piezometric levels with slopes of the day surface. Their hydrodynamic isolation is confirmed by rapid (from 2–3 days to several weeks) drawdown of water resources during pumping (up to drainage) of initially water-bearing rocks and by differences in the chemical composition of water in the neighboring sections.

The author believes that the long-term maintaining of the cryogenic head, generated during freezing under conditions of impeded outflow of subpermafrost waters, is also explained by poor interconnection of the aquiferous sections. The relatively small size of freezing sections prevents the accumulation of significant volumes of cryogenically metamorphosed water and the creating of the heads, sufficient to destroy natural impermeable barriers. Due to poorly studied permafrost history of the Chukotka Upland, the data on the geographically close region of Arctic Yakutia have been involved to analyze the development of permafrost in the Pleistocene and Holocene [*Gavrilov et al., 2000; Gavrilov and Tumskoy, 2001; Anisimov et al., 2002*].

These data suggest that over the last 420 thousand years, the spatial distribution of discontinuous permafrost in the Chukotka Upland has not changed dramatically. However, during the Holocene warming, the permafrost degraded with a decrease of its thickness, apparently, no less than 1.5 times. Therefore, in the mountain areas and river valleys, the fragmentary structure of the subpermafrost aquiferous strata determined impeded water exchange and allowed to preserve the cryogenic head and groundwaters formed more than 420 thousand years ago. The long-term contact of the groundwaters and host rocks contributed to enrichment of waters with salts of carbonic acid due to interaction with carbonaceous-clayey shales and with a chlorine ion leached from them. Activity of water exchange is higher in the hydrogeological massifs of the fault zones. Therefore, it is possible that the subpermafrost waters here is close to the modern age.

CONCLUSIONS

Therefore, the results of drilling, underground mining, and magnetotelluric sounding show the specific features of hydrogeological conditions in the subpermafrost units in the east of the Chukotka Upland and lead to the following conclusions and recommendations:

1. According to the conditions of the groundwater distribution and occurrence in the area of the Chukotka Upland, the hydrogeological massifs with local fracture waters were formed in the granitoid massifs and in the Paleozoic metamorphosed rocks. A classic example of such a massif is the Valkumey massif. The unique natural reservoir was formed on the tectonically active arch-thrust uplifts. This reservoir consists of fractured aquiferous rocks, divided into sections by relatively impermeable screens. The last ones are represented by tectonic breccias, cemented by mylonite, friction clays, quartz and kaolin, as well as by hydrothermal quartz and/or kaolin veins.

2. The sectional structure of the subpermafrost units contributed to the formation of a cryogenic head pressure under all topographic features, including watersheds, with the head level higher than the daylight surface and maintaining these heads up to the present time. The hydrogeological structural features outside the arch-thrust uplifts are poorly studied. Drilling in the river valleys suggests the existence of the subpermafrost sectional structure in these areas.

It is possible that the existence of confined subpermafrost waters in the watersheds with a static level up to 54.3 m above the wellhead may be related to the presence of local open taliks in the upper reaches of streams, for example, in the bottoms of former glacial cirques or kars. Similar taliks are known in the western part of the Chukotka Upland, and may exist in the eastern part, too.

3. Existence of the subpermafrost sections with the impeded water exchange at shallow depths is favorable for the creation of underground storage of liquid products – fresh water for potable water supply, oil products, toxic liquid waste, etc.

4. It is necessary to conduct long-term regime observations of the level, pressure, and composition of subpermafrost waters, to study the age specifics of groundwaters in the entire area of the Chukotka Upland and in the adjacent areas not only in river valleys, but also in watersheds.

5. We recommend implementing the MTS methods into the practice of areal and local permafrost-hydrogeological studies.

Acknowledgments. *The author expresses his gratitude to Lyudmila Petrovna Glotova for her help in data selecting and in the design of this work, to Ibragim Mubarakovich Khasanov, candidate of geological and mineralogical sciences, leading researcher of the Shilo*

North-East Interdisciplinary Scientific Research Institute, Far East Branch, Russian Academy of Sciences for his help in studying the magnetotelluric sounding data, and to the reviewers, whose comments allowed me to improve the text of this article.

References

Abramov, V.Yu., 2014. Cryogenic metamorphization of the chemical composition of groundwater. Exploration and conservation of mineral resources, No. 5, 16–20.

Afanasenko, V.E., Zamolotchikova, S.A., Tishin, M.I., Zuev, I.A., 1989. North-Chukotka region. In: Geocryology of the USSR. Eastern Siberia and the Far East. E.D. Ershova (Ed.). Nedra, Moscow, pp. 280–292 (in Russian).

Alekseev, V.R., Gorin, V.V., Kotov, S.V., 2011. Naledi-taryny of Northern Chukotka. Ice and Snow 51 (4), 85–88.

Anisimov, M.A., Tumskoy, V.E., Savatyugin, L.M., 2002. On the issue of changes in the natural conditions of the New Siberian Islands in the Late Pleistocene and Holocene. News of the Russian Geographical Society, 134 (5), 32–37.

Basic provisions for the compilation of serial legends for state geological maps of scale 1:200,000 and 1:1,000,000, 2001. Geoinform, Moscow, 15 pp. (in Russian).

Belikovich, A.V., Galanin, A.V., Galanin, A.A. et al., 1997. The nature and resources of Chukotka. SVNTs FEB RAS, Magadan, 236 pp. (in Russian).

Byalobzhesky, S.G., Goryachev, N.A., Shpikerman, V.I., 2006. Cratons and Orogenic Belts of the East of Russia. In: Geodynamics, Magmatism and Metallogeny of Russia. V.I. Khanchuk (Ed.). Dalnauka, Vladivostok, Book 1, pp. 144–152 (in Russian).

Danielsen, V.E., Dahlin, T., 2009. Comparison geoelectrical imaging and tunnel documentation at the Hollands's Tunerel, Sweden. Engin. Geol., vol. 107, 118–129.

Efimova, D.V., Romanov, V.V., Seletskiy, Yu.B., Yakubovskiy, A.V., 1978. Tritium and deuterium in the waters of Western and Central Chukotka. In: Materials on geology and mineral resources of the North-East of the USSR. Issue 24. Book. Publishing House, Magadan, pp. 169–174 (in Russian).

Efimova, D.V., Sabelnikov, A.V., Sinitskaya, V.M., 1977. Anyuy-Chukotka region. In: Engineering Geology. Vol. 4. Far East. E.G. Chapovsky (Ed.). Moscow State University, Moscow, 157 pp. (in Russian).

Fotiev, S.M., 2013. Underground waters of the cryogenic region of Russia (classificationn). Kriosfera Zemli [Earth's Cryosphere], XVII (2), 41–59.

Gavrilov, A.V., Tumskoy, V.E., 2001. The evolution of the mean annual ground temperature on coastal lowlands of Yakutia in the Middle and Late Pleistocene. Kriosfera Zemli [Earth's Cryosphere], V (3), 3–16.

Gavrilov, A.V., Tumskoy, V.E., Romanovsky, N.N., 2000. Reconstruction of the mean annual ground temperature dynamic on the Yakutian coastal lowlands and adjoining shelf during the last 420 kyr. Kriosfera Zemli [Earth's Cryosphere], IV (4), 3–14.

Glotov, V.E., 2020.Taliki regions of mountain-valley glaciation in Zapolyarnaya Chukotka. Exploration and protection of mineral resources, No. 5, 28–36.

Glotov, V.E., Glotova, L.P., 2003. Underground waters of the Valkumeysky tin ore deposit. Kolyma, No. 2, 21–28.

Glotov, V.E., Glotova, L.P., 2013. Relationship between the basement of the Okhotsk-Chukotka volcano-plutonic belt and the water resources of the active water exchange zone. Vestnik SVNTs FEB RAS, No. 4, 67–75.

Glotov, V.E., Glotova, L.P., 2015. Hydrogeology of the zone of active water exchange on the Arctic coast of the North of the Far East. Bulletin of the North-Eastern Scientific Center of the Far East Branch of the Russian Academy of Sciences, No. 1, 28–36.

Glushkova, O.Yu., Smirnov, V.N., 2020. Neopleistocene glacial complexes in the North-East of Russia. In: Science in the North-East of Russia: fundamental and applied research in the North Pacific and the Arctic: Materials of Scientific. Conf. (Magadan, 05–06.03.2020). SVKNII FEB RAS, Magadan, pp. 23–26 (in Russian).

Khasanov, I.M., Sharafutdinov, V.M., 2011. The deep structure of the southeast of the Yano-Kolyma fold system according to geophysical data and the characteristic features of the structure of gold ore nodes. Uchenye zapiski Kazan University. Natural Sciences, 153 (3), pp. 1–17 (in Russian).

Pinneker, E.V., 1977. Problems of regional hydrogeology: patterns of distribution and occurrence of groundwater. Nauka, Moscow, 196 pp. (in Russian).

Polzunenkov, G.O., 2018. Estimation of P–T and O_2 conditions of crystallization of monzonitoids of the Velitkenai granite-pegmatite massif (Arctic Chukotka) according to the data of mineral thermobaro- and oxybarometry. Tikhoocean. Geol. 37 (5), 97–111.

Seminsky, K.Zh., 2003. Internal structure of continental fault zones: tectonophysical aspect. Acad. Publ. House "Geo", 243 pp. (in Russian).

Seminsky, K.Zh., Zaripov, R.M., Olenchenko, V.V., 2016. Tectonophysical approach to the interpretation of shallow electrotamography data of fault zones. Geology and Geophysics 57 (9), 1715–1729.

Shepelev, V.V., Tolstikhin, O.N., Pigusova, V.M. et al., 1984. Permafrost-hydrogeological conditions of Eastern Siberia. Nauka, Novosibirsk, 198 pp. (in Russian).

Shumikhina, M.K., 1999. Hydrogeology. In: State Geological Map of the Russian Federation. Scale 1:1,000,000 (new series). Sheet R-59-(60) – Bilibino. Explanatory letter. VSEGEI, St. Petersburg, pp. 68–74 (in Russian).

Tolstikhin, O.N. (Ed.), 1972. Hydrogeology of the USSR. Vol. 26. North-East of the USSR. Nedra, Moscow, 296 pp. (in Russian).

Tolstikhin, O.N., 1974. Overlapping and underground waters of the North-East of the USSR. Nauka, Novosibirsk, 162 pp. (in Russian).

Volkov, A.V., Goncharov, V.I., Sidorov, A.A., 2006. Deposits of gold and silver in Chukotka. SVKNII FEB RAS, Moscow, Magadan, 221 pp. (in Russian).

Zhuravlev, G.F., Kalinin, S.A., 1999. Tectonics. In: State Geological Map of the Russian Federation. Scale 1:1,000,000 (new series). Sheet R-59 (Bilibino). Explanatory letter. VSEGEI, St. Petersburg, pp. 45–61 (in Russian).

URL: vsegei.ru/ru/info/gisatlas/dvfo/chukotsky_ao/index.php (last visited: 10.07.2021).

Received May 13, 2021
Revised July 28, 2021
Accepted September 26, 2021

Translated by V.A. Krutikova